1975

The Dynamic Response Of A Cylindrical Elastic Vessel To Disturbed Flow: A Case For Arterial Resonance

Alexander Stewart Sinclair

THE DYNAMIC RESPONSE OF A CYLINDRICAL ELASTIC VESSEL TO DISTURBED FLOW: A CASE FOR ARTERIAL RESONANCE

by

Alexander Stewart Sinclair, B.Sc., M.Sc.

Department of Biophysics

Submitted in partial fulfillment

of the requirements for the degree of

Doctor of Philosophy

Faculty of Graduate Studies

The University of Western Ontario

London, Ontario

ABSTRACT

Vibrations in biological tissue can lead to a change in the structural properties that appear similar to the 'structural fatigue' in synthetic materials. In arteries, a dilatation of the vessel, known as poststenotic dilatation, can occur distal to a stenosis. The observation of discrete amplitude peaks in the wall vibration spectra distal to an artificial stenosis, in vitro, led to the conclusion that the artery wall was being stimulated at its resonant frequencies. This result provides a plausible explanation for the fatigue that is observed as well as for the generation of cardiovascular sound that is associated with this phenomenon.

Since the question of resonance seems a crucial one for a further understanding of fatigue and the generation of sound, the intention of this thesis is to examine what the resonant frequencies are and what factors are important.

A solution was first considered, analytically, for the membrane analysis of the radial equation of motion for a cylindrical elastic vessel under constant wall stress. The bending energy contribution and the inertial loading of the wall due to fluid internally or externally were also considered and those factors included in the description. This analysis revealed

that the dominant factors determining the resonant frequencies were wall stress, geometry and the acoustic media.

An experimental evaluation of the model was considered by examining the radial wall vibration spectra (measured with an optical sensor) of penrose tubing exposed to either acoustical stimulation (by a loudspeaker) or the random pressure fluctuations of turbulent flow (created by a stenosis). The effect of wall stress was determined from changes in the pressure (circumferential tension) or length (longitudinal tension) and the effect of geometry evaluated by using samples of different radii and length. The inertial loading of the wall was considered by studying the response in air - air, air - fluid, and fluid - fluid (internally and externally, respectively). The predicted mode shapes were confirmed from spatial examination of the amplitude and phase that were obtained by movement of the probe.

Having established that the model adequately described the resonant modes in the above study, a series of tests were then performed on six isolated arteries exposed to turbulent flow. The experimental results supported the model, and analysis of other

data available in the literature agreed with the predictions as well.

This thesis has therefore shown that the analytical expression for the resonant radial vibrations proposed here adequately describes the resonant frequencies of synthetic tubes and isolated arteries. The dominant factors governing this description were wall stress, geometry and the acoustic environment. Although only arterial segments were examined a similar extension to other tissues seems possible.

The frequency range that is characteristic of murmurs and bruits is one which would be expected to contain several resonant modes of the vessel wall as described in the present study. It seems clear therefore, that the arterial wall in these situations is being stimulated at one or more resonant frequencies and that this factor is probably a dominant one in the fatigue that results and the sound that is heard.

ACKNOWLEDGEMENTS

Professor M. R. Roach introduced me to this area of research and has provided constant interest and guidance throughout this particular study. Professor J.E.K. Foreman made this study possible. In addition to his interest and many helpful suggestions, he brought to my attention the optical sensor and provided the facilities for conducting this research. I am deeply grateful to both of these people.

Mr. G. Vandenbrink in Engineering as well as Mrs. D. Elston and Mr. L. Rigutto in Biophysics patiently provided the technical support necessary. Without their help the experimental task would have been insurmountable.

My wife, Pat, has helped with the figures, re-writing and typing. More importantly, she has had to put up with all the frustrations that go with completing a thesis. I think I can finally guarantee her that there will be no more.

Finally, this work was supported by a grant from the Ontario Thoracic Society and the Ontario Heart Foundation. The author wishes to express his gratitude to these organizations and to the Medical Research Council of Canada who provided a studentship throughout the course of this research.

TABLE OF CONTENTS

	Page
CERTIFICATE OF EXAMINATION	ii
ABSTRACT	iii
ACKNOWLEDGEMENTS	vi
TABLE OF CONTENTS	vii
LIST OF PHOTOGRAPHIC PLATES	ix
LIST OF TABLES	ix
LIST OF FIGURES	x
NOMENCLATURE	xv
CHAPTER I - INTRODUCTION	1
CHAPTER II - HISTORICAL REVIEW	3
(i) Dynamic Stresses and Fatigue	3
(ii) Disturbed Flow	8
(iii) Fluid Pressure Spectra	13
(iv) Murmurs	20
(v) Resonance	21
CHAPTER III - THEORETICAL ANALYSIS	26
(i) Introduction	26
(ii) Membrane Analysis	30
(iii) Bending Energy Contribution	38
CHAPTER IV - EXPERIMENTAL ANALYSIS	44
(i) Introduction	44
(ii) Technique	45
(a) Displacement Sensor	45
(b) Signal Conditioning	51
(c) Tape Recorders	54
(d) Measurement of Geometry	55
(iii) Vibration in Air	56
(a) Method - Acoustical Stimulation	57
- Disturbed Flow	62
(b) Results - Acoustical Stimulation	63
- Disturbed Flow	79
(c) Discussion	93
(iv) Vibration in Fluid : Externally	98
(a) Method	98
(b) Results - Acoustical Stimulation	99
- Disturbed Flow	104
(c) Discussion	117
(v) Vibration in Fluid :Internally and Externally	117
(a) Method	117
(b) Results - Disturbed Flow	119
- Geometry	132
- Correlation Studies	147
(c) Discussion	151

Page

(vi) Vibration of Arteries 153
(a) Method 153
(b) Results 158
(c) Discussion 181

CHAPTER V - GENERAL DISCUSSION 192
(i) Evaluation of Model 192
(ii) Dynamic Response to Disturbed Flow 195
(iii) Fatigue 202
(iv) Murmurs 209

CHAPTER VI - SUMMARY 221

CHAPTER VII - SUGGESTIONS FOR FUTURE RESEARCH 226

* * *

APPENDIX I - LIST OF EQUIPMENT USED AND THEIR SPECIFICATIONS 227

REFERENCES 231

VITA 236

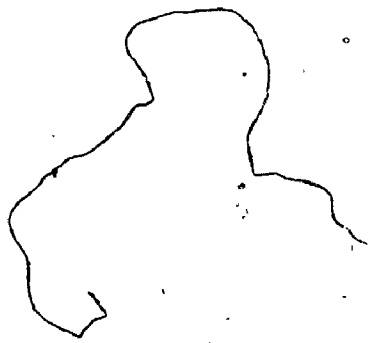

LIST OF PHOTOGRAPHIC PLATES

Plate		Description	Page
1	A	Example of spectral phonocardiography on a noisy murmur.	212
	B	Example of contour plot in spectral phonocardiography on a noisy murmur.	
2	A	Example of a musical murmur due to a partial arterial occlusion.	216
	B	Example of a musical murmur due to calcific aortic valves.	

LIST OF TABLES

1	A summary of the data from Foreman and Hutchison's study of wall vibration spectra distal to an artificial stenosis, in vitro.	185

LIST OF FIGURES

Figure	Description	Page
1	Effect of a stenosis on the structural properties of a dog femoral artery.	6
2	Effect of vibration on the structural properties of dog bronchi.	10
3	Non dimensional fluid pressure spectra in a turbulent boundary layer.	16
4	Wall displacement spectra distal to a stenosis on a human external iliac artery, in vitro.	23
5	Radial vibration modes of a cylinder.	28
6	Operation of photonic sensor.	47
7	Calibration curve for the photonic sensor on penrose tubing.	50
8	Signal conditioning procedure.	53
9	Experimental arrangement for measuring wall displacement.	59
10	Method of acoustical stimulation: A) Externally B) Internally.	61
11	Response to acoustical stimulation: A) Externally B) Internally.	65
12	Change in vibration amplitude with movement of the probe axially and circumferentially.	68
13	Effect of circumferential and longitudinal tension under internal acoustical stimulation in air.	72
14	A plot of f^2 versus T_e for the three resonant peaks in figure 13.	75

Figure	Description	Page
15	A) A plot of f^2 versus m^2 for the three resonant peaks in figure 13.	77
	B) A plot of C_z^2 versus longitudinal strain for the beam mode, n=1, and the circumferential resonance, n=2.	
16	Characteristic wall displacement spectra while under disturbed flow in air.	81
17	Effect of pressure on the wall displacement spectra in air.	83
18	Effect of longitudinal tension on the wall displacement spectra in air.	85
19	A) A plot of f^2 versus T_c' for the circumferential resonance under disturbed flow in figure 17.	87
	B) A plot of f^2 versus the longitudinal strain term for the beam mode n=1 in figure 18.	
20	A plot of f^2 versus T_c' for the n=3 mode in figure 17.	91
21	Wall displacement spectra under different flow rates, during disturbed flow in air, while maintaining the prestress levels constant.	95
22	Calculated resonant frequencies versus the observed values for the results in air, under disturbed flow.	97
23	Comparison of the results from internal acoustical stimulation with and without the loading of external fluid.	101
24	Plot of f^2 versus T_c' for the resonant peaks observed in figure 23 with and without the loading of external fluid.	103
25	Comparison of wall displacement spectra under disturbed flow with and without external fluid.	106

Figure	Description	Page
26	Effect of pressure on the wall displacement spectra with internal fluid.	109
27	Effect of longitudinal tension on the wall displacement spectra with external fluid.	111
28	A plot of f^2 versus T_c' for the resonant peaks in figure 26.	113
29	A plot of f^2 versus longitudinal strain for the resonant peaks in figure 27.	115
30	Comparison of the wall vibration spectra with fluid internally and externally and with air internally and fluid externally.	121
31	Effect of pressure on the wall displacement spectra with internal and external fluid loading while the longitudinal tension was constant.	123
32	Effect of longitudinal tension at constant pressure on the wall displacement spectra with internal and external loading.	125
33	A plot of f^2 versus T_c' for the dominant resonant peak under internal and external fluid loading.	128
34	A plot of f^2 versus T_c' for the higher frequency peak corresponding to n=3.	130
35	A plot of f^2 versus the longitudinal strain factor for the beam mode n=1.	134
36	Comparison of the wall displacement spectra under disturbed flow for the large and small diameters of penrose tubing.	136

Figure	Description	Page
37	A plot of f^2 versus pressure for the large and small samples.	139
38	A plot of amplitude versus axial position for the resonant peak at 235Hz under disturbed flow.	141
39	Wall vibration spectra using the HP3580A spectrum analyzer.	144
40	A plot of f^2 versus T_c' for the results obtained in figure 39.	146
41	Correlograms obtained upon filtering at the circumferential resonant frequencies corresponding to n=2 and n=3.	150
42	Summary of the results obtained on the synthetic tubing with the calculated resonant frequency plotted against the observed value for the three acoustic media.	155
43	Effect of pressure on the wall displacement spectra of a femoral artery under constant tethering and flow.	160
44	Effect of longitudinal tension on the wall displacement spectra of a femoral artery.	162
45	A plot of f^2 versus T_c' for the dominant circumferential resonance of the femoral artery in figure 43.	165
46	A plot of f^2 versus T_c' for the resonant peak corresponding to n=3.	167
47	A plot of f^2 versus the longitudinal strain for the beam mode n=1 of the femoral artery.	170

Figure	Description	Page
48	Wall vibration spectra of a carotid artery with that on the femoral artery included for comparison.	172
49	A plot of f^2 versus m^2 for the three dominant modes associated with n=2 in the carotid artery.	175
50	A plot of f^2 versus T_c' for the resonant peaks in the carotid artery results.	178
51	A plot of f^2 versus T_c' for the n=3 resonant mode in the carotid artery results.	180
52	A plot of calculated resonant frequencies versus the observed values for the six biological samples tested.	183
53	A plot of f^2 versus the circumferential mode factor for the results from Foreman and Hutchisons study, showing the sensitivity of the radius.	188
54	A plot of the calculated resonant frequencies versus the observed valuesfrom the six samples taken from Foreman and Hutchisons study.	191
55	A plot of the rms amplitude of wall displacement versus the inverse of the resonant frequency.	198
56	A plot of the rms amplitude of wall displacement versus the flow rate at constant pressure and length for the circumferential modes n=2 and n=3.	200
57	A plot of the length versus the corresponding frequency producing a dilatation, from Boughners work.	205

NOMENCLATURE

z,r,θ	....	axial, radial and tangential cylindrical coordinate
t	....	time
u,v,w	....	perturbation displacement in axial, circumferential and radial direction, respectively
a	....	mid-surface radius
h	....	wall thickness
L	....	length
ρ_w,ρ_f	....	density of wall and fluid, respectively
$f_{m,n}$	....	resonant frequency for mode shape (m,n)
m	....	number of half waves longitudinally
n	....	number of full waves circumferentially
T_θ^o	....	circumferential tension ($\bar{T}_\theta^o = \Delta p.a$)
T_z^o	....	longitudinal tension ($T_z^o = E_z h\varepsilon_z + \nu T_\theta^o$)
$\bar{T}_c$	....	$T_\theta^o/(2\pi a)^2$
$\bar{T}_L$	....	$T_z^o/(2L)^2$
P	....	transmural pressure, ΔP
p_i,p_e	....	pressure perturbation internally and externally
$\rho_e h$	....	effective density of wall due to loading by internal or external fluid ($\rho_e h = \rho_w h + m_L$)
m_L	....	virtual mass due to internal or external fluid (see equation 15 in text)
C_z^2	....	$[T_z^o + \gamma A_2]/[\rho_e h(2L)^2]$
C_θ^2	....	$[T_\theta^o + n^2\gamma A_1]/[\rho_e h(2\pi a)^2]$

E_i^*, ν ..... anisotropic moduli and poissons ratio, respectively

A_1, A_2^* .... bending term contribution (see equation 24)

γ .... $h^3/(12a^3)$

I_n, I_n', K_n, K_n' .... Modified Bessel functions and their first derivatives of the first and second kind, respectively

ψ .... velocity potential in fluid

C .... velocity of sound in fluid

ω .... circular frequency

k .... $k^2 = \frac{m^2\pi^2}{L^2} - \frac{\omega^2}{C^2} \simeq m^2\pi^2/L^2$

---

*The terms E_i and A_i are referred to throughout the text without reference to their units which are dynes/cm^2.

I INTRODUCTION

It is well known that vibration of a synthetic material can lead to a weakening or failure of that material, known as 'structural fatigue'. A similar effect has been observed in biological tissue that is exposed to dynamic stresses. The vibration of arteries, for example, may lead to a change in the structural properties (Roach, 1972). These structural alterations may be localized as in poststenotic dilatation (Holman, 1954 a,b; Roach, 1963 a,b) or more generalized as in the pulmonary artery with atrial septal defect (Boughner, 1971).

The vibrations occur in the physiological state due to random pressure fluctuations that arise from disturbed or turbulent flow. Foreman and Hutchison (1970b) observed several amplitude peaks in the wall vibration spectra distal to an artificial stenosis, in vitro, and concluded that the artery wall was stimulated over several resonant frequencies. This result has important implications not only with respect to fatigue but in the production of murmurs as well. The relatively large strains (and hence dynamic stresses) possible at resonance seem a plausible explanation for the observed alterations. Furthermore, since any vibrating structure will act as a sound source the increased vibration amplitude at resonance may become the dominating factor in the production of murmurs.

Since resonance seems important for structural fatigue and murmur production, this problem should be studied in detail. The objective of this thesis, therefore, is to determine the resonant modes that were observed or are possible in synthetic and biological tubes, and to evaluate what factors (wall stress, geometry, structural properties) are important.

The thesis will present a mathematical model for the resonant frequencies of a cylindrical, elastic vessel and show that the wall stress and geometry are the most significant factors determining the resonant frequencies. The model will be tested by studying vibration spectra, obtained with a non-contacting, fibre-optic, displacement sensor, under different values of wall stress and geometry. Both accoustical stimulation and exposure to disturbed flow, created by a stenosis, are used to test the model.

The results show that some resonant modes fall within the range of frequencies that are associated with murmurs in the cardiovascular system.

II HISTORICAL REVIEW

(i) Dynamic Stresses and Fatigue

All structural materials have an ultimate tensile strength to which they can be stressed without failure. This is true of both biological and synthetic materials. When, however, a substance is exposed to dynamic[1] or cyclic stresses the material is observed to fail at loads considerably below those that it stands statically. This phenomena is known as structural fatigue, with the dynamic stress amplitude and the number of cyclic deformations governing the time to failure (Hayden, Moffat and Wulff, 1965).

Holman (1954 a, b) was the first to suggest that structural fatigue might occur in biological tissue; for example, in the phenomenon of poststenotic dilatation, a localized dilatation of the arterial wall is observed downstream from an arterial stenosis. An excellent review of this phenomena is provided in the same publication, which outlines the association with various types of arterial constriction.

Using rubber tubes, Holman produced similar dilatations downstream from an artificial stenosis exposed to pulsatile flow. With dye studies, he observed that the region of turbulent eddies was identical with the position of largest dilatation and also corresponded to the location of greatest thrill or bruit (Holman, 1954 b). Along with Bruns and others (Bruns et al, 1959) he produced pressure fluctuations in the lumen of penrose tubing with a vibrating reed and again observed a dilatation at the point of maximum vibration.

---

[1] 'Dynamic' is used synonymously with 'cyclic' when referring to stresses in this text.

Roach (1963, a,b) extended the analysis of the phenomenon of poststenotic dilatation by studying the structural properties of arteries that were partially occluded by artificially created stenoses which resulted in a disturbed flow distally. She examined the elastic properties distal and proximal to the stenosis both in vitro (Roach, 1963a, b), using human and dog iliac arteries, and in vivo (Roach, 1963a, b,) using dog femoral and carotid arteries. Figure 1 characterizes her results, indicating not only a dilatation (larger radius) distally, but an increased distensibility. From her previous studies on the elastic properties of arteries (Roach and Burton, 1957) she suggested that an alteration in the elastic fibers or the links between collagen fibers had occurred.

Following the observations made by Holman, she noted that the degree of dilatation was related to the presence of a thrill or bruit, which she attributed to turbulent flow (Roach and Harvey, 1964). When the thrill or bruit was absent, as was the case with a minimum stenosis (10-39%) no dilatation was observed. However, when a moderate stenosis (45-72%) was created, a thrill or bruit was observed and a dilatation occurred. In these latter tests when the thrill or bruit was classified as weak the dilatation was slight (10-28%) whereas when it was strong the dilatation was more severe (31-63%). These results lend further credence to the idea that dynamic strains, indicated by vibrations of the wall (thrills), lead to a structural weakening or alteration.

The study was extended further by exposing arteries to

FIGURE I

Effect of a stenosis (obtained by putting a nylon taffeta band around the artery) on the structural properties of a dog femoral artery. Reproduced with permission from Roach (1963b). Pre-stenotic refers to the region immediately upstream of the stenosis while post-stenotic refers to the wall region immediately downstream. Distal to dilation refers to the wall region further downstream from the point of dilatation.

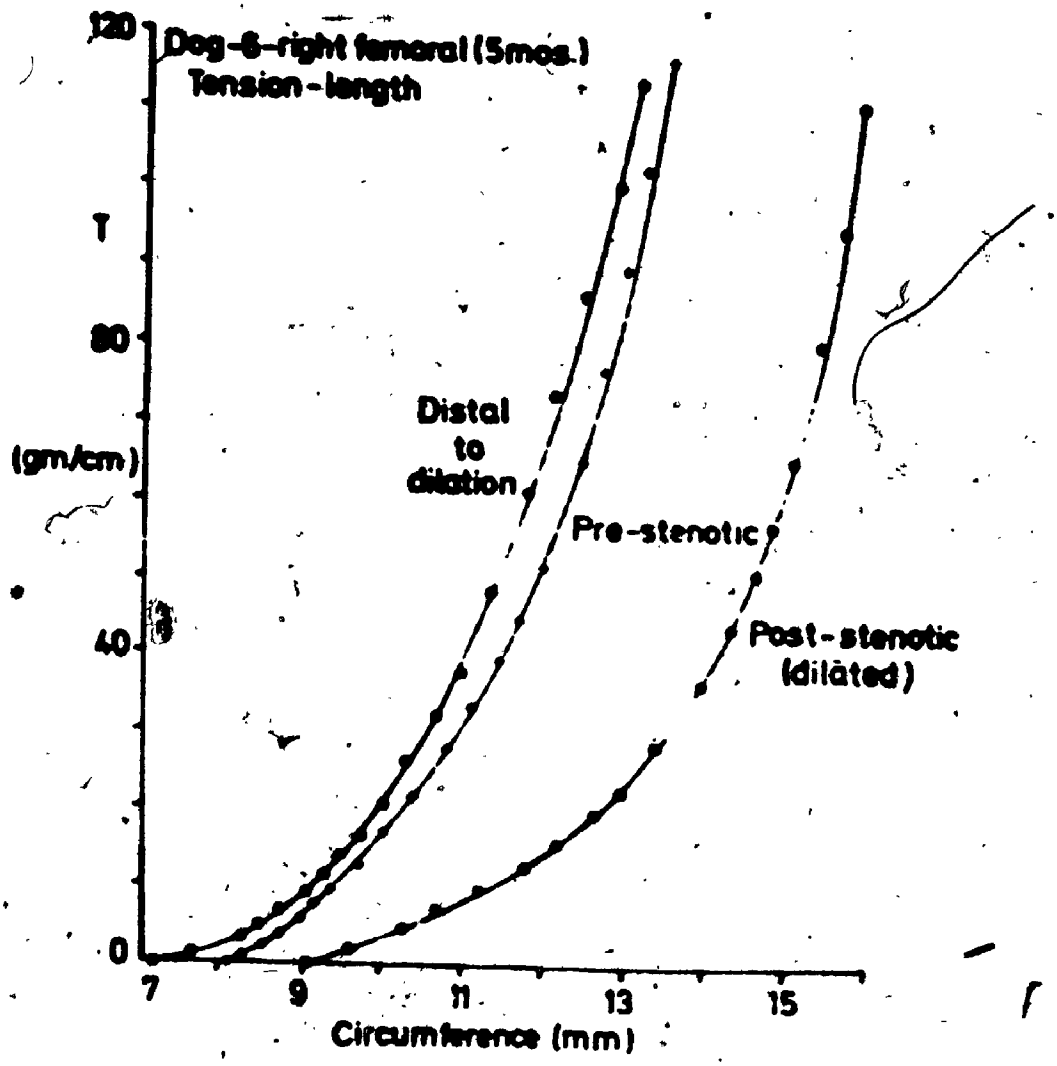
Dog-6-right femoral (5mos.)
Tension-length
120
T
80
(gm/cm)
40
0
Distal to dilation
Pre-stenotic
Post-stenotic (dilated)
7
9
11
13
15
Circumference (mm)

dynamic stresses created by a cocktail shaker (Roach, 1963 a), a phonocatheter used in reverse (Roach and Melech, 1971) and by a loudspeaker (Boughner, 1971). In each case structural alterations were observed similar to those occurring in poststenotic dilatations. That is, the vessels became more distensible.

In Boughner's study, however, he found the frequency of stimulation to be important. Some frequencies would cause a vessel to dilate while others would not. He correlated his findings with age and found that the older the artery the higher the frequency required to produce a dilatation.

Following Roach's idea that turbulent flow is the factor involved, Boughner (1971) looked for a situation where turbulence was present in the absence of a stenosis to see if there were structural alterations present. He examined patients with atrial septal defects, a congenital defect where a hole exists in the septum dividing the two atrium. This abnormality allows part of the blood returning from the lungs (to the left atrium) to pass back through the right atrium with the venous return into the pulmonary artery. This increased volume of flow raises the Reynolds number (Boughner, 1971) past the critical value and a murmur is heard. When he examined the elastic properties of the pulmonary artery, angiographically, he found the artery was more distensible and the change was similar to that occurring with pulmonary valve stenosis.

Sinclair (1972) recently examined the response of isolated dog bronchi to vibratory stress. Isolated segments of bronchi were

perfused with a turbulent air jet which produced considerable vibration or a fluttering of the wall, and significant alterations in the geometry and properties occurred. Again, those regions exposed to the greatest vibratory stress underwent the most significant alterations. This point is illustrated in Figure 2.

Although the exact nature of the structural alterations in biological tissue is not clear, the important facts of similarity to 'structural fatigue' are. The necessity of dynamic strains occurring within the biological vessels, as evidenced by palpable thrills, has been shown to be a prerequisite. Furthermore, the fact that the degree of structural alteration was related qualitatively to the degree of dynamic stresses induced, provides further support for this idea.

(ii) Disturbed Flow

To produce dynamic stresses within the walls of biological vessels the flow must be disturbed so that pressure fluctuations interact with the wall. Flow disturbances may arise from the interaction of the flow with boundaries or from the shear between layers of fluid. Once initiated, the disturbance may then grow (turbulent) or decay (laminar) depending upon the stability of the fluid, which is represented by the Reynolds number.

It was not until the recent use of hot film probes that quantitative analysis of blood flow in the major arteries became possible. Using a hot film anemometer to obtain the velocity profiles in dog aortas, Nerem, Seed and Wood (1972) have established

FIGURE 2

Effect of vibration on the structural properties of isolated dog bronchi, induced by a turbulent air jet. This was produced from two types of cannulae acting as stenoses, as shown in the diagram. 'Elastance' is related to the modulus of elasticity by, Elastance = Eh, where h is the wall thickness. The normalized value is obtained from the ratio after exposure to that before, so that a value greater than 1.0 indicates an increasing stiffness. The results (mean and standard error for seven samples, total) indicate a significant alteration in the properties both longitudinally and circumferentially over the region exposed to the greatest vibratory stress. The use of different cannulae demonstrates a shifting of this point of maximum structural alteration with the point of maximum vibration. Reproduced from Sinclair (1972).

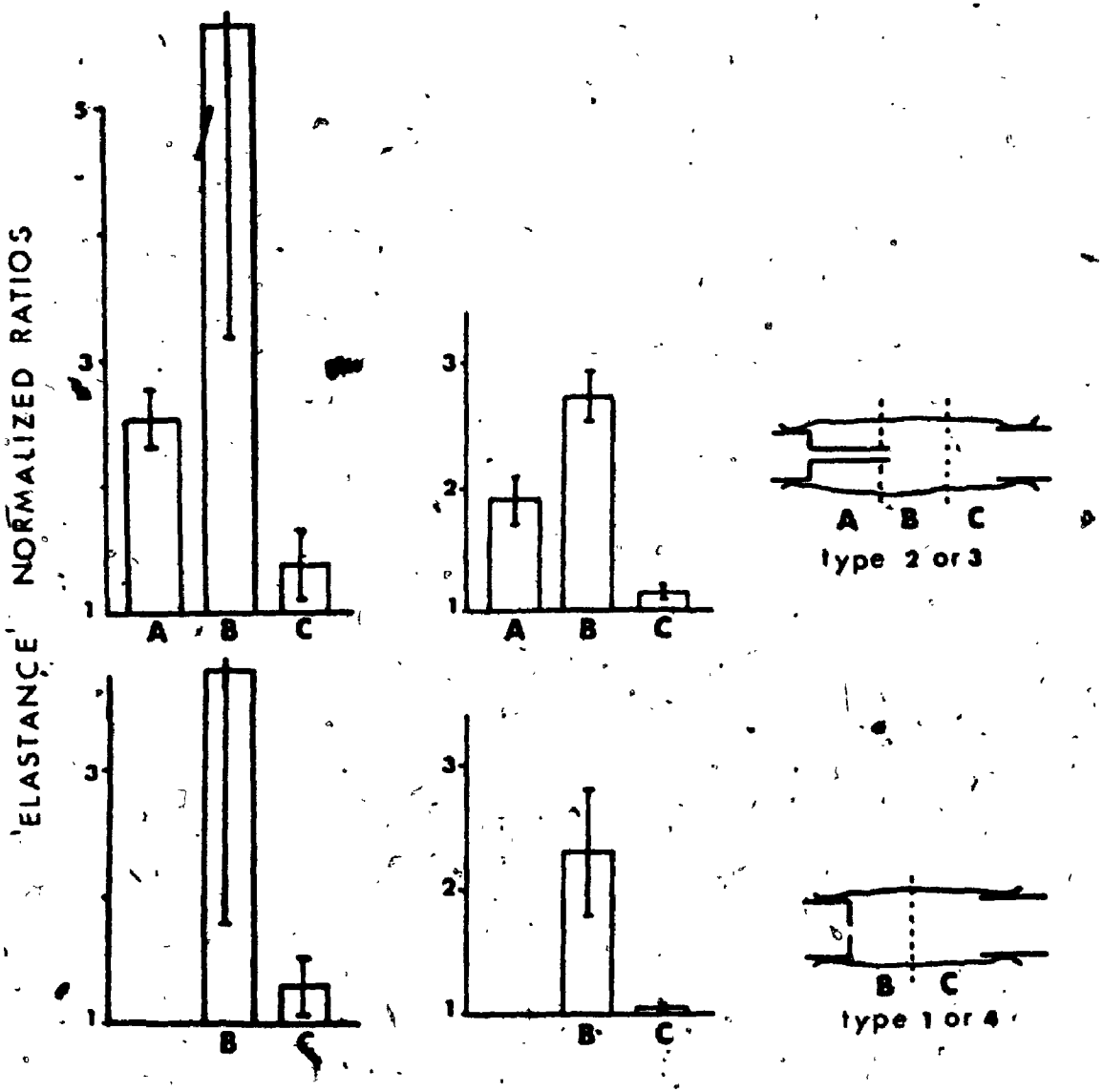
CIRCUMFERENTIAL
LONGITUDINAL
CANNULA
ELASTANCE NORMALIZED RATIOS
5
3
1
A
B
C
3
2
1
A
B
C
A B C
type 2 or 3
3
1
B
C
3
2
1
B
C
B C
type 1 or 4

stability criteria for disturbed flow in terms of the peak Reynolds number and the unsteadiness parameter ' α ' ($\alpha = R\sqrt{\omega/\nu}$), where R = radius, ω = circular frequency and ν = kinematic viscosity). They characterize the flow in terms of the existence of high frequency (h.f.) velocity components as follows.

1) Undisturbed (laminar) - negligible h.f. components
2) Disturbed - h.f. components only at peak systole
3) Turbulent - h.f. components persist through the decelerative phase of systole.

They found stability boundaries of $Re_c = 250\alpha$ for the thoracic aorta and $Re_c = 150\alpha$ for the ascending aorta. Their results suggested that a state of transitional or turbulent flow exists in dogs under normal conditions. Clark and Schultz (1973), using similar probes, did not see turbulent flow under normal conditions in dogs, although low frequency disturbances were present.

In any event we are concerned not with the normal physiological conditions where structural alterations are absent but those abnormal states where highly disturbed or turbulent flow occurs. These states will occur when the Reynolds number for the flow exceeds the critical value, either by changing the Reynolds number associated with the flow itself or by lowering the critical value. An important diagnostic indication of these abnormal states of flow disturbance is the presence of murmurs or bruits upon auscultation. McKusick (1958), presents an extensive analysis of murmurs and other cardiovascular sounds, using spectral phonocardiography to illustrate his points.

The Reynolds number, $\frac{VD}{\nu}$, (V = average velocity, D = diameter and ν = kinematic viscosity) associated with the flow can be increased by altering the various parameters involved. McKusick (1958) discusses various abnormal states where the Reynolds number increases and a murmur occurs. For instance, in anemia where the kinematic viscosity decreases, or in thyrotoxicosis or exercise where blood flow increases, murmurs develop. Other examples of murmurs resulting from increased flow are patent ductus arteriosus (Dawes, Mott and Widdicombe, 1955) and atrial septal defect (Boughner, 1971).

The critical Reynolds number can be lowered by boundary induced flow alterations such as bifurcations or stenoses. Ferguson (1972) demonstrated a lowering of the critical Reynolds number in dye studies of glass model bifurcations and its dependence on angle (the greater the angle the lower the critical Reynolds number). Other studies, using hot film anemometry at branches in glass models (Gutstein, Schneck and Marks, 1968) and at the junction of the dog aorta and iliac arteries in vivo (Gutstein, Farrel and Schneck, 1970), also show the existence of disturbances at low Reynolds numbers.

The lowering of the critical Reynolds number with an arterial stenosis has been studied by several authors, using dye studies (Roach, 1972), birefringence techniques (Meisner and Rushmer, 1963 a), and hot film anemometry (Young and Tsai, 1973 a, b). With stenoses of various dimensions, Roach (1972) found the Re_c depended on geometry, with the diameter or degree of constriction being more important than the length of the stenosis. Young and Tsai (1973 a, b) have performed

an extensive analysis of the flow characteristics of model stenoses, for steady and unsteady flow, using hot film probes. Using instantaneous Reynolds number they found, as above, a lowering of Re_c for the onset of turbulence with increasing degrees of narrowing. They also noted that mildly stenosed models were more stable under oscillatory flow, whereas severe constrictions showed little difference between steady and pulsatile flow. Sacks, Tickner and Macdonald (1971) found a stability boundary between the critical Reynolds number and stenosis geometry, using the occurrence of a murmur as the criteria for critical Reynolds number. They found a convenient empirical relation $Re_c = 2000 \left(\frac{d}{D}\right)^2$ where d is the occluded diameter and D is the normal diameter of the lumen. Their results showed good agreement between the time duration of a murmur and the duration of 'super critical' flow.

In summary, disturbed flow occurs when the Reynolds number associated with the flow exceeds the critical value. This will occur normally when the appropriate values of flow rate or diameter increase or the kinematic viscosity decreases beyond the normal physiological values. However, an effective lowering of the critical Reynolds number will provide the same effect under normal physiological values. This arises from boundary induced flow alterations such as bifurcations or stenoses.

(iii) Fluid Pressure Spectra

The previous discussion has emphasized some of the conditions where abnormal flow states result in disturbed flow. A knowledge of the magnitude and frequency range of the pressure fluctuations

arising from this disturbed flow is important in studying the question of fatigue. The spectra of fluid motion has been studied by many authors, using birefringence techniques (Meisner, and Rushmer, 1963 a, b; Anne et al, 1967), spectral phonocardiography (McKusick, 1958; Winer et al, 1965; Lees and Dewey, 1970), pressure fluctuations (Yellin 1966; Foreman and Hutchison, 1970 a) and hot film velocity fluctuations (Nerem, Seed and Wood, 1972; Kim and Corcoran, 1973; Giddens et al, 1973). All of these studies indicate an increase in the magnitude and frequency range of disturbances as the flow rate increases.

Foreman and Hutchison (1970 a) measured the wall pressure fluctuations produced by flow through stenoses in rigid tubes. Their results indicate an increase in the magnitude and frequency range of pressure fluctuations when either the flow rate or degree of constriction is increased. Kim and Corcoran (1973) observed similar results using a hot film probe to measure velocity fluctuations in rigid tubes. An in vivo analysis on dog aortas has been recently performed by Giddens et al (1973) obtaining both velocity and pressure fluctations. As in rigid models, they found an increase in magnitude and frequency range of disturbances as the vessel is narrowed.

The spectra of wall pressure fluctuation in a turbulent boundary layer for different flow rates can be characterized in terms of the non-dimensional power spectral density and the non-dimensional frequency (Willmarth, 1959; Bull, 1968; Clinch, 1969). This relationship is shown in Figure 3 redrawn from Clinch (1969). Lees and

FIGURE 3

Non-dimensional fluid pressure spectra in a turbulent boundary layer. Redrawn from Clinch (1970).

ϕ - power spectrum of the pressure fluctuations

ρ - fluid density

d - diameter of pipe

U_∞ - centerline velocity

f - frequency

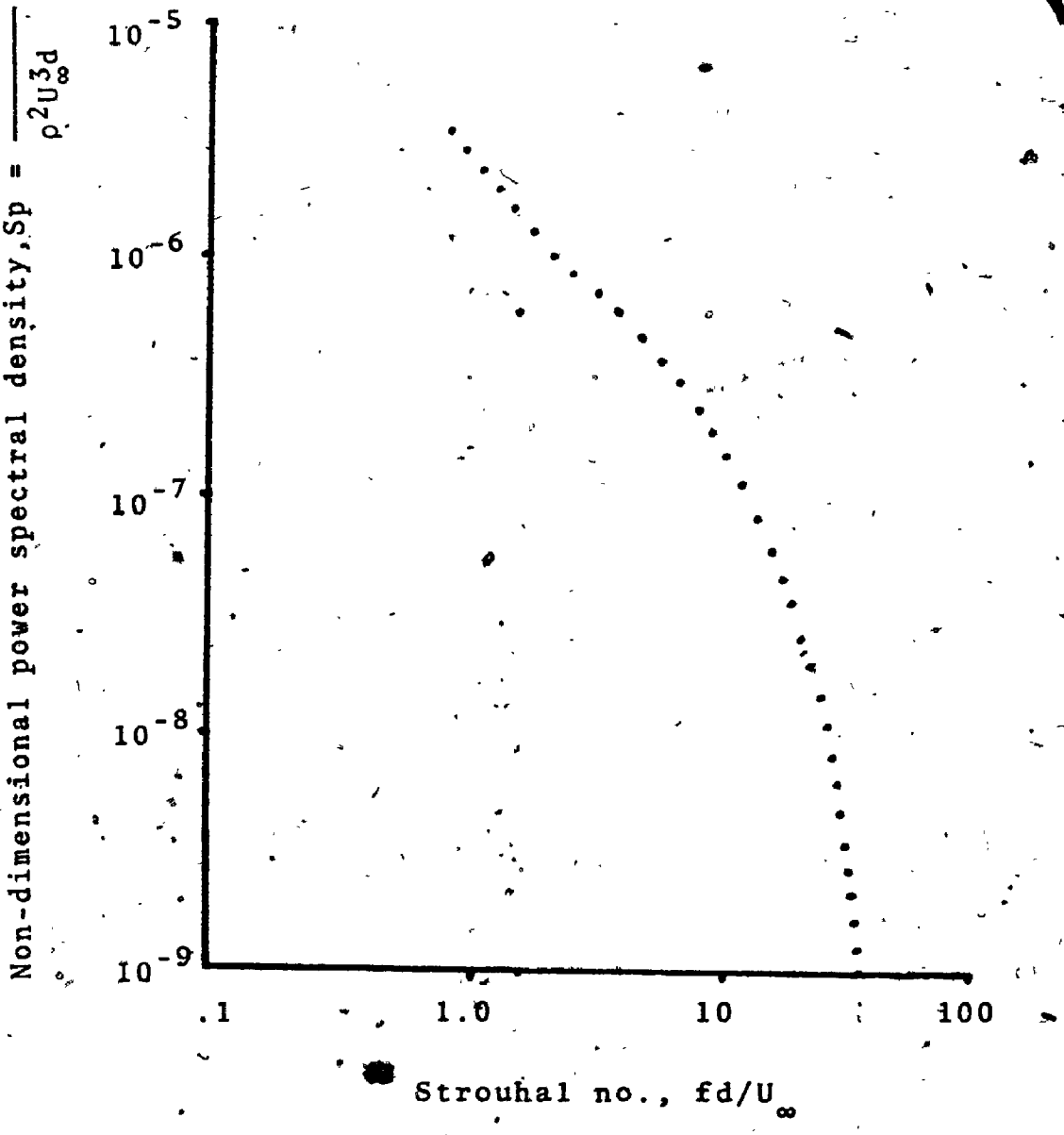
Non-dimensional power spectral density, Sp = $\frac{\phi(f)}{\rho^2 U_\infty^3 d}$
10^{-5}
10^{-6}
10^{-7}
10^{-8}
10^{-9}
.1
1.0
10
100
Strouhal no., fd/U_∞

Dewey (1970) have adopted this approach to represent the loud carotid bruits observed in patients with severe atherosclerosis. They noted that there are substantial differences between the pulsatile turbulent jets arising from stenotic occlusions and the constant mean velocity pipe flow with its constant non-dimensional intensity. In spite of these differences, however, they feel that their results "suggest that the fluid jet produced by a stenosis rapidly establishes a universal turbulent spectrum just distal to the point of partial occlusion".

There are two wall regions associated with a stenotic jet where we would expect different wall pressure spectra. Just distal to the stenosis between where the boundary layer separates and reattaches is a 'separated region' where there are low frequency disturbances (Young and Tsai, 1973 a). Distal to the point of reattachment of the boundary layer the fluid is highly disturbed containing a much higher frequency content and intensity (Young and Tsai, 1973 a). Both regions are dependent on stenosis geometry and Reynolds number. Roach (1972) demonstrated the effect of stenosis diameter on the point of reattachment and length of the highly disturbed region. The results indicate a movement of the reattachment point closer to the stenosis and a larger zone of highly disturbed flow as the degree of constriction is increased. This provides qualitative agreement with the observation of Roach and MacDonald (1970) that the length of poststenotic dilatation was inversely related to the stenosis diameter in renal arteries.

This could correspond to an increased region of highly disturbed flow with its greater spectral content.

In spite of the large number of pressure spectra studies performed, no absolute values of the pressure fluctuations within the lumen of biological vessels are reported. Even in spectral phonocardiography few absolute values are reported, with relative intensity, timing and duration the quantities of interest. Murmurs are generally quantified as loudness on a 6 point scale, which is largely subjective as reported by Lepeschkin (1957). He made attempts to analyze murmurs objectively with an electric stethoscope. In normal persons he found levels of 20 to 60 dB for the first heart sound and 30 to 70 dB for the second heart sound. The loudness of systolic murmurs ranged up to 40 dB while some high pitched musical murmurs reached 50 dB. These are all levels recorded at the body surface, however. Wallace et al (1959), using a phonocatheter intravascularly, calculated an amplitude of 45 dB with respect to 1 dyne/ cm^2 sound pressure level (or approximately 120 dB with respect to threshold) for the second heart sound in the right ventricle. However, they provide no other levels for their intravascular studies.

It is clear from the above discussion that increasing the flow or severity of constriction (once the critical Reynolds number has been exceeded) will result in a greater spectral content of pressure fluctuations acting on the wall, as well as changing the region over which it acts. The significance of these facts in view of the observations made by Roach (1970), relating the degree and

zone of structural weakness to the degree of occlusion, is now in perspective. However, whether it is the general increase in intensity of the pressure fluctuations or the increase at higher frequencies or both is not clear.

(iv). Murmurs

One important aspect of the response of an elastic vessel to disturbed flow is in the production of murmurs. The essential factor here is that the wall is flexible and can vibrate in response to the turbulent boundary layer. The result of this motion is an additional sound field that may have a much greater intensity than that associated with the flow. This point is demonstrated by the fact that a turbulent jet in a rigid tube does not produce a murmur, whereas if an elastic vessel is exposed to the same Reynolds number a murmur is heard (McKusick, 1958). Meisner and Rushmer (1963b) demonstrated that the more flexible cellophane tubing produced sounds that were 10 times louder than the more rigid tygon tubing under the same flow conditions.

Bruns (1959b) recognized that turbulence alone could not account for murmurs but suggested that periodic wake fluctuations of vortex shedding were responsible. The previous spectral analysis of pressure fluctuations, however, does not provide evidence for a periodic nature of the flow. McKusick (1958) correctly summed it up by stating that "Murmurs are produced through a complex interplay between the disturbed flow and the wall or other boundary structure". It is clear that a further understanding of murmur production requires an understanding of the dynamic response of the enclosing structures involved.

(v) Resonance

The response of a biological vessel to disturbed flow is one of considering the effect of a fluctuating force on an elastic system. In particular, if that driving force has a frequency content that includes the natural frequency or frequencies of the elastic system, resonance may occur. The development of this condition with its large vibratory strains would have considerable effect on the problem of fatigue or weakening of the wall. The previous section has discussed the frequency content of the stimulating force under the abnormal flow states. The question that remains to be answered is - what are the resonant frequencies of biological vessels and have they been observed?

In reference to this question Foreman and Hutchison (1970) obtained wall displacement spectra of isolated dog and human iliac arteries distal to an artificial stenosis perfused (in vitro) with steady flow. Using a non contacting capacitive displacement transducer they obtained results similar to that in figure 4, which clearly shows three amplitude peaks at 130, 310 and 550 Hz. They considered whether these were true resonant peaks of the wall by stimulating the vessel externally with a constant level sinusoidal pressure from a loudspeaker. Their results demonstrated several resonance peaks which showed excellent correlation with that obtained under disturbed flow.

FIGURE 4

Wall displacement spectra distal to a stenosis on a human external iliac artery, in vitro. Reproduced with permission from Foreman and Hutchison (1970 b).

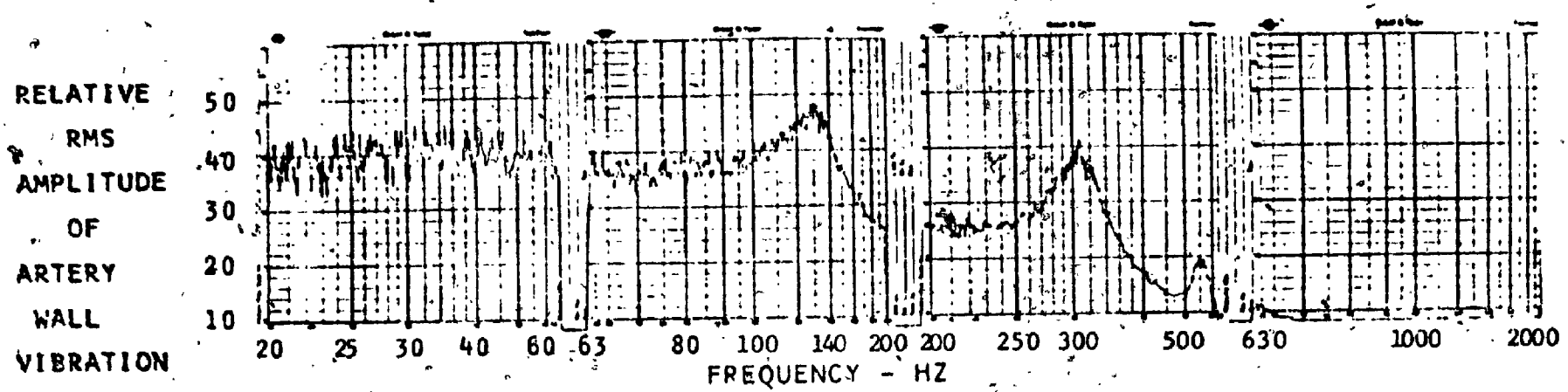

FREQUENCY SPECTRUM OF ARTERIAL WALL DISPLACEMENT DISTAL TO A 45% STENOSIS IN AN ISOLATED HUMAN EXTERNAL ILIAC ARTERY, WITH FLOW RATE OF 1000 ML/MIN THROUGH ARTERY. (UNITS ON ORDINATE REFER TO VOLTAGE LEVEL OF SIGNAL AT INPUT TO FREQUENCY ANALYZER).

They concluded that "fluid flow through isolated arteries with an experimental stenosis excites the artery wall to vibrate over a wide range of frequencies that coincide with the resonant frequencies of the artery wall."

Boughner and Roach (1971), who found the dilational response of arteries to be frequency dependent, suggestive of resonance did not find resonant peaks in their vibration studies. However, their use of a pressure transducer (Pitran Model PT, Stow Laboratories) to quantify wall displacements is questionable.

Other investigators have considered the wall vibrations in response to disturbed flow. Meisner and Rushmer (1963b) used a phonocartridge in contact with the walls of tygon and cellophane tubing. Although no sharp resonant peaks were found the spectra obtained were fairly complex, possibly containing several peaks close together. Recently; Kim and Corcoran (1973) have obtained 'wall' spectra using a microphone in contact with tubing of different thickness. They did find resonance, particularly in the thinner walled vessels. Placing a phonocatheter against the wall of cerebral aneurysms, in vivo, in humans, Ferguson (1970) has observed musical murmurs and suggested that resonance may be involved.

Except for the study by Foreman and Hutchison the question of arterial resonance has been examined poorly.

The use of pressure transducers to evaluate wall vibration is questionable. The former study, on the other hand, could not provide information on the resonant modes of vibration nor were the properties altered to see the effect on the resonant frequencies. It seems clear that an analytical and experimental evaluation of the resonant modes of a biological vessel is necessary for a further understanding of murmur production and fatigue.

II THEORETICAL ANALYSIS

(i) Introduction.

To understand the dynamic response of a biological vessel we must consider the propagation of a perturbation of the vessel surface. The disturbance propagates outwards from the point of initiation, characterized by the wave propagation speeds C_z and C_θ. It is easy to see that if the frequency of the stimulating force is such that the returning perturbation circumferentially is in phase then a standing wave will occur. Similarly, if there was some acoustical discontinuity longitudinally, to allow part or all of the disturbance to be reflected, then longitudinal standing waves might be set up. The corresponding resonant modes are shown in figure 5.

To determine the frequencies involved in the above resonances, the wave propagation characteristics must be known. The study of wave propagation has concerned many investigators interested in the propagation of the arterial pressure pulse, beginning with Thomas Young in 1808 (Skalak, 1966). Excellent reviews of the development of wave propagation theories, all limited by consideration of axisymmetric disturbances, are provided by Skalak (1966) and Noordergraaf (1972).

FIGURE 5

Radial vibration modes of a cylinder.

m= number of half waves longitudinally

n= number of full waves circumferentially

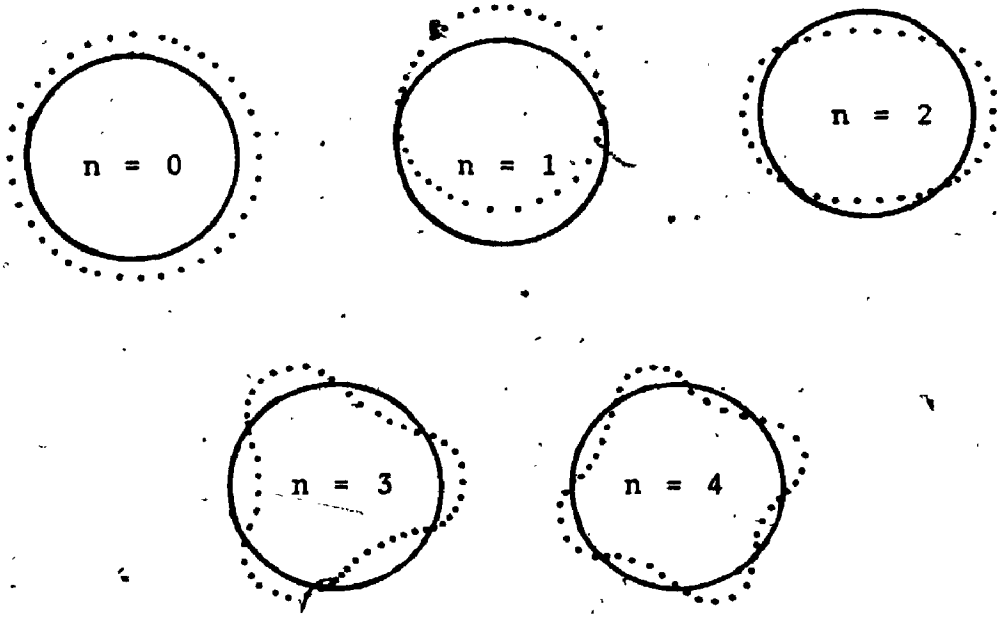

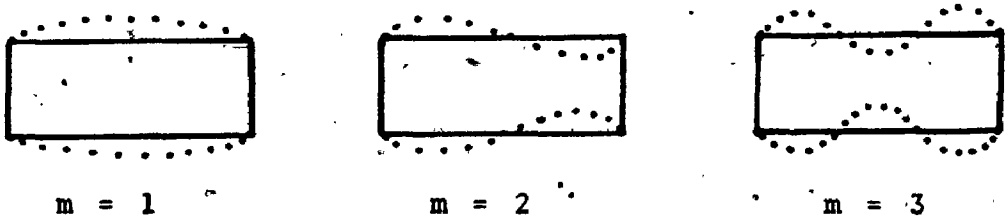

VIBRATIONAL MODES OF A CYLINDER

The most comprehensive analysis of wave propagation, theoretically and experimentally, that includes non axisymmetric disturbances is by Anliker and his colleagues (Anliker and Maxwell, 1966; Maxwell and Anliker, 1968; Anliker, 1972; Moritz and Anliker, 1974). Their analysis considers the in place axial (u) and tangential (v) movement in addition to the radial motion (w). These results indicate that three types of waves - axial, torsional, and pressure - can be propagated, characterized by their dominant motion u, v and w, respectively.

The most general description of the motion of a cylindrical vessel comprises three equations relating the translational motion and two equations relating the shear. From our point of view, however, we are interested primarily in the radial motion of the vessel. The motions longitudinally (u) and tangentially (v), are of little interest since movement in these directions would not result in an additional sound field. The radial vibrations, however, can lead to a new sound source. Since an additional sound source seems probable in the production of murmurs or bruits (interaction of the flow with an elastic structure (McKusick, 1958)), which appears necessary for fatigue (Roach and Harvey, 1964), it would seem that our concern should be with the resonant modes of radial vibration.

(ii) Membrane Analysis

The equation of motion in the radial direction is (Dym, 1974):

$$\frac{1}{R}\frac{\partial(Q_z R)}{\partial z} + \frac{1}{R}\frac{\partial Q_\theta}{\partial \theta} - \frac{T_z}{R_z} - \frac{T_\theta}{R_\theta} - \rho h \frac{\partial^2 w}{\partial t^2} + F_r = 0 \qquad (1)$$

where T_z, T_θ are the stress resultants (tensions), $\frac{1}{R_z}$, $\frac{1}{R_\theta}$, the principle curvatures, longitudinally and circumferentially. F_r is the total body surface force acting in the radial direction. Q_z and Q_θ are the transverse shear resultants related to the bending moments by

$$Q_z R = \frac{\partial(M_z R)}{\partial z} + \frac{\partial M_{\theta z}}{\partial \theta} - M_\theta \frac{\partial R}{\partial z} \qquad (2a)$$

$$Q_\theta R = \frac{\partial(M_{z\theta} R)}{\partial z} + \frac{\partial M_z}{\partial \theta} + M_{\theta z} \frac{\partial R}{\partial z} \qquad (2b)$$

However by making the assumption of a thin wall ($h/R << 1$) the transverse shear resultant become small so that equation (1) reduces to the membrane equation:

$$-\frac{T_z}{R_z} - \frac{T_\theta}{R_\theta} - \rho h \frac{\partial^2 w}{\partial t^2} + F_r = 0 \qquad (3)$$

Noting that $r = Z\,\hat{k} + R(z,\theta,t)\,\hat{r}$ and $R(z,\theta,t) = a + w(z,\theta,t)$, where a is the mid surface radius, then the principle curvatures are (Dym, 1974):

$$\frac{1}{R_z} = \frac{-\frac{\partial^2 R}{\partial z^2}}{\left[1+\left(\frac{\partial R}{\partial z}\right)^2\right]^{3/2}} = \frac{\frac{\partial^2 w}{\partial z^2}}{\left[1+\left(\frac{\partial w}{\partial z}\right)^2\right]^{3/2}}$$

$$\therefore \frac{1}{R_z} \simeq -\frac{\partial^2 w}{\partial z^2} \qquad (4a)$$

Similarly

$$\frac{1}{R_\theta} = \frac{1}{R} - \frac{1}{R^2}\frac{\partial^2 R}{\partial \theta^2} = \frac{1}{a+w} - \frac{1}{(a+w)^2}\frac{\partial^2 w}{\partial \theta^2}$$

$$= \frac{1}{a}\left(1-\frac{w}{a}\right) - \frac{1}{a^2}\frac{\partial^2 w}{\partial \theta^2}$$

ignoring the higher order terms in w.

Thus $$\frac{1}{R_\theta} = \frac{1}{a} - \frac{1}{a^2}\left(w + \frac{\partial^2 w}{\partial \theta^2}\right) \qquad (4b)$$

Substituting these into equation (3) we obtain:

$$T_z \frac{\partial^2 w}{\partial z^2} + \frac{T_\theta}{a^2}\left(w + \frac{\partial^2 w}{\partial \theta^2}\right) = \rho h \frac{\partial^2 w}{\partial t^2} + \frac{T_\theta}{a} - F_r$$

If we consider that the time dependent part of the tension due to the perturbation ($T = T^o + T'$), is small relative to the prestressed level T^o, then $T \simeq T^o$ and

$$T_z^o \frac{\partial^2 w}{\partial z^2} + \frac{T\theta^o}{a^2}\left(w + \frac{\partial^2 w}{\partial \theta^2}\right) = \rho h \frac{\partial^2 w}{\partial t^2} + \Delta p - F_r \qquad (5)$$

where $T\theta^o \simeq \Delta p a$. This is the same approach taken when considering the motion of a string under tension. If the last two terms in equation (5) are ignored we have

the dynamic equation for a cylindrical membrane under tension in a vacuum. This may be compared to the more familiar equation for a rectangular membrane

$$\frac{T_z}{\rho h}\frac{\partial^2 w}{\partial z^2} + \frac{T_y}{\rho h}\frac{\partial^2 w}{\partial y^2} = \frac{\partial^2 w}{\partial t^2}$$

which reduces to the wave equation:

$$\nabla^2 w = \frac{1}{C^2}\frac{\partial^2 w}{\partial t^2}, \quad C^2 = \frac{T}{\rho h}$$

when the tensions are equal, ie. $T_z = T_y$. The two equations differ by the term w/a^2 arising from the permanent curvature. Hence we can rewrite the cylindrical equation as

$$C_z^2 \frac{\partial^2 w}{\partial z^2} + \frac{C\theta^2}{a^2}\left(w + \frac{\partial^2 w}{\partial \theta^2}\right) = \frac{\partial^2 w}{\partial t^2} \qquad (6)$$

where $C_z^2 = \frac{T_z}{\rho h}$ and $C\theta^2 = \frac{T_\theta}{\rho h}$.

For a cylindrical shell of finite length the normal modes of radial vibration are (Warburton, 1961):

$$w = Wo \cos(n\theta)\sin\left(\frac{m\pi}{L} z\right) e^{i\omega t}$$

where n (0, 1, 2, ...) is the number of full waves circumferentially and m (1, 2, 3...) is the number of half waves longitudinally. Substituting into (6) we find

$$C_z^2 \frac{m^2\pi^2}{L^2} w + \frac{C\theta^2}{a^2}(n^2-1)w = \omega^2 w$$

or

$$f_{m,n}^2 = m^2 \frac{C_z^2}{(2L)^2} + (n^2-1) \frac{C_o^2}{(2\pi a)^2} \qquad (7)$$

since $\omega = 2\pi f$.

Thus if the geometry and prestress levels of the membrane are known the resonant frequencies, $f_{m,n}$ can be calculated. As in the case of a string or a rectangular membrane, when the tension is increased the wave propagation speed increases, thereby raising the resonant frequencies. The resonant modes or standing waves of the membrane are shown in figure 5.

For the biological cases of interest, however, we have a fluid contained within the vessel and tissue surrounding it, as in arteries or veins, or just the surrounding tissue, as in bronchi. The dynamic response of a vessel containing fluid or enclosed by it is substantially different from the results in a vacuum or in air (Warburton, 1961). Not surprisingly, this results from the additional inertial response due to the respective movement of the fluid itself. That is, any perturbation of the vessel wall is also reflected by a similar motion of the fluid or tissue.

The fluid motion is determined from the continuity equation in terms of the velocity potential (Warburton, 1961)

$$\nabla^2 \psi = \frac{1}{C^2} \frac{\partial^2 \psi}{\partial t^2} \qquad (8)$$

where C is the velocity of sound in the fluid and the velocity of the fluid motion is $V = -\nabla\Psi$. Thus, the boundary condition relating the motion of the wall to the fluid at the wall is

$$\frac{\partial w}{\partial t} = \left(\frac{\partial \Psi}{\partial r}\right) r = a_i \qquad (9)$$

Following Warburton (1961) a solution of the wave equation is

$$\Psi = F(r) \cos(n\theta) \sin\left(\frac{m\pi z}{L}\right) e^{i\omega t}$$

where $F(r) = AI_n(kr) + BK_n(kr)$

if $k^2 = \frac{m^2\pi^2}{L^2} - \frac{\omega^2}{C^2} > 0.$

For frequencies less than 1000 Hz, ω^2/C^2 is of order 10^{-3} so that we may write $k^2 \simeq \frac{m^2\pi^2}{L^2}$, for L not too large.[1]

I_n and K_n are Modified Bessel function of the first and second kind, respectively. K_n approaches infinity as $r \to 0$ and $I_n \to \infty$ as $r \to \infty$. Because the solution must be finite at r = o we find that B = 0 for the internal fluid, ie.

$$\Psi i = AI_n(kr) \cos(n\theta) \sin\left(\frac{m\pi z}{L}\right) e^{i\omega t} \qquad (10a)$$

Similarly for the external media where Ψe must be finite as $r \to \infty$,

$$\Psi e = BI_n(kr) \cos(n\theta) \sin\left(\frac{m\pi z}{L}\right) e^{i\omega t} \qquad (10b)$$

---

[1] L less than 15 cm. for 5% correction.

The constants A and B are evaluated from the boundary condition (9). Thus

$$i\omega W_o \cos(n\theta) \sin\left(\frac{m\pi z}{L}\right) e^{i\omega t}$$

$$= Ak I_n'(k a_i) \cos(n\theta) \sin\left(\frac{m\pi z}{L}\right) e^{i\omega t}$$

so that $A = \frac{i\omega W_o}{kI_n'(ka_i)} \approx \frac{i\omega W_o}{kI_n'(ka)}$

Similarly, $B = \frac{i\omega W_o}{kI_n'(ka)}$

Therefore we can write

$$\Psi_i = \frac{i\omega W_o}{k} \frac{I_n(kr)}{I_n'(ka)} \cos(n\theta) \sin\left(\frac{m\pi z}{L}\right) e^{i\omega t}$$

$$= i\omega \frac{I_n(kr)}{I_n'(ka)} w \qquad (11a)$$

and $\Psi_e = i\omega \frac{K_n(kr)}{K_n'(ka)} w \qquad (11b)$

The pressure perturbation due to the disturbance is obtained from the velocity potential by

$$p' = -\rho \frac{\partial \Psi}{\partial t}$$

thus $p_i' = \omega^2 \frac{I_n(kr)}{kI_n'(ka)} w \qquad (12a)$

and $p_e' = \omega^2 \frac{K_n(kr)}{kK_n'(ka)} w \qquad (12b)$

Evaluating the pressure perturbation at the wall the total body surface force F_r of equation 5 can now be

written as

$$F_r = \Delta P + (p_i' - p_e')$$

$$= \Delta P + \rho_f \frac{\omega^2}{k} \left[\frac{I_n(ka)}{I_n'(ka)} - \frac{K_n(ka)}{K_n'(ka)} \right] w$$

Substituting this into equation 5 we obtain

$$T_z{}^o \frac{\partial^2 w}{\partial z^2} + \frac{T_\theta{}^o}{a^2} \left(w + \frac{\partial^2 w}{\partial \theta^2}\right) = \rho h \frac{\partial^2 w}{\partial t^2} - \rho_f \frac{\omega^2}{k} \left[\frac{I_n}{I_n'} - \frac{K_n}{K_n'}\right] w$$

We can simplify the right hand side into the more informative form

$$RHS = \left(\rho h + \frac{\rho_f}{k} \left[\frac{I_n}{I_n'} - \frac{K_n}{K_n'}\right]\right) \frac{\partial^2 w}{\partial t^2} .$$

That is, the extra term provides an additional mass per unit area associated with the shell. Calling this the virtual mass (per unit area) (Clinch, 1970)

$$m_L = \frac{\rho_f}{k} \left[\frac{I_n}{I_n'} - \frac{K_n}{K_n'}\right] \qquad (13)$$

we may write the effective mass per unit area as:

$$\rho_e h = m_s + m_L \qquad (14)$$

so that the dynamic equation reduces to equation (6) but with $\rho_e h$ replacing ρh. Thus we obtain the same form as equation (7) except that

$$Cz^2 = \frac{Tz^o}{\rho_e h} \text{ and } Ce^2 = \frac{Te^o}{\rho_e h}$$

The expression (13) for the virtual mass can be simplified if we consider $ka \leq 1$ and $n > 0$. For these approximations

$$\frac{I_n}{I'_n} = \frac{ka}{n} \text{ and } R_e\left[-\frac{K_n}{K'_n}\right] = \frac{ka}{n}$$

(Warburton, 1961), so that the virtual mass becomes

$$m_L = 2\frac{\rho_f a}{n} \tag{15a}$$

Note that if either the external or internal fluid is present by itself then $m_L = \rho_f a/n$. These results show that the inertial term will be dependent upon the modal response circumferentially. Thus, the dynamic response is considerably more complex than that in a vacuum.

One other factor that has been ignored in this analysis is the coupling of the in-plane motions U and V. Following Warburton the significance of these contributions to the present analysis is one of providing an additional term to the virtual mass, ie.

$$m_L = \frac{2\frac{\rho_f a}{n}}{\left[1+\left(\frac{U_o}{W_o}\right)^2+\left(\frac{V_o}{W_o}\right)^2\right]} \tag{15b}$$

For the dominant radial motion of interest, however, the terms $\frac{U_o}{W_o}$ and $\frac{V_o}{W_o}$ are considered small except for the beam mode (n = 1) where U = 0 and V = W, such that equation (15b) becomes $m_L = \frac{\rho_f a}{n}$.

The preceding analysis with its development analogous to that of a vibrating string or membrane provides a relatively simple description of the resonant modes of vibration for a biological vessel. By assuming that the vibrations are small enough to consider the wall stress or tension as approximately constant we have achieved considerable simplicity over the equations describing a shell. The assumption of constant tension is seen to be a reasonable one in the following analysis. The perturbation tension circumferentially is given by $T_\theta' = E_\theta h(\frac{w}{a})$. Considering $E_\theta h$ as approximately 10^6 dynes/cm and using the result $\frac{w}{a} \simeq .2\times10^{-4}$ (from the present studies) then $T_\theta' \simeq 200$ dynes/cm. However, for P = 100 cm H_2O and a = 1 cm then $T_\theta^o \simeq 10^5$ dynes/cm, so that T_θ' is only 0.2% of the prestressed value and can be ignored.

(iii) Bending Energy Contribution

The first major assumption was that the wall was thin ($h/a \ll 1$) allowing us to drop the transverse shear terms from the equation of motion (equation (1)). The cut off value is generally h/a = 1/10, which is not

unreasonable for the larger arteries at physiological pressures (Bergel, 1972). However, as the modal pattern increases (m or n increase) the contribution due to bending moments becomes necessary. We may expect that the higher circumferential modes (n) have a significant contribution due to the smaller dimension circumferentially.

The bending moments are given by

$$M_z = \int_{-h/2}^{h/2} \sigma_z \, \xi(1 + \xi/R\theta) \, d\xi \qquad (16)$$

with M_θ, $M_{z\theta}$, $M_{\theta z}$ of similar form. Using the orthotropic nature of biological vessels (Patel et al., 1969; Botwin, 1973) to describe the perturbation stresses we can write the total stresses as:

$$\sigma_z = \sigma_z^o + E_z \varepsilon_z + E_{\theta\nu}\varepsilon_\theta \qquad (17a)$$

$$\sigma_\theta = \sigma_\theta^o + E_\theta \varepsilon_\theta + E_{z\nu}\varepsilon_z \qquad (17b)$$

$$\sigma_{\theta z} = E_{\theta z} \varepsilon_{\theta z} \qquad (17c)$$

where E_z, E_θ, $E_{\theta\nu}$, $E_{z\nu}$ and $E_{\theta z}$ are related to the anisotropic moduli and the strains are given by (Dym, 1974)

$$\varepsilon_z = [\frac{\partial u}{\partial z} - \xi \frac{\partial^2 w}{\partial z^2}]/[1 + \xi/R_z] \qquad (18a)$$

$$\varepsilon_\theta = [\frac{1}{a}(w + \frac{\partial v}{\partial \theta}) + \frac{\xi}{a^2}(\frac{\partial v}{\partial \theta} - \frac{\partial^2 w}{\partial \theta^2})]/[1 + \xi/R_\theta] \qquad (18b)$$

$$\varepsilon_{\theta z} = \left[\frac{\partial v}{\partial z} + \frac{\xi}{a}\left(\frac{\partial v}{\partial z} - \frac{\partial^2 w}{\partial z \partial \theta}\right)\right]/\left[1 + \frac{\xi}{R_\theta}\right]$$

$$+ \left[\frac{1}{a}\frac{\partial v}{\partial \theta} - \frac{\xi}{a}\left(\frac{\partial^2 w}{\partial \theta \partial z} - \frac{1}{a}\frac{\partial v}{\partial \theta}\right)\right]/\left[1 + \frac{\xi}{R_\theta}\right] \qquad (18c)$$

The quantities u, v are the in plane longitudinal and tangential motions described previously. Substituting the strains into equations (17) the bending moments can be evaluated.

$$\text{Thus } M_z = \frac{h^3}{12a^3}\left[\sigma_z{}^o a^2 + E_z a^2\left(\frac{\partial v}{\partial z} - a\frac{\partial^2 w}{\partial z^2}\right) + E_{\theta\nu} a\left(\frac{\partial v}{\partial \theta} - \frac{\partial^2 w}{\partial \theta^2}\right)\right] \qquad (19a)$$

$$M_\theta = -\frac{h^3}{12a^3}\left[(\sigma_\theta{}^o + E_{z\nu})a^3\frac{\partial^2 w}{\partial z^2} + E_\theta a\left(w + \frac{\partial^2 w}{\partial \theta^2}\right)\right] \qquad (19b)$$

$$M_{\theta z} = M_{z\theta} = E_{\theta z}\frac{h^3}{12a}\left[\frac{\partial v}{\partial z} - 2\frac{\partial^2 w}{\partial \theta \partial z}\right] \qquad (19c)$$

The transverse shear terms in equation (1) can be simplified to

$$\frac{1}{R}\frac{\partial(Q_z R)}{\partial z} + \frac{1}{R}\frac{\partial Q_\theta}{\partial \theta} = \frac{\partial^2 M_z}{\partial z^2} + 2\frac{\partial^2 M_{\theta z}}{\partial \theta \partial z} + \frac{1}{a^2}\frac{\partial^2 M_\theta}{\partial \theta^2}$$

$$= BT \qquad (20)$$

where higher order terms in w (ie. w^2) are ignored. This requires that w is small. Substituting the bending moments into (20) we find:

FIGURE 6

Operation of the photonic sensor.

A) Voltage output versus distance between the probe and reflecting surface, showing the two linear regions A and C.

B) Illustration of the principle involved. As the reflecting surface moves further away from the probe more surrounding fibers transmit until some light 'spills out' and is lost.

where $U^1 = \frac{U_o}{W_o}$, $V^1 = \frac{V_o}{W_o}$. We can rewrite this as

$$BT = -w[(n^2-1)n^2 \frac{\gamma A_1}{a^2} + (\frac{m\pi}{L})^2 \gamma A_2] \qquad (24)$$

where $A_1 = E_\theta a$ and $A_2 = n^2 E_1 a + nE_2 a^3 V^1$

$$+ E_z a^2((\frac{m\pi}{L})^2 + (\frac{m\pi}{L})V^1).$$

Thus the bending terms above provide a correction to the expression for resonant frequency (7) such that we can write modified forms of C_z^2 and C_θ^2 as

$$C_\theta^2 = \frac{T_\theta^o + n^2\gamma A_1}{\rho_e h} \qquad (25a)$$

and

$$C_z^2 = \frac{T_z^o + \gamma A_2}{\rho_e h} \qquad (25b)$$

When h/a is small as in the veins or pulmonary artery (approximately 0.02 as reported by Bergel (1972)) the value of γ is negligible and the additional terms in (25) due to bending can be ignored. With vessels such as the aorta, however, the value of h/a is approximately 0.1 giving a value of $\gamma \simeq 10^{-4}$ so that the bending terms may not be ignored, particularly for the higher circumferential modes n.

The complete expression for the resonant frequencies

of a cylindrical vessel is therefore

$$f^2_{m,n} = \frac{m^2}{\rho_e h} \frac{T_z^{\circ}+\gamma A_2}{(2L)^2} + \frac{n^2-1}{\rho_e h} \frac{T_\theta^{\circ}+n^2\gamma A_1}{(2\pi a)^2} \quad * \quad (26)$$

Experimentally we can evaluate this model by changing the prestress values T_θ° and T_z° and observing the change in the different resonant modes shapes (m, n). Similarly the radius, a, or the length, L, can be changed and the corresponding changes in frequency noted.

IV EXPERIMENTAL ANALYSIS

(i) Introduction

An experimental evaluation of the model was obtained by measuring the radial vibrations of cylindrical segments of both synthetic tubing and arteries. The wall vibrations were obtained from an optical displacement sensor and the spectral content of this signal was obtained from standard electronic filters that are used extensively in the field of acoustics. Thus, by varying the values of wall stress or tension (changing the length or pressure) the predicted changes in the resonant modes could be compared with those obtained from the wall displacement spectra. This was augmented by spatial information on phase and amplitude (obtained by movement of the probe) providing evidence of the mode shape, m,n.

The significance of the surrounding or enclosed acoustic media (as predicted by the model) was examined by performing tests on the synthetic tubing in air, enclosed by fluid with air internally, and then with fluid internally and externally. This provided a continuity for the tests performed on arteries which were exposed to the latter conditions. In all these tests a disturbed or turbulent flow created by a stenosis was the stimulating force acting on the vessel. However, during the first two tests on synthetic tubing with air internally, the samples were stimulated acoustically with a loudspeaker for comparison.

(ii) Technique:Displacement Sensor

The radial wall displacement was obtained by using a commercially available non-contacting, fibre-optic, displacement sensor, which permitted vibrations less than one micro-inch to be measured. The 'photonic sensor' (Model KD-45A) (Mechanical Technology Inc.) consists of a randomly arranged bundle of optical fibers, half of which transmit light from a source of constant but adjustable intensity and the other half transmitting any reflected (plus background) light to a photo sensitive diode, which produces a voltage proportional to the intensity of light received. Therefore if the relative distance between the probe head and reflecting surface changes a corresponding change in the output voltage from the diode is observed. Figure 6A shows this change in voltage with distance.

This distribution, with the two linear regions, A and C, can be qualitatively described as follows. When the probe head is in contact with a flat surface there will be no light received at the diode. As the surface is moved away, however, an increasing amount of reflected light is received by adjacent fibers (see figure 6B), reaching a maximum when all the surrounding fibers transmitting to the diode are receiving light. As the distance is increased further some of the reflected light 'spills out' past the active head and is lost. The

FIGURE 6

Operation of the photonic sensor.

A) Voltage output versus distance between the probe and reflecting surface, showing the two linear regions A and C.

B) Illustration of the principle involved. As the reflecting surface moves further away from the probe more surrounding fibers transmit until some light 'spills out' and is lost.

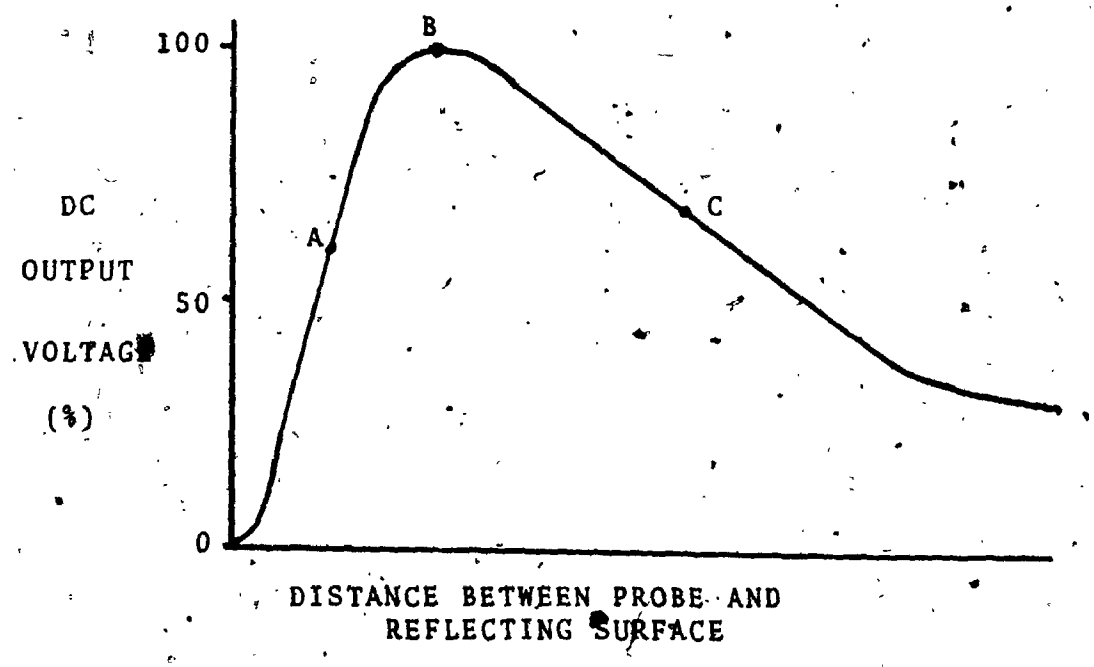
100
50
0
DC
OUTPUT
VOLTAGE
(%)
A
B
C
DISTANCE BETWEEN PROBE AND
REFLECTING SURFACE

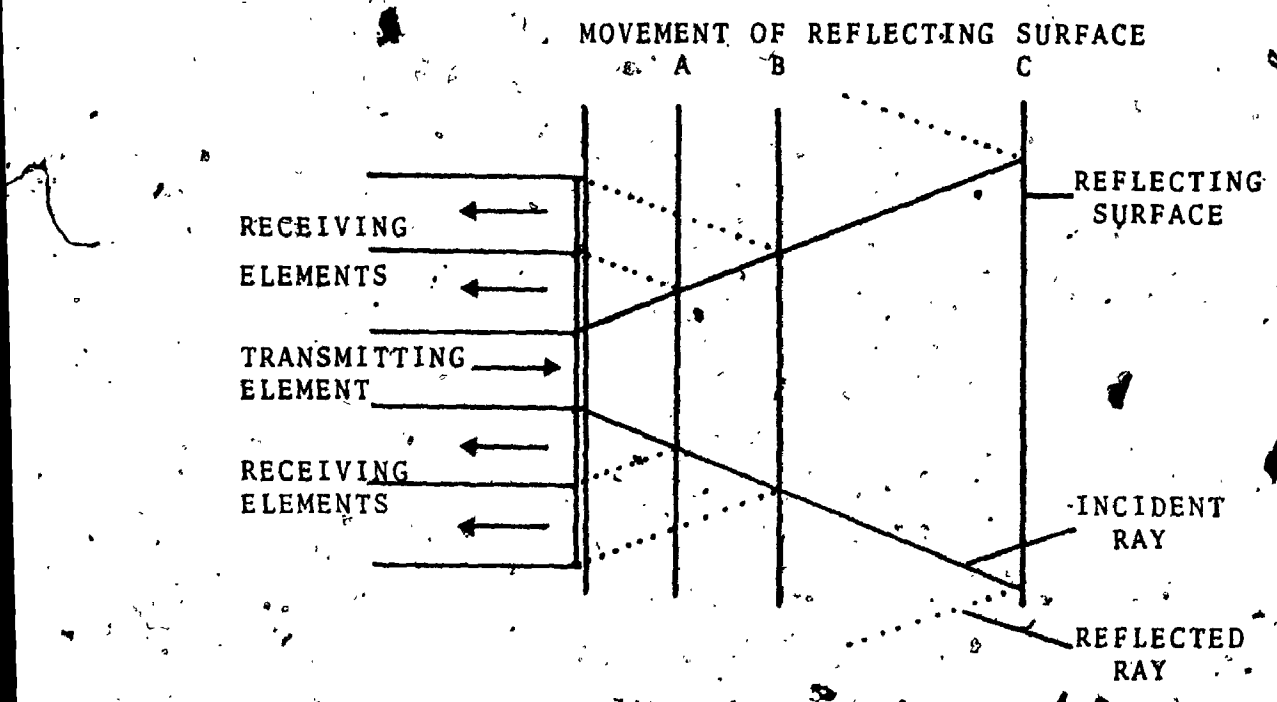
MOVEMENT OF REFLECTING SURFACE
A
B
C
RECEIVING
ELEMENTS
TRANSMITTING
ELEMENT
RECEIVING
ELEMENTS
REFLECTING
SURFACE
INCIDENT
RAY
REFLECTED
RAY

intensity therefore decreases, following the distribution shown in 6A. Thus, by centering the probe at either position A or C, vibrations of the surface can be measured with a frequency response limited by the diode itself (DC to 100 kHz).

The calibration levels from a cylindrial section of penrose tubing, 6.4 mm in diameter, are shown in figure 7, demonstrating the same form of distribution as that for a flat surface. The expected difference is that a position of zero voltage does not occur due to the curvature of the vessel wall. To allow for any changes in calibration due to surface geometry or reflectivity, however, each sample that was studied had calibration measurements performed before each test. These were obtained by placing the sensor in a micro manipulator (with a resolution of 1/400 mm), positioning the probe to the region of interest (generally point A), and recording the voltage change upon moving the probe about the mean position.

Since the biological tissue and penrose tubing used in the experimental analysis was partially transparent, an extremely fine aluminum spot was generally sprayed on the surface to increase the reflectivity. Tests conducted with and without the small spot in air revealed no difference in response, when the different sensitivities were accounted for. This technique was

FIGURE 7

Calibration curve for the photonic sensor on penrose tubing (smaller sample, radius 0.32 cm) with fluid internally and externally. Note the change in scale on the abscissa to allow for the more sensitive front portion of the curve. Maximum DC output voltage was 2 volts and the probe was usually positioned to the linear operating range at 60% on the front part of the curve. The displacements at 40, 50, 60, 70 and 80% were then recorded for calibration before each test.

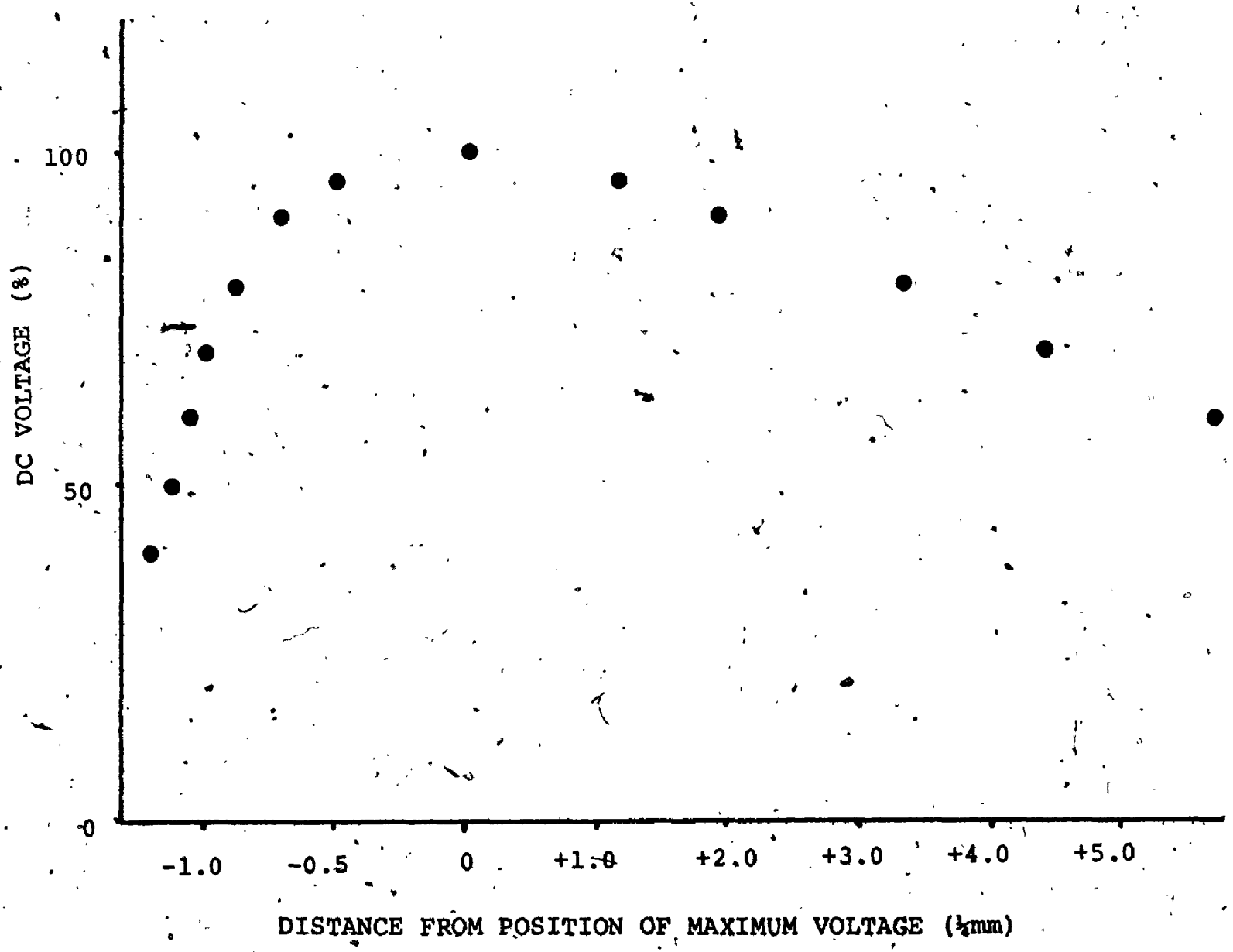
100
50
0
DC VOLTAGE (%)
-1.0
-0.5
0
+1.0
+2.0
+3.0
+4.0
+5.0
DISTANCE FROM POSITION OF MAXIMUM VOLTAGE (½mm)

found necessary to raise the very small signals of the higher order modal patterns above the inherent noise levels of the instrumentation.

Signal Conditioning

The signal voltage from the photonic sensor was conditioned in several ways, as shown in figure 8. The signal could be passed directly to a frequency analyzer, for information on the frequency content of the signal. Two different sets of electronic filters were used in the following studies. The first system consists of a Bruel & Kjaer (B & K) 2107 Frequency Analyzer synchronized with a B & K Level Recorder. In this system the paper of the recorder is pre-calibrated such that a spectral analysis of the input signal is obtained, similar to that shown in figure 4. The relatively poor resolution of this constant percentage bandwidth analyzer at the higher frequencies was circumvented in the later stages of this study when a Hewlett Packard 3580A Narrow Bandwidth Analyzer became available. This latter system allowed a constant bandwidth analysis as small as 1Hz. When coupled with an xy recorder the output could be recorded permanently.

In the final stages of the research program, a second photonic sensor became available that permitted the simultaneous analysis of two signals from different positions on the vessel, longitudinally and circumferentially. For these trials a Model 820A Random Signal

FIGURE 8

Signal conditioning procedure.

SIGNAL CONDITIONING

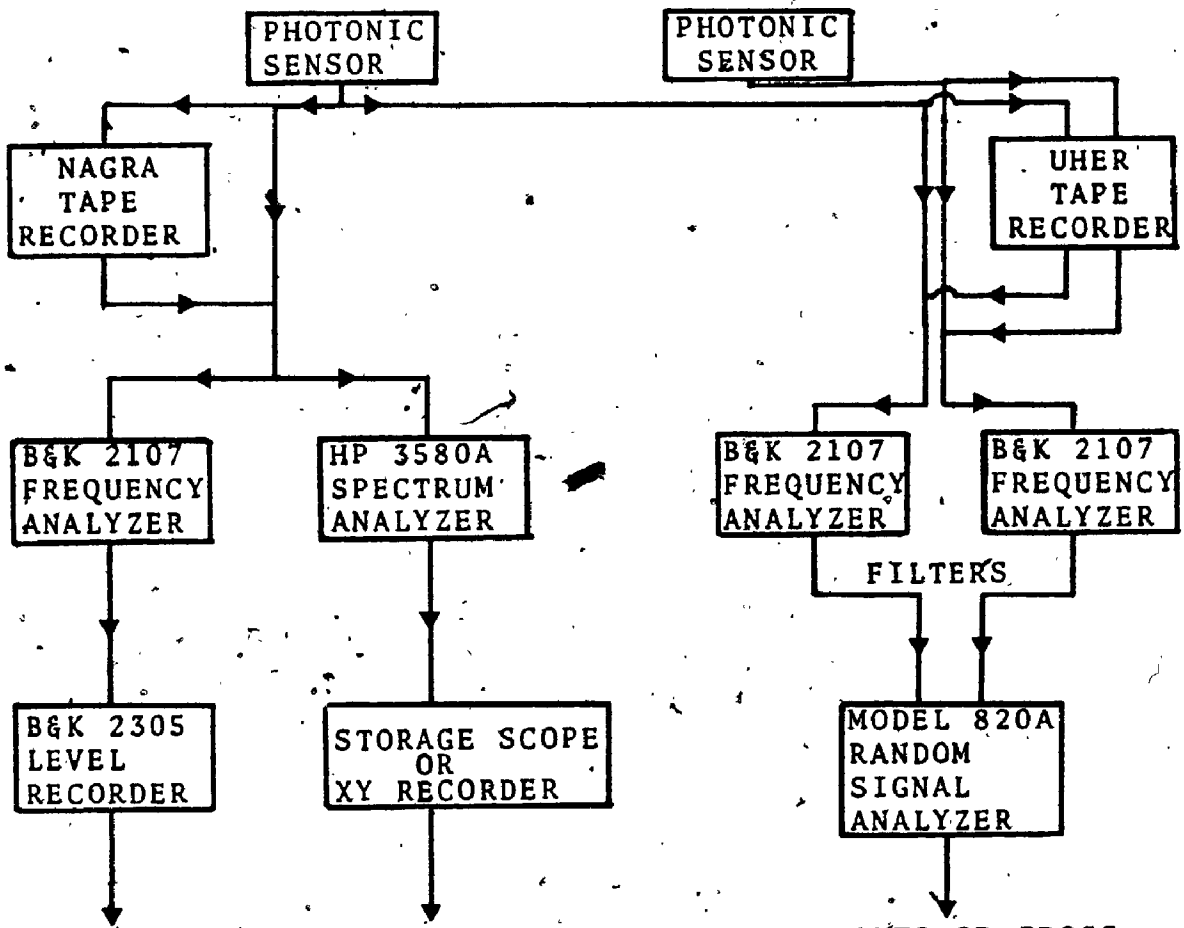

SPECTRUM ANALYSIS

CORRELATION

Analyzer (Physical Data Inc.) was used to perform auto and cross-correlograms, providing further evidence of the resonant response of the vessels.

Tape Recordings

Instead of sending the signal directly to the conditioning facilities, it could be stored on tape for future analysis. There were two reasons for this procedure. First, it permitted tape loops to be constructed and played back so that considerable smoothing of the spectrum was permitted. Secondly, when biological samples were used, it was desirable to perform the tests as quickly as possible before any degradation could occur. There were many tests performed on one sample, so that direct recording involving almost one half hour per test would run into more than 8 hours analysis.

For most of the tests when only one sensor was available a high quality, single channel, Nagra IVL tape recorder was used. The gain of the recorder was adjusted to zero and the signal from the photonic sensor passed through the amplifying circuit of the B&K 2107 Frequency Analyzer (filtering mode off). The known gain of this amplifying circuit was then adjusted to obtain a suitable recording level from which a one minute record was obtained. At a convenient time after the experimental test a short tape loop of 7 to 8 seconds was constructed from the middle of the one minute record and the wall displacement spectra obtained as done

previously. When the second sensor became available a two channel Uher 4000 Report L recorder was used, permitting simultaneous recording of the two signals.

The dynamic range and calibration levels of all the equipment used is contained in Appendix I. The weakest link in this chain of analysis is with the tape recorders, particularly the Uher, where the low frequency information is lost. As it turns out, however, the resonant modes of interest occur within the linear operating range of the equipment.

Measurement of Geometry

The length and outside diameter of the cylindrical segments under study were measured with calipers. This was sufficiently accurate for the length but introduced the possibility of an error in the smaller diameter measurement, perhaps by squeezing the sides too far. Since the diameter became narrower when either the length increased or the pressure decreased, it had to be measured under each condition. The resting wall thickness was measured with a travelling microscope from a thin slice cut from the end of the sample studied. Then using incompressibility ($h = h_o \frac{Ro\ Lo}{R\ L}$) the wall thickness could be estimated at the prestressed values of interest. Using this value of wall thickness the mid surface radius, a, could be calculated from the external diameter measurements.

With these measurements of geometry the prestressed values of circumferential ($T\theta^o$) and longitudinal (Tz^o) tension could be calculated. The circumferential tension was calculated from $T\theta^o = Pa$, where the pressure was measured from a water manometer under the various tests. The longitudinal tension, $Tz^o = E_z h \varepsilon_z + \nu T_\theta^o$ was calculated from a knowledge of the strain, $\varepsilon z = \frac{\Delta L}{Lo}$, and the modulus of elasticity, longitudinally, Ez. This latter value was obtained from a simple force-extension test done on a sample of the synthetic material, giving a linear value of $E_z = 1.55 \times 10$ dynes/cm^2 over the region 0 to 25% extension. Since the longitudinal modulus of elasticity for arteries is non-linear and because it also varies with pressure, no longitudinal extension tests were done on arteries. Thus the longitudinal prestress was not calculated for the arteries studied.

(iii) Vibration in Air

Our starting point in testing the validity of the model presented in chapter III is to consider the dynamics in air. This removes the more complex situation with the inertial dependence on the mode of vibration. Another factor favouring this simplication is that it becomes much easier to stimulate the vessel (acoustically), in air. Finally, it should permit an evaluation of the technique to measure the wall vibrations.

Method

Cylindrical segments of penrose tubing of radius 0.42 cm and of various relaxed lengths, L, ($L/a > 15$) were attached to rigid cylindrical sections (similar dimensions) of plastic or stainless steel (see figure 9). Penrose tubing was used because its properties would not degenerate throughout the test and because it was thin walled ($h/a = 0.1$) with an elastic modulus (although isotropic) similar to arteries at physiological pressures (approximately 10^7 dynes/cm^2).

The sample was pressurized and its length stretched producing the prestressed levels, T_θ^o and T_z^o. By changing the pressure or length the prestressed levels could be varied and its effect compared to the predicted changes for a particular mode of vibration.

As shown in figure 9 the photonic sensor could be used to scan longitudinally so that determination of the longitudinal mode (m) was possible. This was done by plotting the amplitude at each resonance versus longitudinal position.

Acoustical Stimulation

The dynamic response was evaluated initially by accoustically stimulating the vessel under various prestressed levels, both internally and externally. During external stimulation a plastic bifurcation was attached to a cone from a loudspeaker (see figure 10A) such that one branch led to the point of stimulation and the other

FIGURE 9

Experimental arrangement for measuring wall displacement. As shown, the probe could be moved to different longitudinal positions, thereby providing information on the longitudinal mode shape, m.

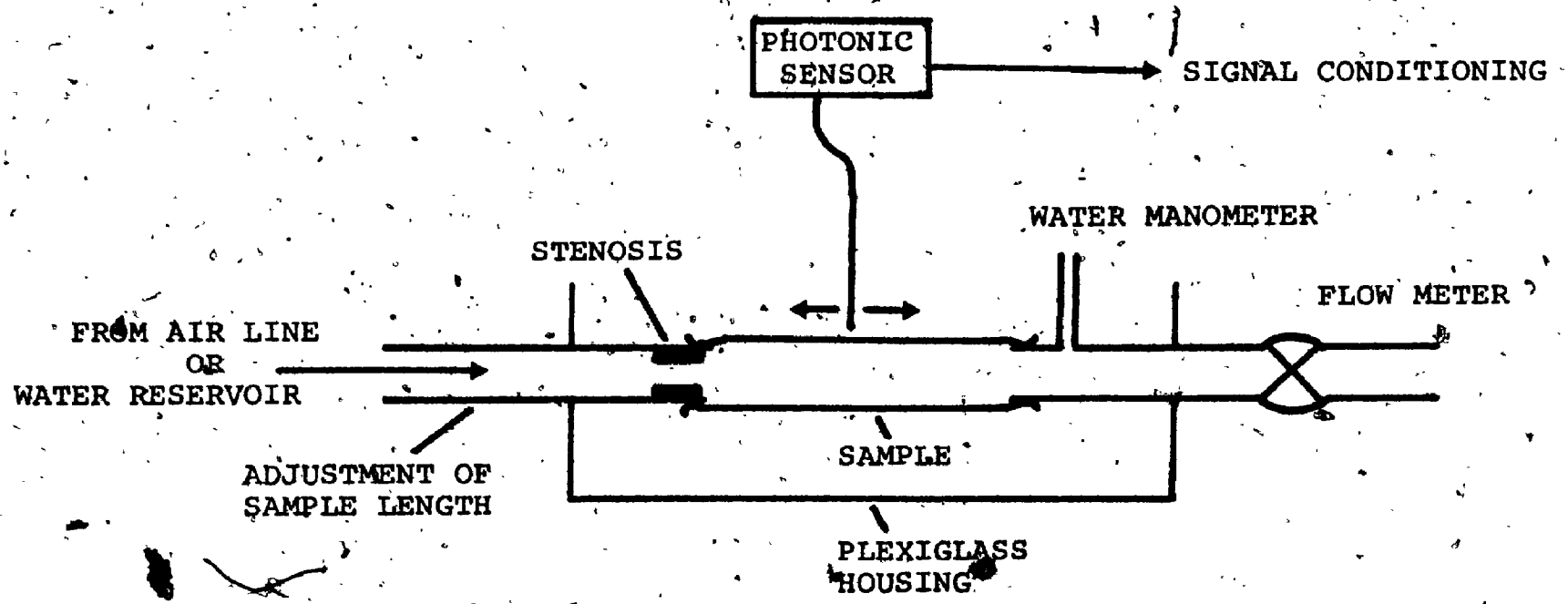
PHOTONIC SENSOR
SIGNAL CONDITIONING
WATER MANOMETER
STENOSIS
FLOW METER
FROM AIR LINE OR WATER RESERVOIR
SAMPLE
ADJUSTMENT OF SAMPLE LENGTH
PLEXIGLASS HOUSING

FIGURE 10

Methód of acoustical stimulation:

A) Externally B) Internally

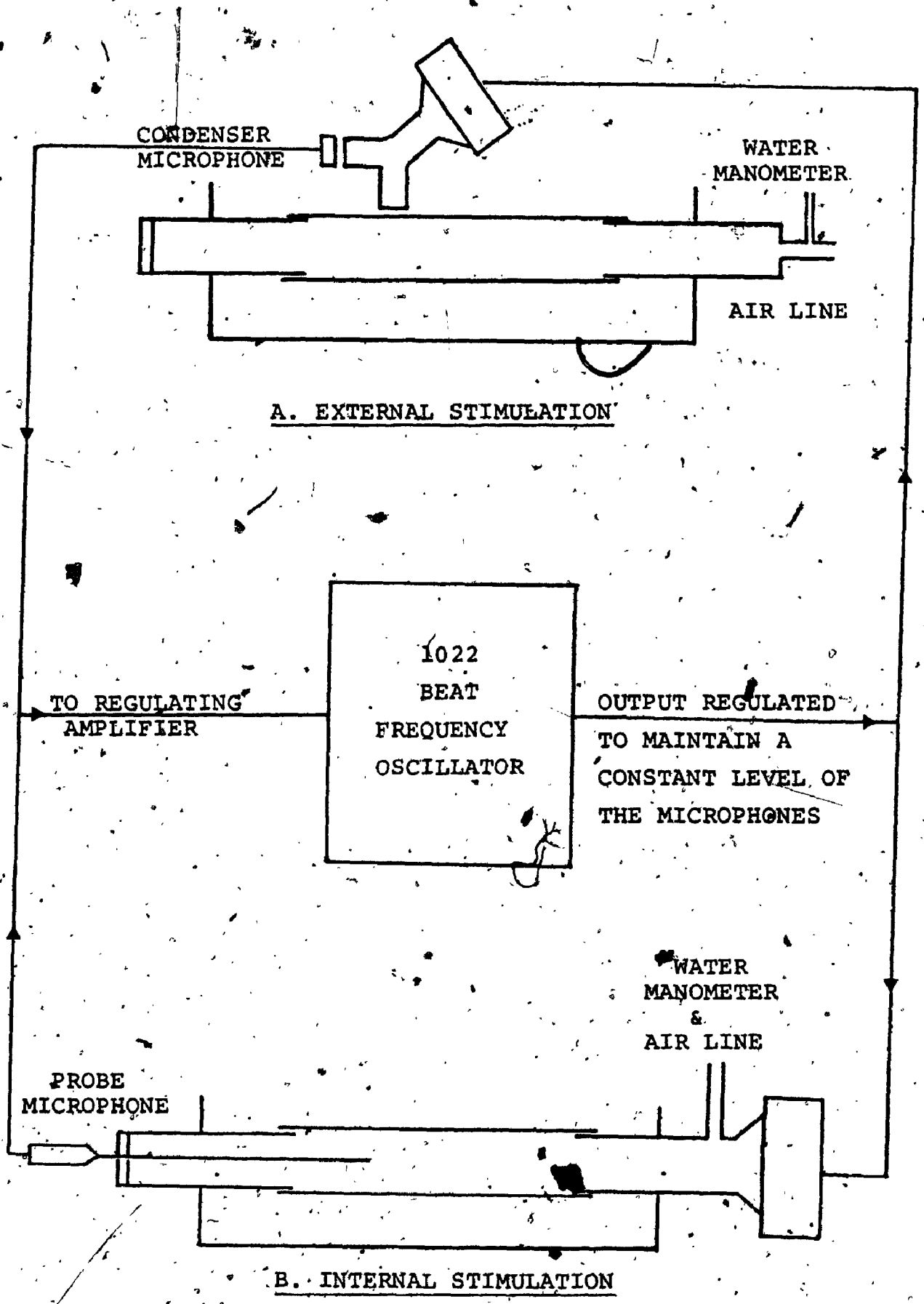
CONDENSER MICROPHONE
WATER MANOMETER
AIR LINE
A. EXTERNAL STIMULATION
1022 BEAT FREQUENCY OSCILLATOR
TO REGULATING AMPLIFIER
OUTPUT REGULATED TO MAINTAIN A CONSTANT LEVEL OF THE MICROPHONES
WATER MANOMETER & AIR LINE
PROBE MICROPHONE
B. INTERNAL STIMULATION

to a ½" condenser microphone. The condensor microphone acted as a control transducer, maintaining a constant sound pressure level by feedback to the compressor circuit of a Beat Frequency Oscillator B.F.O, (B & K model, 1022) that was driving the loudspeaker. When the B.F.O. was synchronized (mechanically linked) to a B & K Level Recorder (model 2305) the output from the photonic sensor was passed directly to the recorder with its frequency pre-calibrated paper. With the level recorder driving the B.F.O., the system was scanned through the frequency range of interest (20HZ to 2,000 HZ) and the dynamic response of the vessel determined.

The procedure was indentical for internal stimulation except that the speaker was accoustically connected to one end internally and a probe microphone (acting as control), (Muirhead H-112) located in the lumen of the vessel (see figure 10B). The probe microphone was positioned approximately midway along the tube centerline and the end plugged with plasticine to permit pressurization.

Disturbed Flow

A series of tests were then performed to determine the vibrational response when disturbed flow was present in the lumen. Disturbed flow was created by inserting a plug (33% stenosis) at one end and allowing air to flow through. The flow was kept constant during a particular

test and monitored using a Fisher Flow meter. Apart from the tests done at different prestress levels the flow rate was also varied (from 420 to 2500 cc/min or Reynolds numbers of 125 to 740) to see what effect this had.

The signal from the photonic sensor was passed to a B & K 2107 Frequency Analyzer coupled to a Level Recorder which permitted automatic recording of the spectra on frequency calibrated paper. The spectrograms were obtained at maximum selectivity (6% bandwidth) during each test to permit the maximum resolution of the dynamic response.

Results

Acoustic Stimulation

Examples of the response to internal and external acoustical stimulation are shown in figure 11. Both results appear to show several resonant peaks with many close together. The major peak around 400Hz in figure 11B, for example, appears to consist of more than one. Although the degree of prestress is not exactly the same in the two cases, the major resonant frequencies are considerably different.

The reason for the difference quickly became apparent when the pressure and longitudinal tension were varied. For the case of external stimulation the major resonance at 65Hz was found to be insensitive to pressure changes but responded to changes in the longitudinal tension. Conversely the resonance at

FIGURE 11

Response to acoustical stimulation.

A) Externally at 75 dB sound pressure level (top display) with sample at 5cm H_2O pressure and length = 9.7 cm (strain = 3%).

B) Internally at 80 dB (bottom display) with sample at 30cm H_2O pressure and length = 10.0cm (strain=2%).

Probes were located at approximately ¼ the sample length.

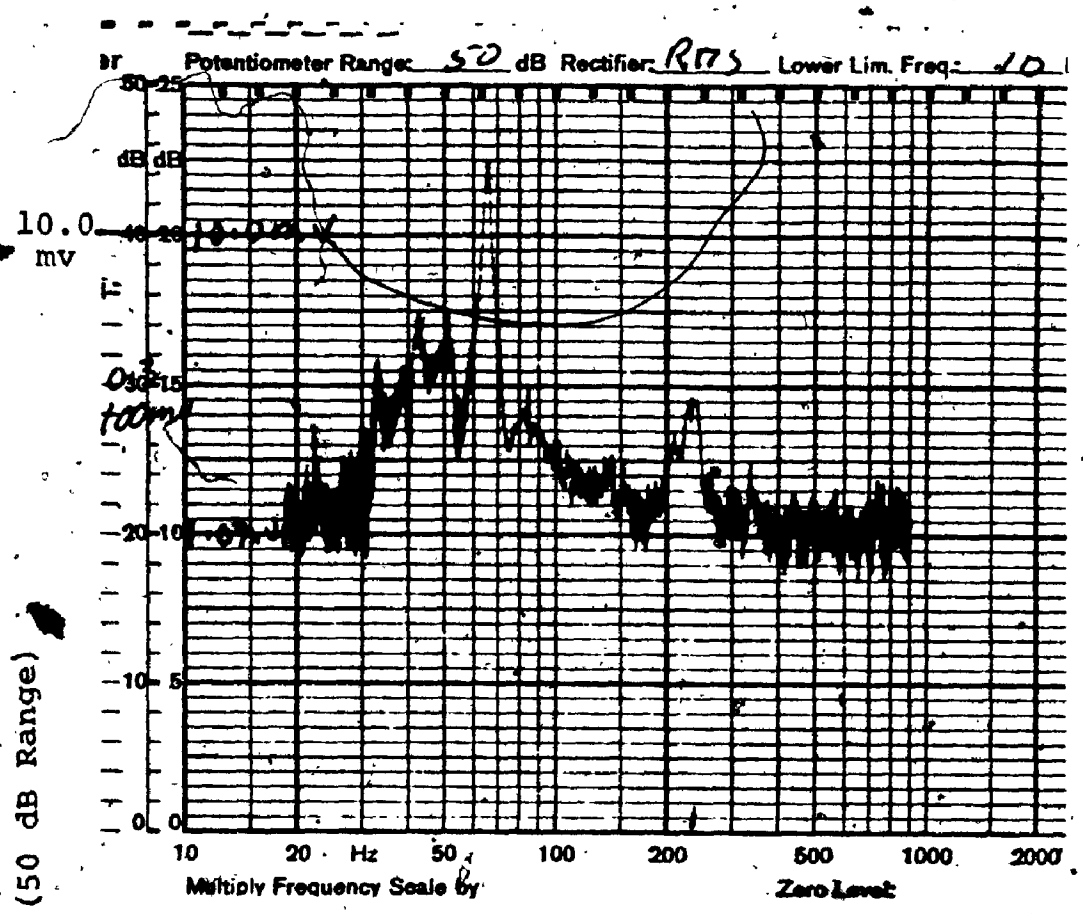
Potentiometer Range: 50 dB Rectifier: RMS Lower Lim. Freq: 10
10.0 mv
10 20 Hz 50 100 200 500 1000 2000
Multiply Frequency Scale by
Zero Level

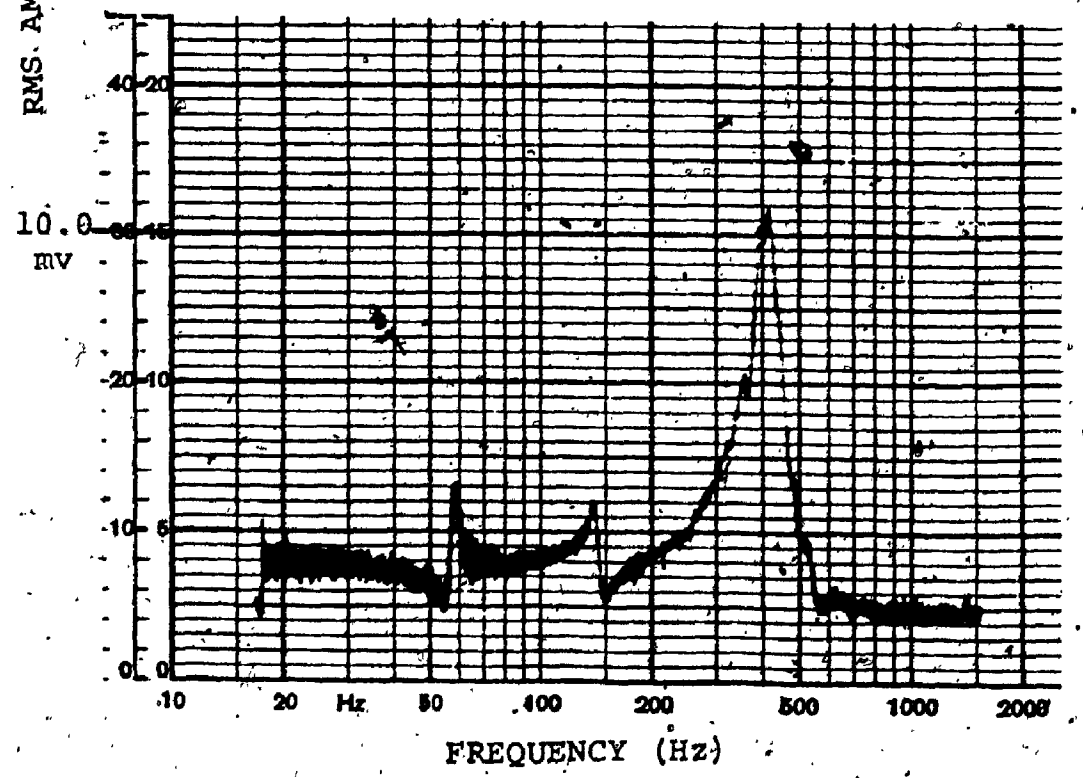
RMS AMPLITUDE (50 dB Range)
10.0 mv
10 20 Hz 50 100 200 500 1000 2000
FREQUENCY (Hz)

400 Hz in 11B was very sensitive to pressure changes and changed only slightly to longitudinal tension. The smaller peak at 60 Hz, however, behaved in the same way as the major peak in 11A. Similarly the smaller peak at 230 Hz in 11A changed in a similar manner to the major resonance in 11B. It was becoming clear that the resonant modes were the same but that the method of stimulation favoured certain modes. Not surprisingly, the dominant mode in external stimulation was the beam mode, with n = 1, m = 1.

This result was justified by setting the frequency of the B.F.O. to the resonance frequency 68Hz and scanning the vessel longitudinally. The result is displayed in figure 12A, clearly showing m = 1. To scan the vessel circumferentially, the sample was rearranged to a vertical position so that the sensor could be moved circumferentially. The result is shown in figure 12c, giving n = 1, which was expected from the insensitivity to pressure ($n^2 - 1 = 0$). The same circumferential results for stimulation at 160Hz were observed and figure 12B shows the results of a longitudinal scan, suggesting m = 2, n = 1. The fact that this mode was barely observable in figure 11A is due to the probe being positioned midway, which would be a node for m = 2.

One of the problems of this technique is that a 'slave' filter was not available for simultaneous filtering of the signal at the frequency of stimulation,

FIGURE 12

Effect of moving the probe position axially and circumferentially while the sample was stimulated externally at one of the resonant modes.

A) Axial variation with stimulation at 68 Hz suggesting m=1.

B) Axial variation with stimulation at 160 Hz suggesting m=2.

C) Circumferential variation with stimulation at 68 Hz suggesting n=1. Same result was observed for 160 Hz stimulation.

2 4

OF/DE

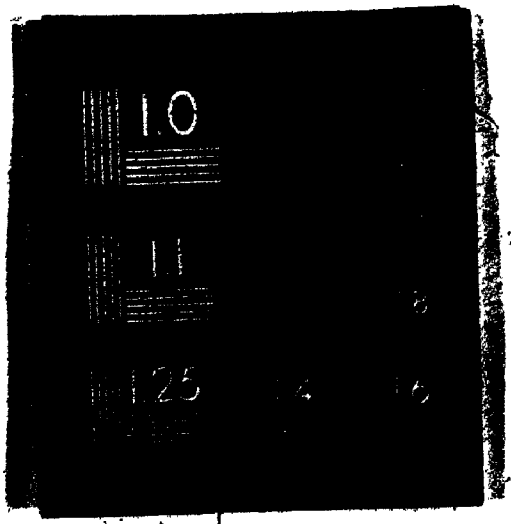

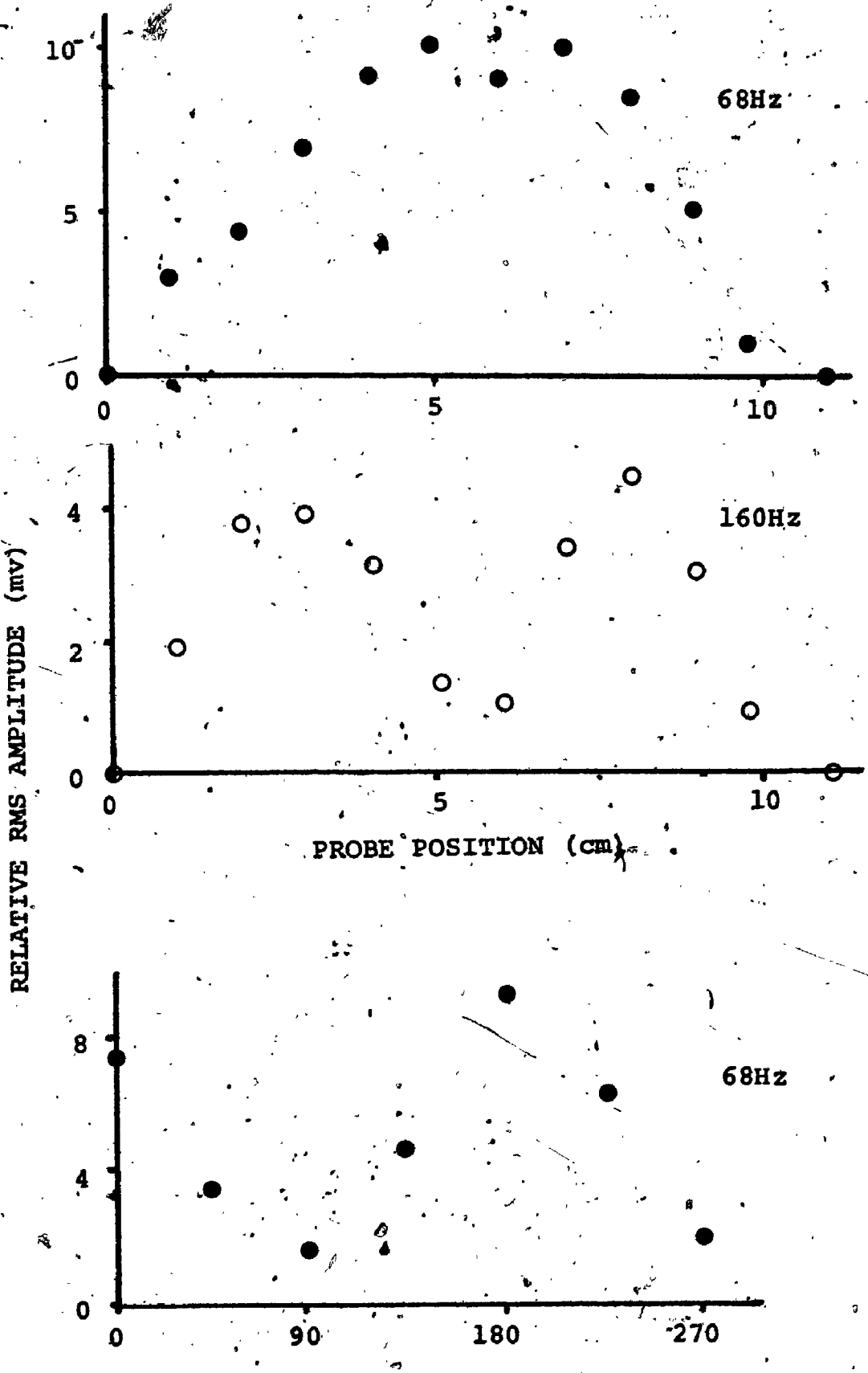
68Hz
160Hz
68Hz
RELATIVE RMS AMPLITUDE (mv)
PROBE POSITION (cm)
ANGLE BETWEEN SPEAKER
AND PROBE (DEGREES)
0
5
10
2
4
8
90
180
270

resulting in some artifacts due to distortion in the speaker. Particularly during external stimulation, amplitude peaks were observed at 1/2 and 1/3 the dominant resonance but when the signal was analyzed at these frequencies the vibration was at that of the dominant resonance. For example, in figure 11A, the smaller peaks at ½ (33) and 1/3 (22) the major peak at 65Hz were not resonances but vibration at 65 Hz.

This artifact was observed with the probe microphone at the lower frequencies and became more distorted when smaller plastic bifurcations were used. For example, maintaining the same sound pressure level (85dB) and using three bifurcations with diameters approximately 2, 1, and ½x the diameter of the penrose tubing the artifact at ½ the dominant frequency was 23dB, 15dB and 9dB down from the major resonance, respectively.

As a result of this distortion and the domination of the beam mode it was felt that internal stimulation would provide a more natural response. Accordingly, this method was used extensively to study the resonant modes under various prestress conditions. It is also obvious from figure 11 that the frequency scale must be expanded to obtain proper resolution of the resonant frequencies. As well as expanding the frequencies scale by a factor of 10 the system was scanned slowly and stopped at a resonance peak. The signal was then filtered to see if it corresponded to the stimulation frequency and then recorded on the chart.

Figure 13 illustrates some of these results under different values of prestress with the expanded scale permitting a separation of the individual modes that were obscure in figure 11B. As mentioned previously, these modes are extremely sensitive to pressure and less so to changes in longitudinal tension. The fact that the frequency increases with pressure rather than decreases suggests from equation 7 that they may correspond to the circumferential mode n = 2. Furthermore the separation between the three modes appears to increase with increased longitudinal tension, suggesting that they correspond to different longitudinal modes, m.

These modes were found to correspond to m = 1,2, 3 by noting the respective phase of motion during a longitudinal scan. An indication of the relative phase was obtained by taking the signal from the oscillator and using it to drive the horizontal sweep on an oscilloscope. By moving the sensor longitudinally abrupt reversals in phase (180^{o}) were observed as a nodal line was passed (as well as the corresponding decrease in amplitude).

Sufficient information was now available to evaluate the expression for resonant frequency

$$f_{m,n}^2 = m^2 \frac{C_s^2}{(2L)^2} + (n^2-1)\, C_\theta^2/(2\pi a)^2$$

where $C_z^2 = (T_z^o + \gamma A_2)/\rho h$ and $C_\theta^2 = (T_\theta^o + n^2 \gamma A_1)/\rho h$

FIGURE 13

Effect of pressure (circumferential tension) and longitudinal strain (tension) on the dominant resonant peaks occurring under acoustical stimulation, internally, at 85 dB in air.

A. Effect of Pressure

B. Effect of Length

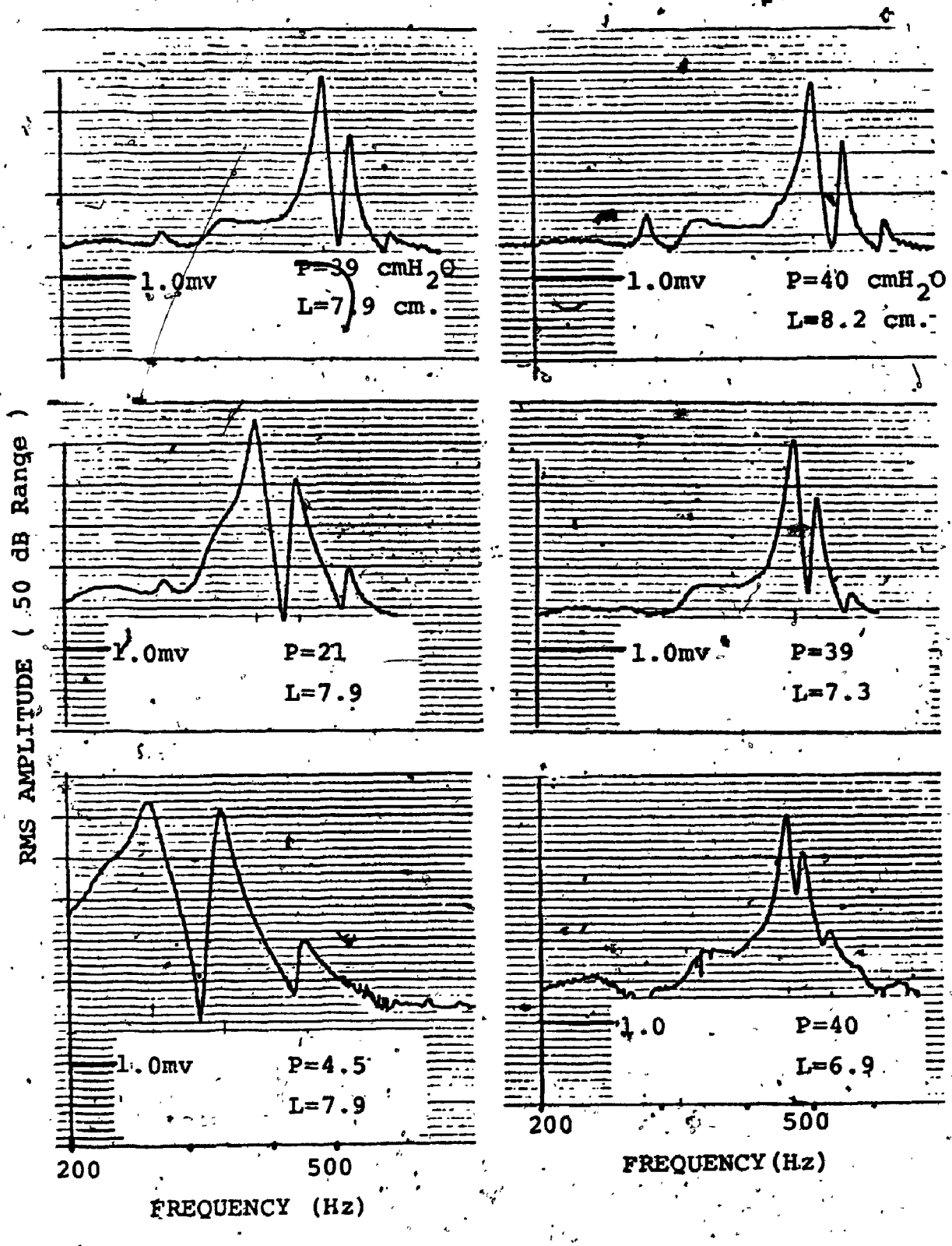

By plotting f^2 versus circumferential tension T_θ^o or $T_c' = T_\theta^o/(2\pi a)^2$ then from the slope = $(n^2-1)/\rho h$ we would be able to evaluate whether n=2 is correct. This result is shown in figure 14 for each of the three modes observed. As expected the slopes are linear and the same but with different intercepts which is expected from intercept = $m^2C_z^2/(2L)^2 + \frac{(n^2-1)}{\rho h} \cdot \frac{n^2\gamma A_1}{(2\pi a)^2}$ where increasing m results in a greater intercept.

The slope from figure 14 was found to be 71.5 so that $(n^2-1)/\rho h = 71.5$. Substituting the calculated values for $\rho h = 0.039$ we find $n^2 = 3.8$ which is very close to n=2.

Since all the quantities in the intercept above are constant except for m the difference between intercepts 1-2 and 2-3 should be in the ratio 3:5 or 1.67. This agrees very well with the observed difference of 3.2:5.5 or 1.71 giving a value of $C_z^2/(2L)^2 = 1.1 \times 10^4$. This same result can be obtained by plotting f^2 versus m^2, as shown in figure 15A for different longitudinal tensions. The slopes give the quantity $C_z^2/(2L)^2$ and the intercepts $(n^2-1)C_\theta^2/(2\pi a)^2$. The intercepts change with increasing length because of a thinning of the wall and a narrowing. This result was obvious from plots of f^2 versus T_c' at different lengths where the slopes are inversely related to thickness $(3/\rho h)$. The assumption of incompressibility $(h = h_o \frac{R_o L_o}{R.L})$ provided excellent agreement with the thickness calculated from the slopes.

FIGURE 14

A plot of f^2 versus the circumferential term T_c' with the length constant for the three resonant peaks observed in figure 13.

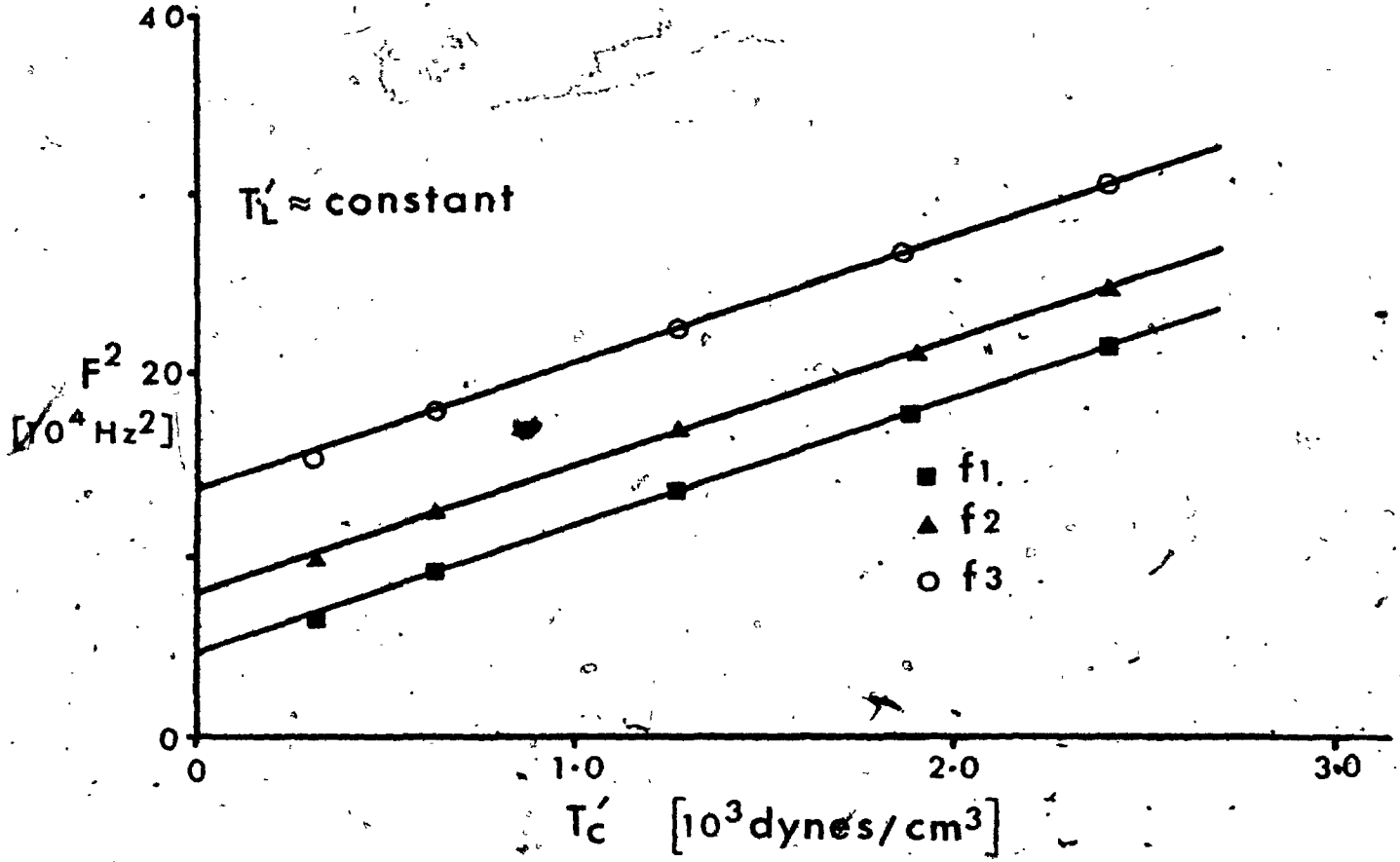
40
20
0
$T_L' \approx$ constant
F^2
$[10^4 Hz^2]$
f1
f2
f3
0
1·0
2·0
3·0
T_C' $[10^3 dynes/cm^3]$

FIGURE 15

A) A plot of f^2 versus m^2 for the three resonant peaks in figure 13 at different longitudinal strains. The three resonant peaks have been assumed to be m=1, 2, and 3.

B) A plot of C_z^2 versus the longitudinal strain for the beam mode (n=1) stimulated externally, and for the values obtained from the slopes in part A above.

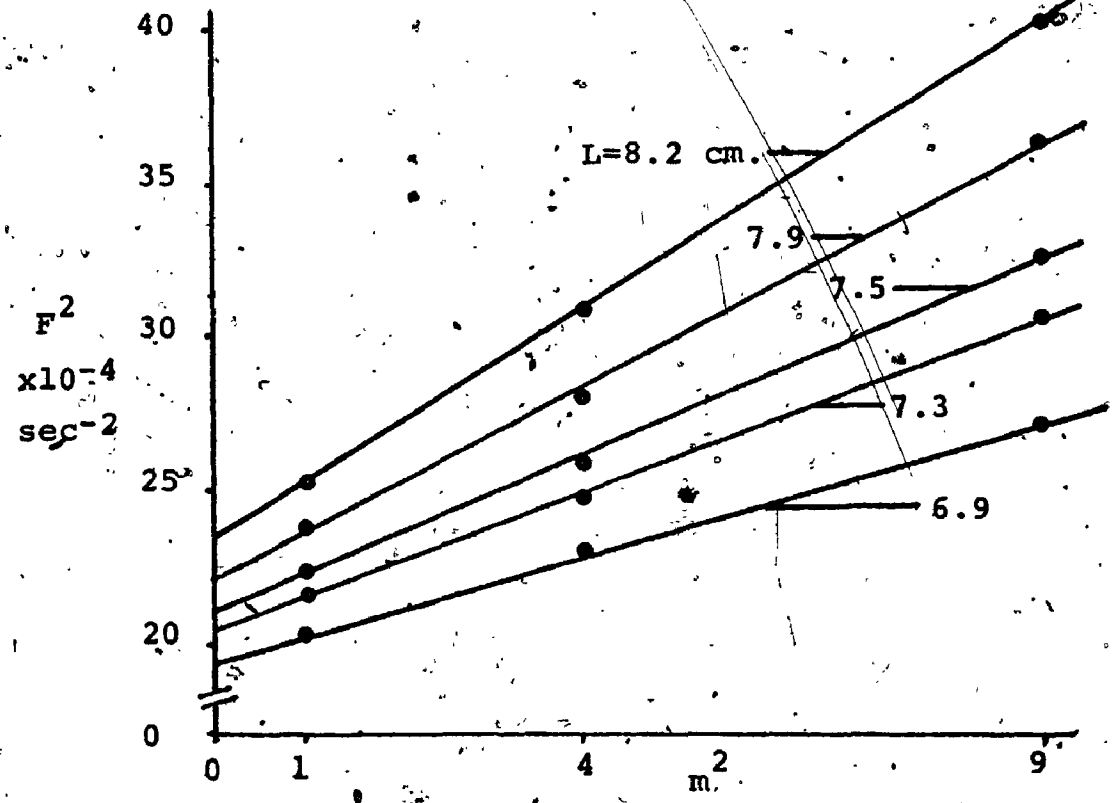
40
35
30
25
20
0
F^2
$x10^{-4}$
sec^{-2}
L=8.2 cm.
7.9
7.5
7.3
6.9
0
1
4
9
m^2

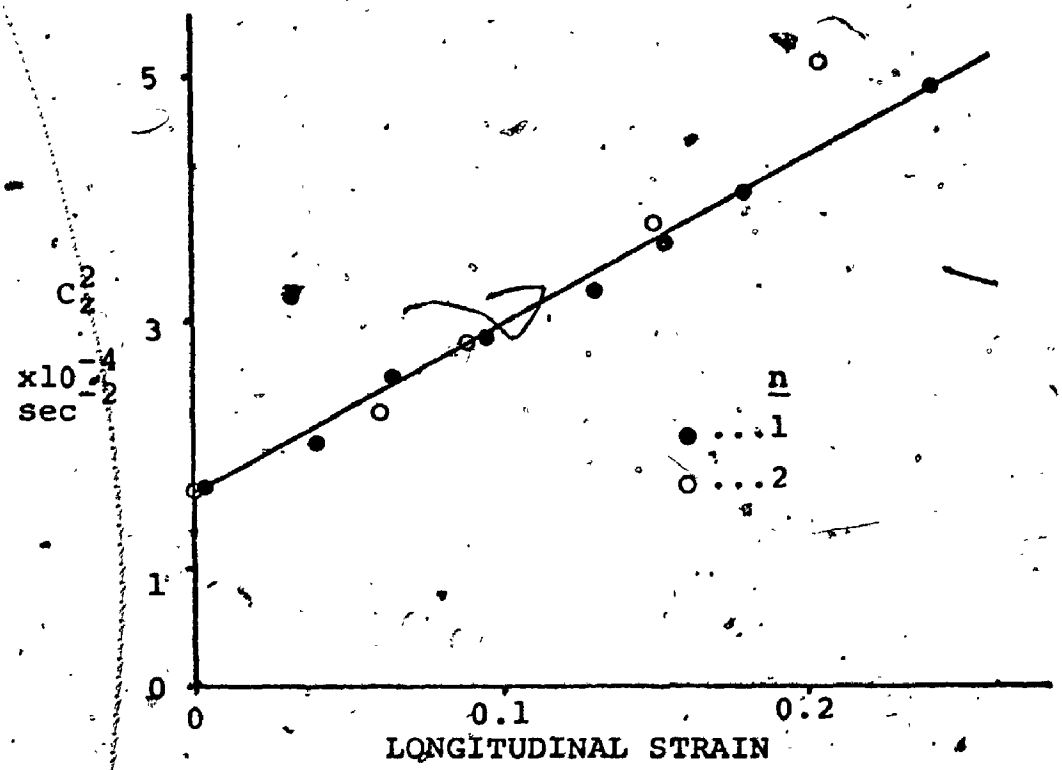
5
3
1
0
C_2^2
$x10^{-4}$
sec^{-2}
n
●...1
o...2
0
0.1
0.2
LONGITUDINAL STRAIN

Since we can write $T_z^o = E_z h\epsilon_z$ then

$C_z^2 = \frac{E_z h\epsilon_z + \gamma A_1}{\rho h} = \frac{E_z \epsilon_z}{\rho} + \frac{\gamma A_1}{\rho h}$. Thus, by plotting C_z^2 versus ϵ_z we can obtain the slope $\frac{E_z}{\rho}$ and the intercept $\frac{\gamma A_1}{\rho h}$. This has been done in figure 15B using the results in figure 15A for the circumferential mode n = 2. The results for the beam mode (m=1,n=1) are also shown for the same sample excited externally, indicating a much better ~~fit than the~~ results for n=2. This latter value gives a slope of 1.43×10^7 or $E_z = 1.6 \times 10^7$ which agrees quite well with the value 1.55×10^7 obtained from a force extension test. The intercept (1.6×10^6) gives $\gamma A_2 = 6.4 \times 10^4$ or $A_2 = 6.4 \times 10^8$ for $\gamma = 10^{-4}$. Even though the value of A_2 is difficult to estimate the value obtained experimentally appears to be too high.

The term γA_1 can be determined from the intercept in figure 14, knowing the contribution of $\frac{C_z^2}{(2L)^2}$. Using this value as 1.1×10^4 then

$$\frac{(n^2-1)}{\rho h} \frac{n^2 \gamma A_1}{(2\pi a)^2} = 3.2 \times 10^4$$

so that $\gamma A_1 = 7.9 \times 10^2$ or $A_1 = 7.9 \times 10^6$ (using $\gamma = 10^{-4}$). Now $A_1 = E_\theta a$ so that E_θ is determined as 1.9×10^7 dynes/cm^2. Assuming that the penrose tubing is isotropic this value is not substantially different from the result $E_z = 1.6 \times 10^7$ obtained above. This result would seem to be quite promising in demonstrating that the bending term correction is accurate.

Disturbed Flow

There are several reasons why the exposure to disturbed flow was studied. First, this type of exposure is most similar to that occurring naturally. Secondly, artifacts due to acoustical stimulation will be eliminated. Finally, since acoustical stimulation in fluid was more difficult and therefore not done, this technique will provide some continuity between the results in air and in fluid.

Figure 16 shows a characteristic wall vibration spectra under this type of flow, demonstrating a complex response dominated by two peaks, one at 55 Hz and the other at 450Hz. Keeping in mind the logarithmic nature of the plot these peaks are quite pronounced, with the one at 450 Hz 17dB or approximately 8x greater than its immediate background. Following the results of acoustical stimulation the order of magnitude of the two major peaks suggests that they correspond to the beam mode n = 1 and the higher order circumferential mode n = 2.

These suggestions are confirmed in figures 17 and 18 which show the spectra under different prestressed conditions. Figure 17 demonstrates the sensitivity of the higher frequency peak to pressure, similar to that under acoustical stimulation. Figure 18 demonstrates the dependence of the lower frequency peak on longitudinal tension, similar to the beam mode before. Figure 19

FIGURE 16

Characteristic wall displacement spectra while under disturbed flow in air.

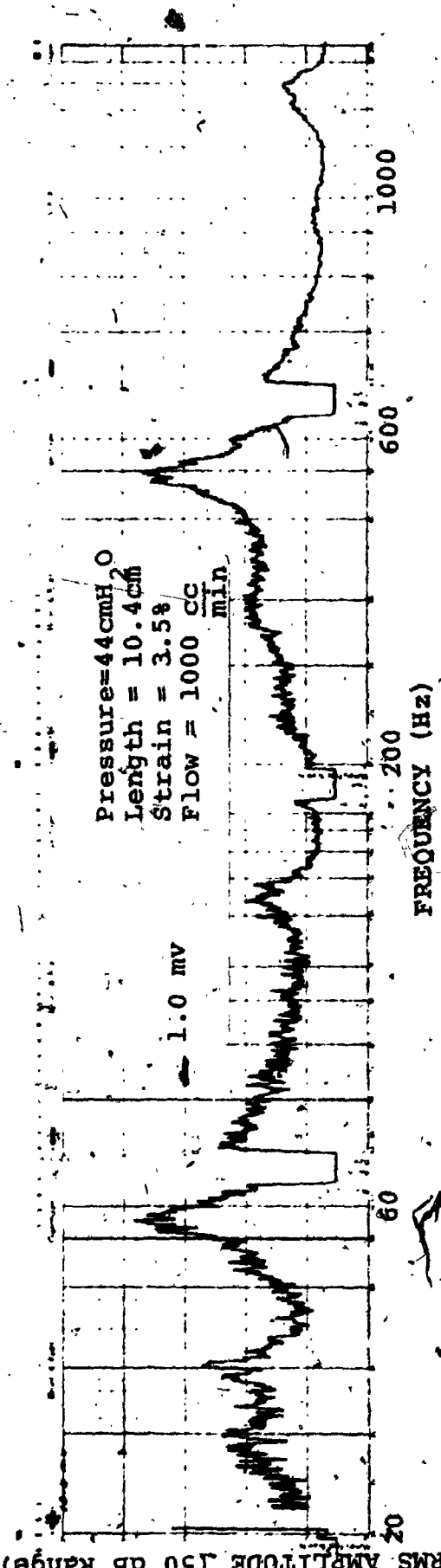
RMS AMPLITUDE (50 db Range)
FREQUENCY (Hz)
0
20
60
200
600
1000
1.0 mv
Pressure=44cmH2O
Length = 10.4cm
Strain = 3.5%
Flow = 1000 cc/min

FIGURE 17

Effect of pressure on the wall displacement spectra, in air, while maintaining the length at 10.6 cm (strain = 6%) and the flow at 1000 cc/min.

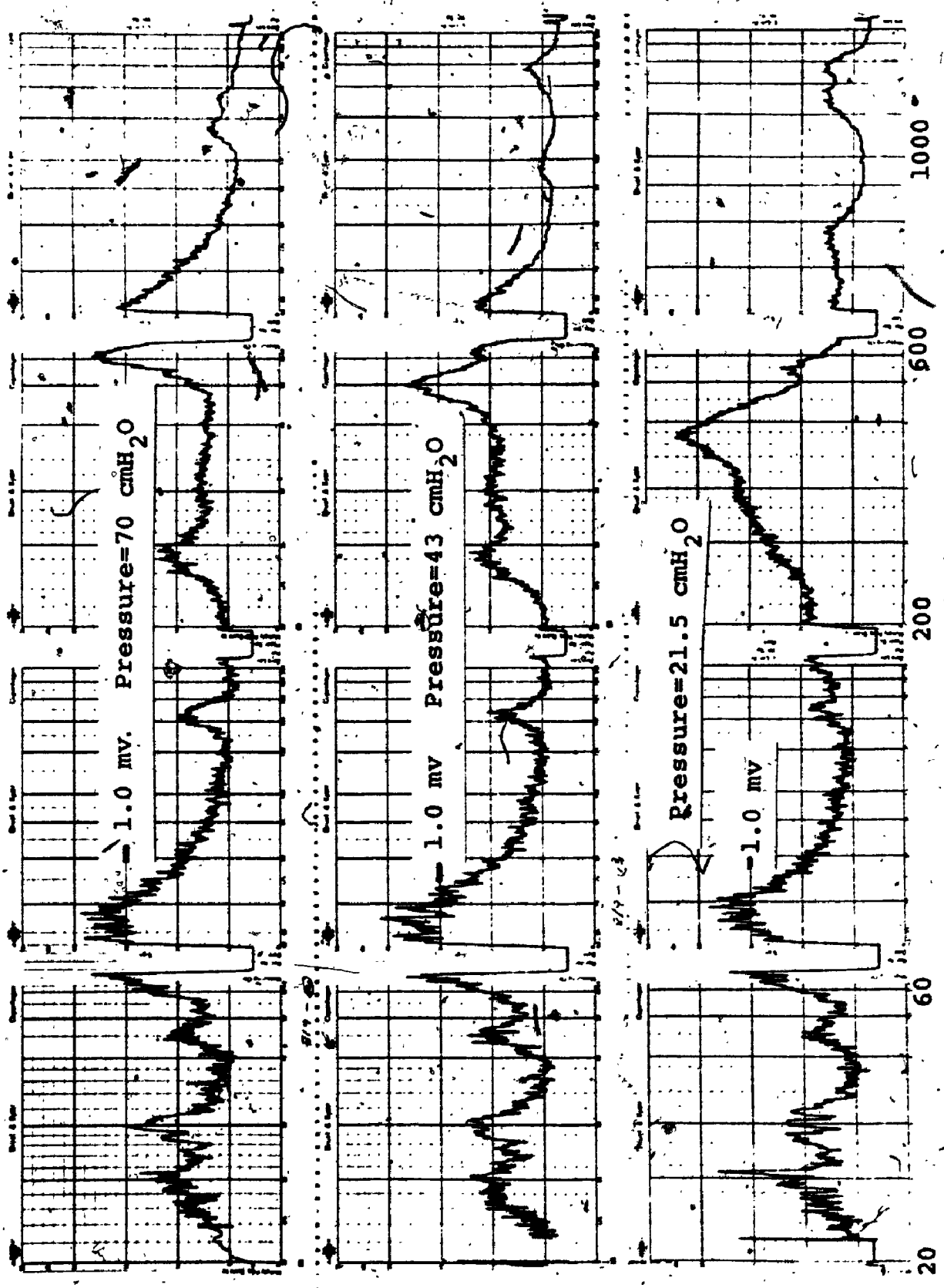
1.0 mv. Pressure=70 cmH2O
1.0 mv Pressure=43 cmH2O
1.0 mv Pressure=21.5 cmH2O
RMS AMPLITUDE (50 dB Range)
FREQUENCY (Hz)
20
60
200
600
1000

FIGURE 18

Effect of longitudinal tension on the wall displacement spectra, under disturbed flow in air, while maintaining the pressure constant at 70 cm H_2O and the flow at 1000 cc/min.

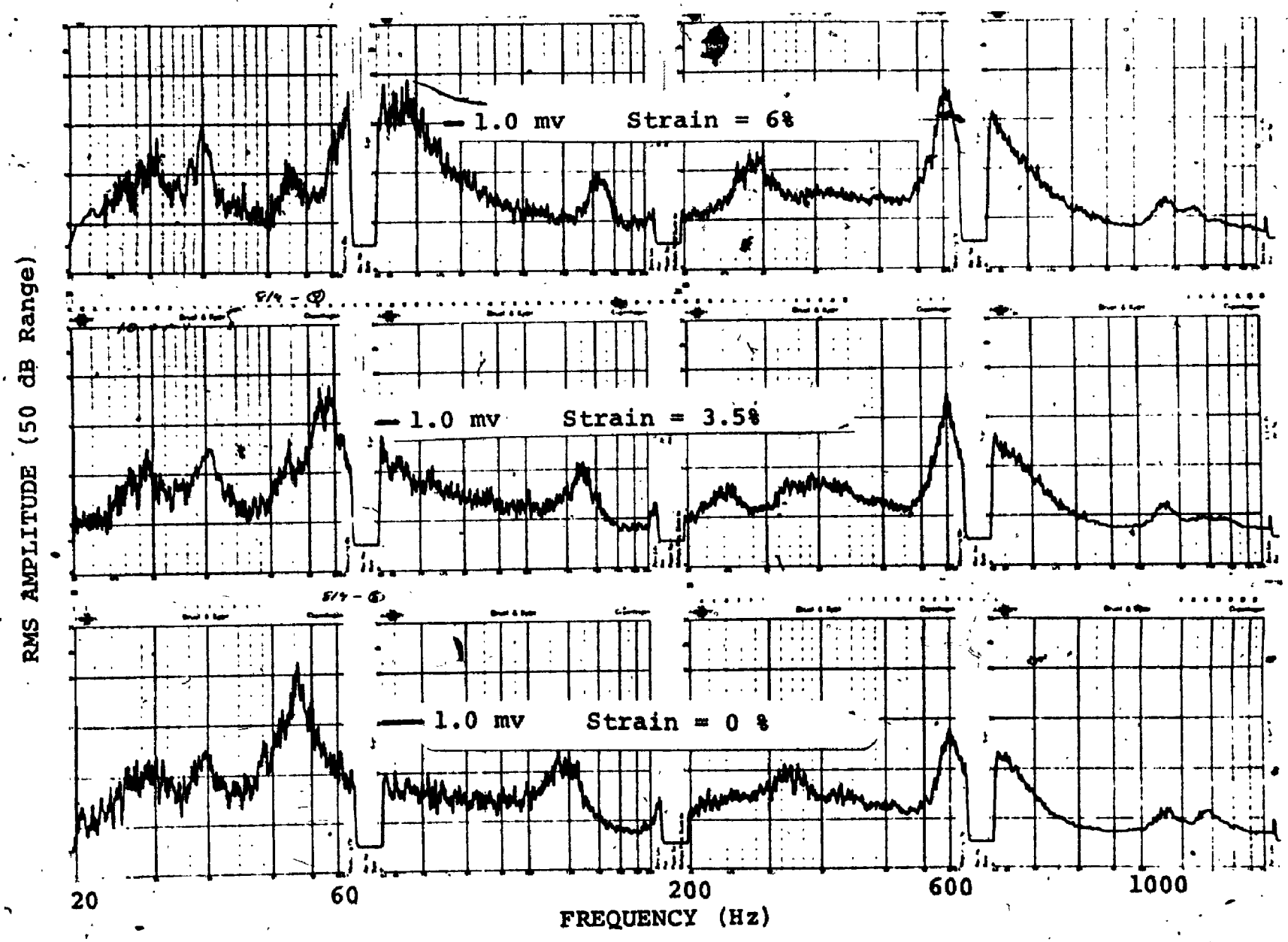
1.0 mv Strain = 6%
1.0 mv Strain = 3.5%
1.0 mv Strain = 0 %
RMS AMPLITUDE (50 dB Range)
20
60
200
600
1000
FREQUENCY (Hz)

FIGURE 19

A) A plot of f^2 versus T_c' for the dominant high frequency peak in figure 17.

B) A plot of f^2 versus the longitudinal strain term for the beam mode (n=1) in figure 18.

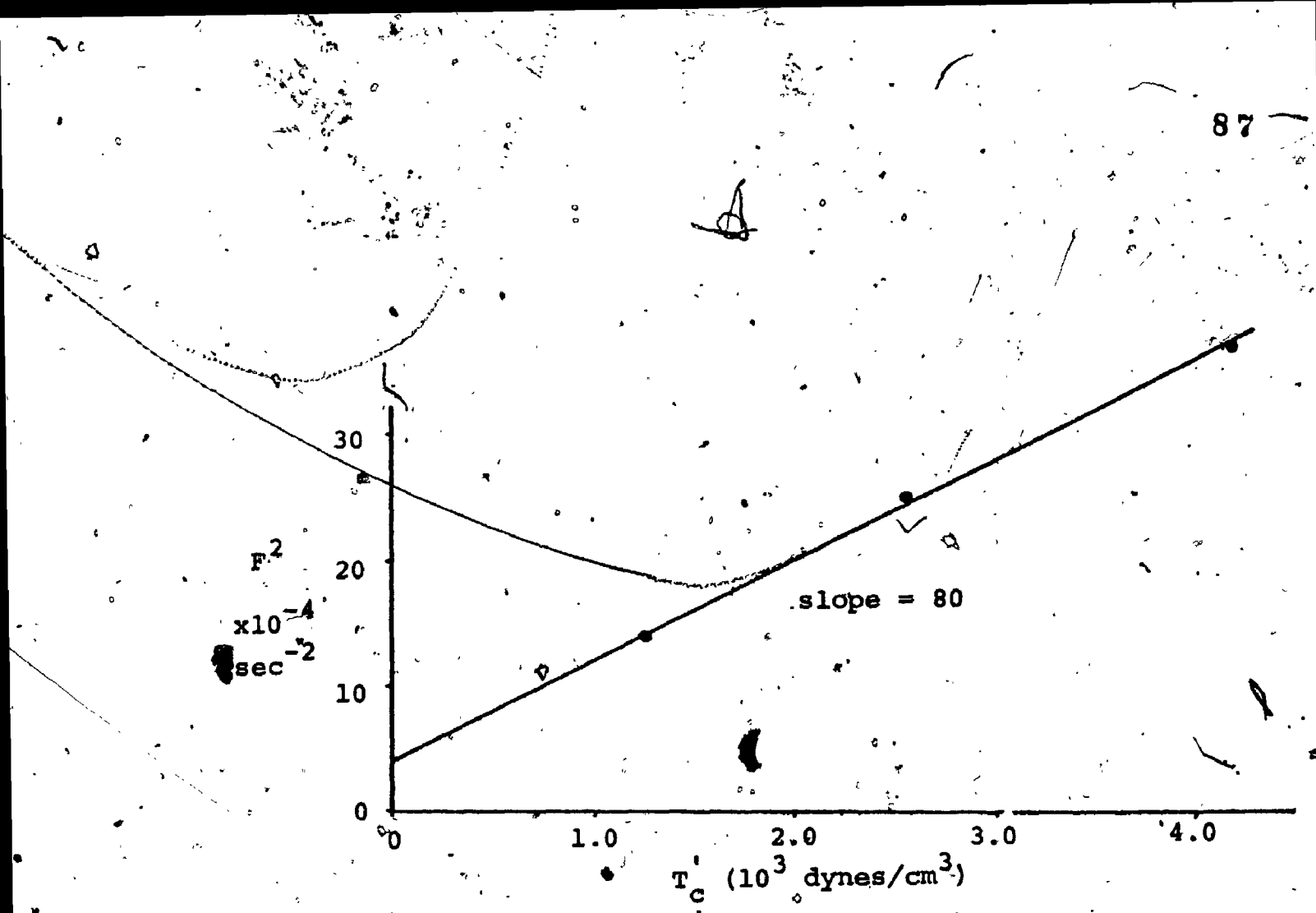
30
20
10
0
F^2
$x10^{-4}$
sec^{-2}
slope = 80
0
1.0
2.0
3.0
4.0
T_c' (10^3 dynes/cm^3)

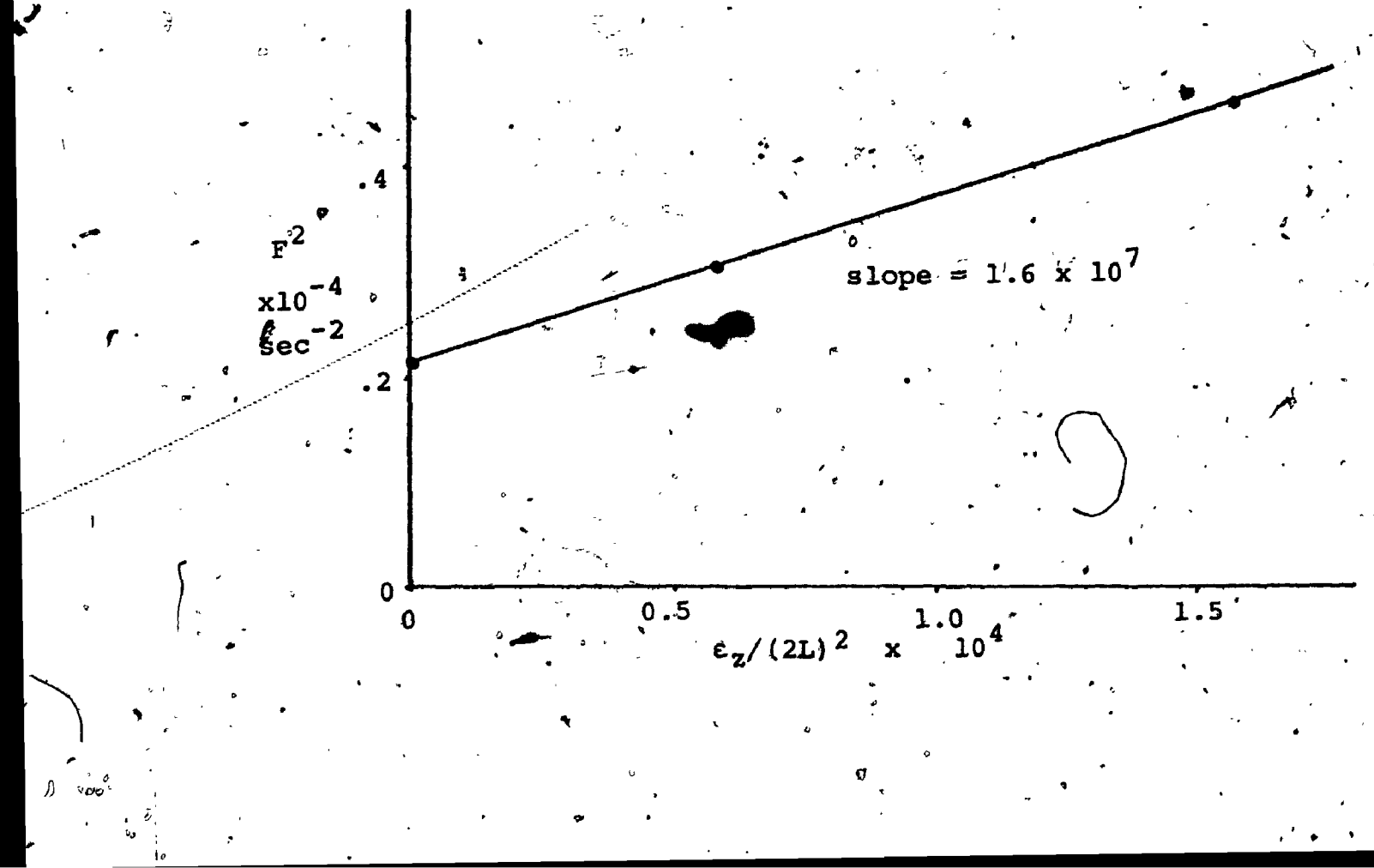
.4
.2
0
F^2
$x10^{-4}$
sec^{-2}
slope = 1.6 x 10^7
0
0.5
1.0
1.5
$\epsilon_z/(2L)^2$ x 10^4

shows these results plotted as a function of the prestress values.

In spite of the fact that only three points are used the results give values similar to that with acoustical stimulation. That is in 19A the slope = 80 which gives the value of n = 2 for this mode. Using the value of n = 2 the thickness is calculated as 0.034cm. which agrees quite well with the value (using incompressibility) of 0.035. In figure 19B, f^2 for the beam mode is plotted against $\epsilon_s/(2L)^2$ which should give a slope of E_s/ρ as discussed before. The measured slope of 1.6×10^7 is in excellent agreement with the previous result by external acoustical stimulation, 1.6×10^7.

The other smaller peaks, such as the ones at 145Hz and 240 Hz in figure 18A appear to be the beam modes m=2 and m=3 from their respective changes with longitudinal tension. The lower frequency peaks at 25,30 and 45Hz are a result of some background vibration, since these levels persist after the flow is reduced to zero. The one at 30Hz seemed to be due to a compressor in an adjacent room since it disappeared when the compressor was shut off. Greater vibration isolation was considered to eliminate the background levels but rejected. The increased experimental complexity was not considered necessary in view of the dominance of the true signals and the ability to observe their changes through varying the prestress levels.

The smaller peak at 540 Hz in 17C and 640Hz in 17B would appear to be a higher order longitudinal mode m of the n = 2 circumferential mode. The gradual disappearance of it in figure 17A may be due to the dominating effect of the C_e^2 term as the pressure increases. The higher frequency peaks in 17A would appear to be higher order circumferential modes, particularly the first peak at 1150Hz. For example it appears to shift to 960 Hz in 17B and then to 760 Hz in 17C as the pressure is lowered.

Plotting these results in figure 20b in the same manner as figure 19A, a straight line with slope = 253 is obtained. Using the value of h = 0.035cm. we can estimate n from slope = $\frac{n^2-1}{\rho h}$

so that $n^2-1 = \rho h\,(253)$ which gives $n^2 = 9.6$. Thus the nearest value of n would be n = 3. Considering that only three data points were used the error seems quite small.

Recall that the model gives an intercept of

$$\frac{m^2 C_a^2}{(2L)^2} + (n^2-1)\ \frac{n^2 \gamma A_1}{\rho h}$$

if f^2 is plotted against T_c. Hence a greater circumferential mode n would give a considerably higher value for the intercept, if m is constant. This is precisely what figure 20 shows with an intercept of 27×10^4 in contrast to a value of 4.2×10^4 in figure 19A. From the

FIGURE 20

A plot of f_2 versus T_c for the n=3 mode in figure 17.

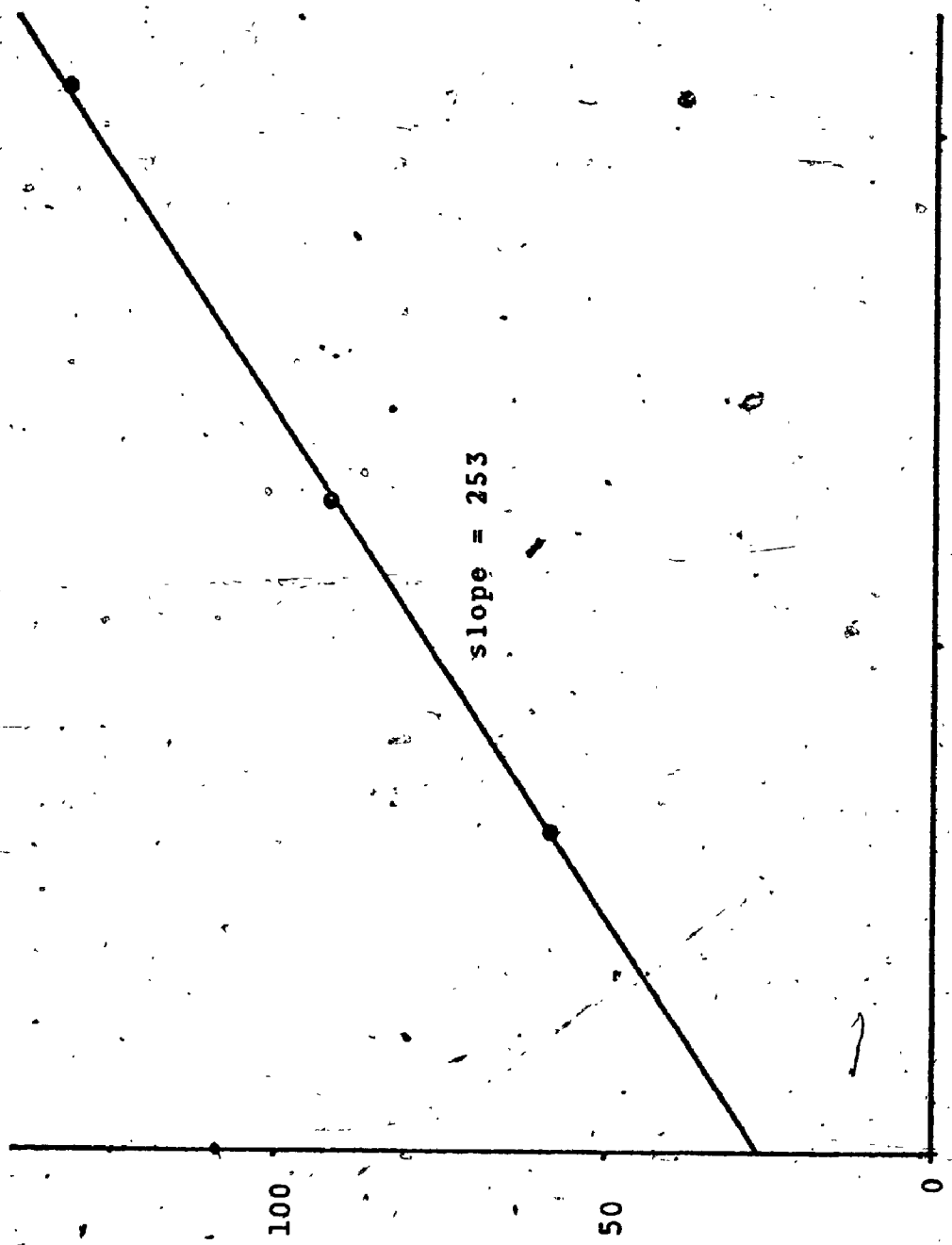
slope = 253
100
50
0
0
2.0
4.0
F^2 x10^{-4} sec^{-2}
T_c' (10^3 dynes/cm^3)

second term of the intercept we would expect a ratio of: $\frac{(n^2-1)n^2}{n}\Big|_{n=3} : \frac{(n^2-1)n^2}{n}\Big|_{n=2} = 6:1$ between the two measured intercepts.

Assuming that m is constant and using the value of $\frac{Cs^2}{(2L)^2} \simeq 0.20\times10^4$ given in 19B then the observed ratio is 26.5/4 = 6.6:1. This result would seem quite good considering the possible sources of error.

Considering the relationship to be true

$$\frac{(n^2-1)n^2}{(2\pi a)^2}\gamma\frac{A_1}{\rho h} \simeq 26.5 \times 10^4 \text{ then } \frac{\gamma A_1}{(2\pi a)^2}\frac{1}{\rho h} = 0.37\times10^4.$$

Using this result for the prestressed values in 17A with $f^2 = 13.7 \times 10^4$ then $\frac{n^2-1}{\rho h}\frac{Te^o}{(2\pi a)^2}$ is approximately 12.2×10^4 or $\frac{Te^o}{\rho h\,(2\pi a)^2} \simeq 4.1\times10^4$. Hence for n = 4 we would expect $f^2 = 150\times10^4$ or $f \simeq 1225$ Hz which seems reasonably close to the first higher frequency peak in figure 17A (ie ≃1300 Hz).

In none of these results could any peak be found that would correspond to the axi symmetric mode n = o. This is not too surprising since modes below a certain value of m will not exist. For example, with the prestressed values corresponding to figure 17C we find $\frac{Te^o}{\rho h(2\pi a)^2} \simeq 11\times10^4$ and $\frac{Cs^2}{(2L)^2} \simeq 0.46 \times 10^4$ so that $f^2_{m,0} = m^2(0.46) \times 10^4 - 11.0\times10^4$. Thus values below m = 5 are negative and therefore don't exist. The other possibility that discourages these modes is that the nature of the turbulent flow may favour asymmetrical modes.

The effect of increasing the turbulent intensity of the flow is shown in figure 21. Here the spectra at different flow levels has been recorded demonstrating that the same resonant modes are occurring at the same frequency. As expected, with increasing flow the vibration levels increase, particularly at the higher frequencies.

Discussion

The results both for acoustical stimulation and exposure to disturbed flow have demonstrated that the model presented adequately describes the resonant frequencies of an elastic vessel in air. The results obtained under disturbed flow indicate that the wall is driven over a fairly large frequency range, one which includes many resonant modes of vibration. The dominant modes turn out to be the beam mode (n=1) and the second order circumferential mode (n=2).

Using the values of $E=1.6\times10^7$, $\gamma A_2 = 6.4\times10^4$ and $\gamma A_1 = 790$ the results of the resonant modes are calculated and compared with the observed frequencies under disturbed flow. These results are summarized in figure 22 for several modes under the different prestressed values of figures 17 and 18. The resulting fit is quite good indicating the success of the model in describing the resonant frequencies in air. These results also demonstrate that the photonic sensor adequately depicts the radial wall vibrations of interest.

FIGURE 21

Wall displacement spectra under different flow rates during disturbed flow in air while the pressure remained constant at 21 cm H_2O and the length constant at 11.0 cm (strain = 4%).

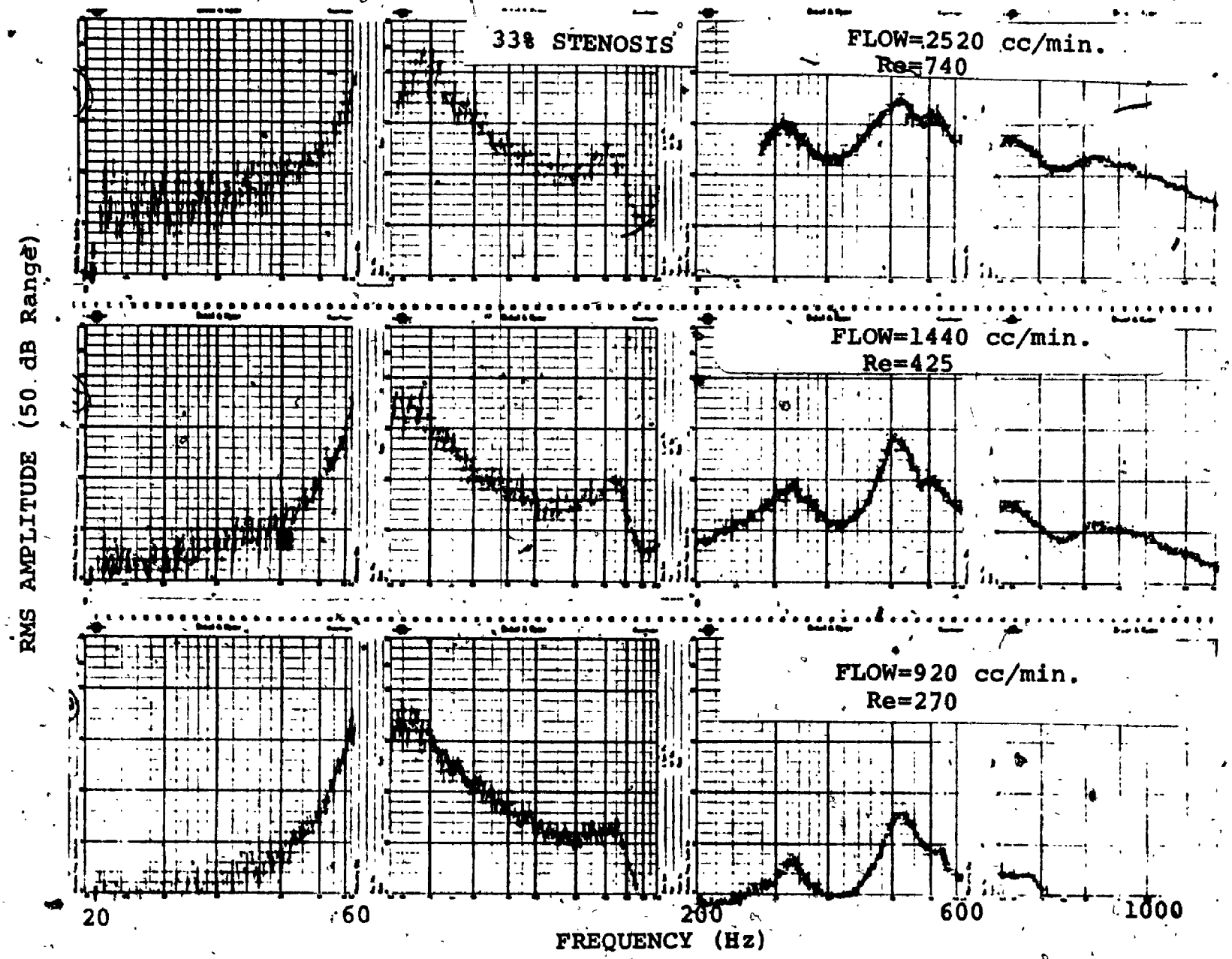
33% STENOSIS
FLOW=2520 cc/min.
Re=740
FLOW=1440 cc/min.
Re=425
FLOW=920 cc/min.
Re=270
RMS AMPLITUDE (50 dB Range)
20
60
200
600
1000
FREQUENCY (Hz)

FIGURE 22

Calculated resonant frequency versus the observed value under disturbed flow in air for the mode shapes m, n listed.

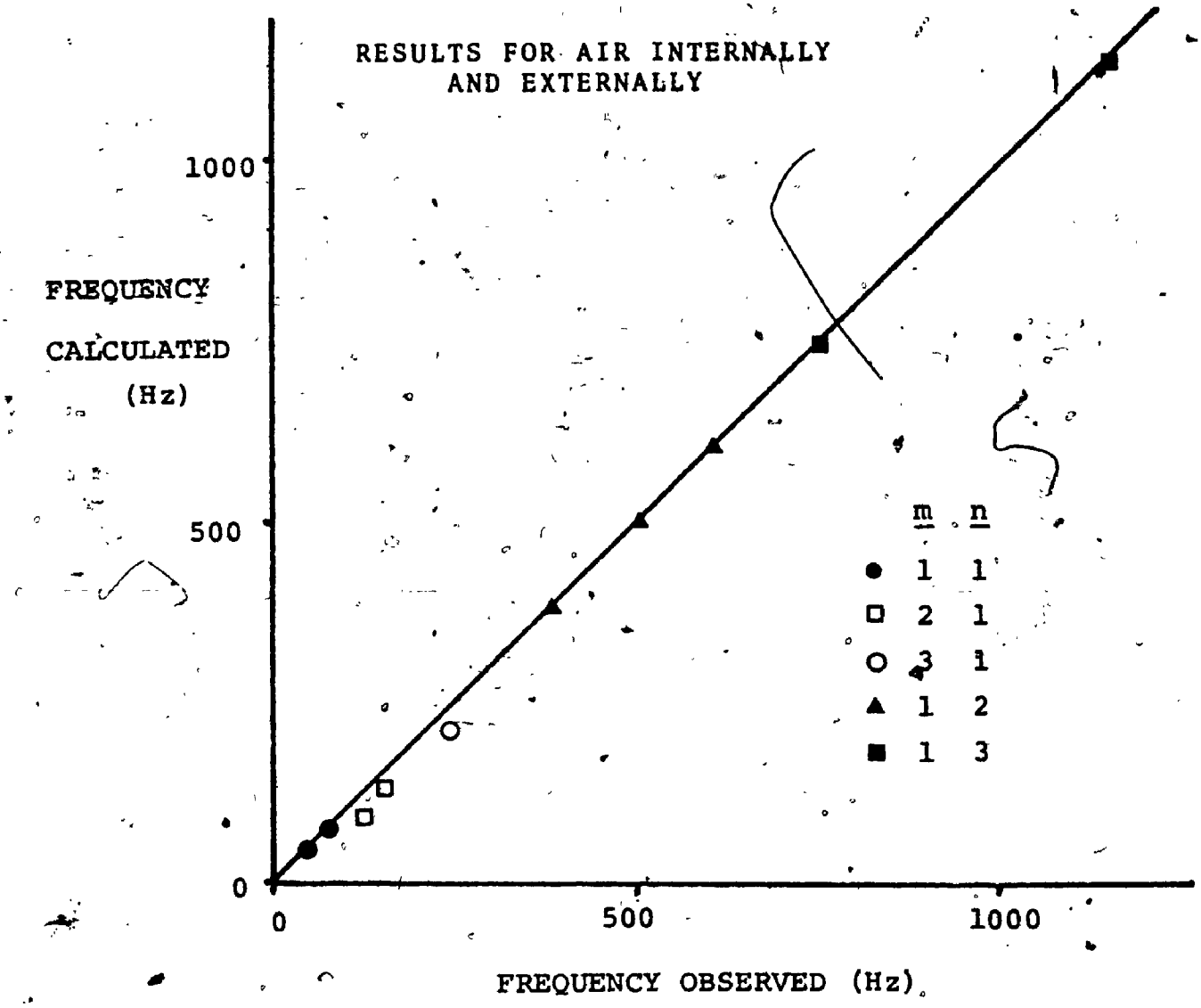
RESULTS FOR AIR INTERNALLY
AND EXTERNALLY
FREQUENCY
CALCULATED
(Hz)
1000
500
0
0
500
1000
FREQUENCY OBSERVED (Hz)
m n
1 1
2 1
3 1
1 2
1 3

(iv) Vibrations in Fluid: Externally.

The extension to vibrations with an external medium may be compared to that of bronchi. The use of water externally will not provide the elastic nature of the tissue surrounding bronchi but may reflect its inertial response. This extension is fairly simple, experimentally, since the same arrangement may be used as in the past except for having fluid in the bath.

Method

The same penrose tubing was used as in the previous method, in the same experimental arrangement. The only difference being that water was added to the bath enclosing the sample. The fluid level was approximately 2cm above the top of the rubber tubing. The amount of reflected light from the bare surface was substantially lower so that small aluminum spots (approximately 2x diameter of probe) were sprayed on.

Acoustical stimulation (at 85dB) was similar to the past experiment except that there was no external stimulation. For the tests under acoustical stimulation a 1/3 octave band pass filter (B & K 1612) was synchronized with the level recorder and B.F.O. This permitted a filtering of the signal over 1/3 octave bands which would eliminate artifacts due to distortion of the speaker, as noted previously. The tests under disturbed flow were performed as in the previous tests.

Results

Acoustical Stimulation

The dramatic inertial effect of the external fluid is demonstrated in figure 23 which shows the response before and after the addition of fluid. The change in the dominant circumferential mode (n=2) from 500Hz in air to 200Hz in fluid[1] is considerable. Note that the distorted response in figure 23 in comparison to those done before is due to the 1/3 octave band pass filter. The small downward spikes indicate a decrease in amplitude due to the switching between filters. The advantage of this technique was noted in that the response of figure 23A showed a very large peak (8dB down from major peak) at 250Hz (ie. ½ the major resonance) when the filter was shut off.

The nature of the major resonance in figure 23A and 23B seems to be similar each with a smaller higher frequency peak at approximately 580 and 250 Hz respectively, probably a higher order longitudinal mode associated with n = 2. Figure 24 shows a plot of f^2 versus T_c^{-1} for these two resonances both in air and fluid. The similar slopes between the two peaks as a function of circumferential stress confirm the idea of them being different longitudinal modes.

As we discussed in the previous chapter a plot of f^2 versus T_c^{-1} should have a slope $\frac{n^2-1}{\rho_e h}$.

---

[1] The term "fluid" has been incorrectly used for "liquid" throughout this text, since "fluid" refers to both liquids and gases.

FIGURE 23

Comparison of the results from internal acoustical stimulation at 95 dB with and without the loading of external fluid (A-air, B- fluid). The length and pressure were constant at 10.3 cm (strain =3%) and 56cm H_2O.

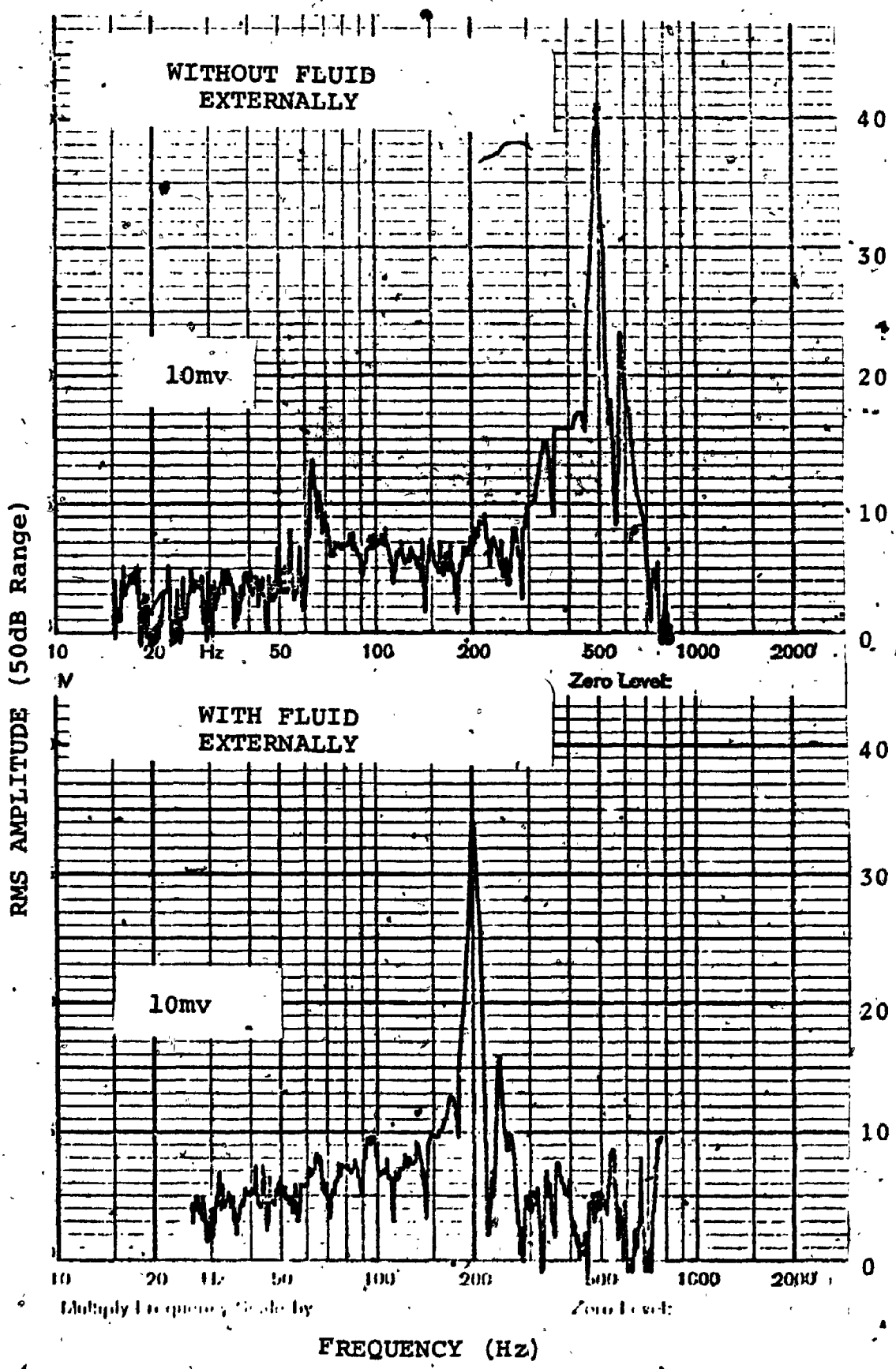
WITHOUT FLUID
EXTERNALLY
10mv
40
30
20
10
0
10
20
Hz
50
100
200
500
1000
2000
Zero Level
WITH FLUID
EXTERNALLY
10mv
RMS AMPLITUDE (50dB Range)
FREQUENCY (Hz)

FIGURE 24

A plot of f^2 versus T_c for the two dominant resonances in figure 23 with both air and fluid externally. f_1 refers to the dominant resonance and f_2 is the second peak.

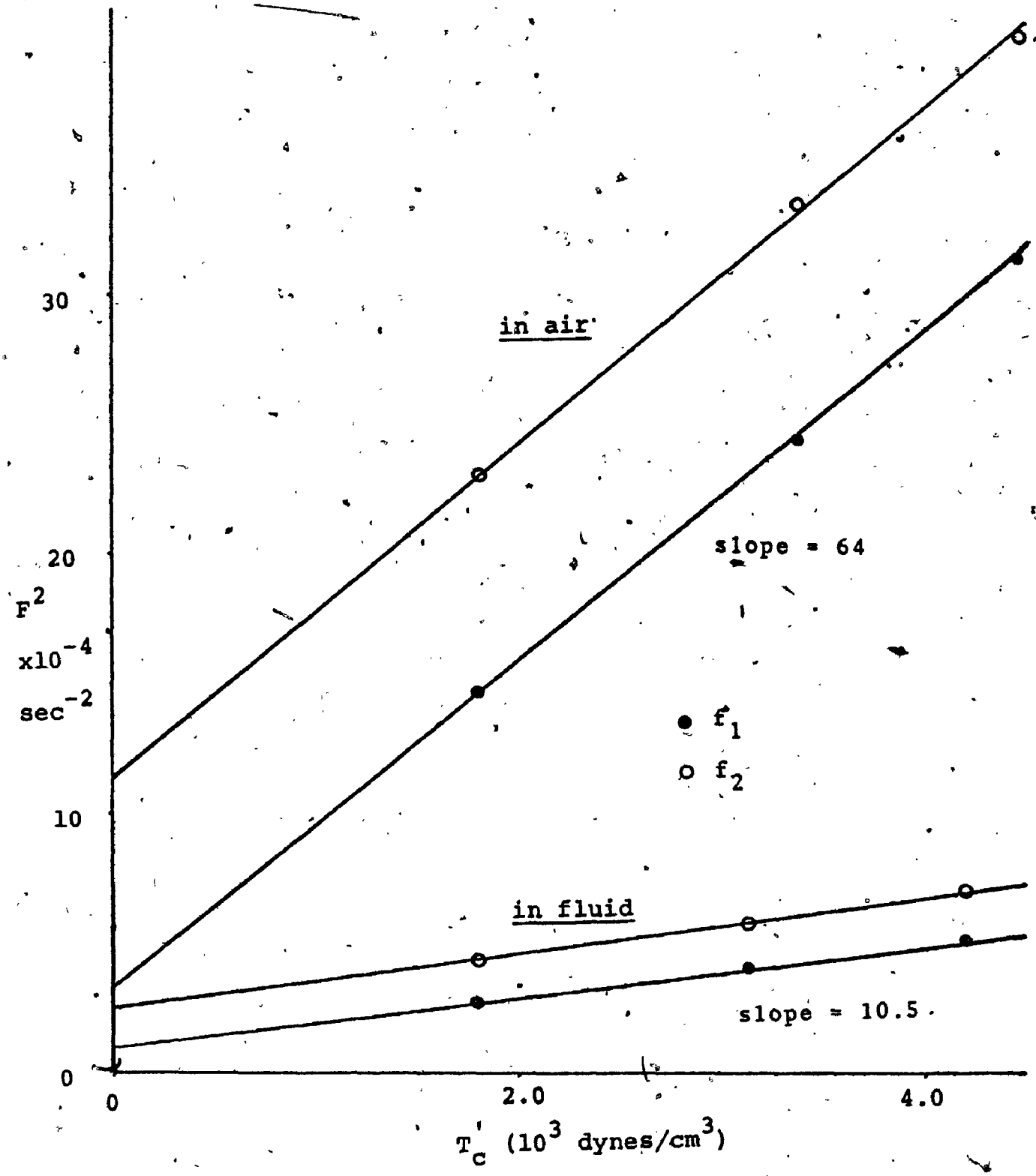
30
20
10
0
F^2
$x10^{-4}$
sec^{-2}
in air
slope = 64
f_1
f_2
in fluid
slope = 10.5
0
2.0
4.0
T_c' (10^3 dynes/cm^3)

Hence for the same circumferential mode n the ratio of slopes between the results for air and fluid should be $\rho_e h/\rho_w h$.

But $\rho_e h = \rho_w h + \rho_f a/n$ for external fluid so that $\frac{\rho_e h}{\rho_w h} = 1 + \frac{\rho_f \frac{a}{n}}{\rho_w h}$. Since $\frac{\rho_f a}{\rho_w h} = 10.5$ and $n = 2$ then $\frac{\rho_e h}{\rho_w h} = 6.5$. However the measured slopes from figure 24 are in the ratio 64:10.5 which gives a ratio of 6.1. Considering the resolution available from charts like those in figure 23, the agreement is quite good. Using the slope from figure 24 of 10.5, however, we find $\rho_e h$ = 0.285 which is about 20% higher than the measured value of 0.23.

Changes in longitudinal tension were not performed in this series so that interpretation of the longitudinal mode number was not possible.

Disturbed Flow

The same dramatic lowering of the resonant frequencies when fluid is added externally is shown in the wall vibration spectra in figure 25, when the flow is turbulent. The fluid was added immediately after the top spectra was obtained so that the same prestress conditions exist in the wall (except for a lowering of the transmural pressure, 2 cmH_2O, by the addition of fluid 2cm above the level of the tubing).

FIGURE 25

A comparison of the wall displacement spectra under disturbed flow with and without fluid externally while maintaining a constant length of 10.6cm (6% strain), pressure of 70cm H_2O and flow of 1000 cc/min.

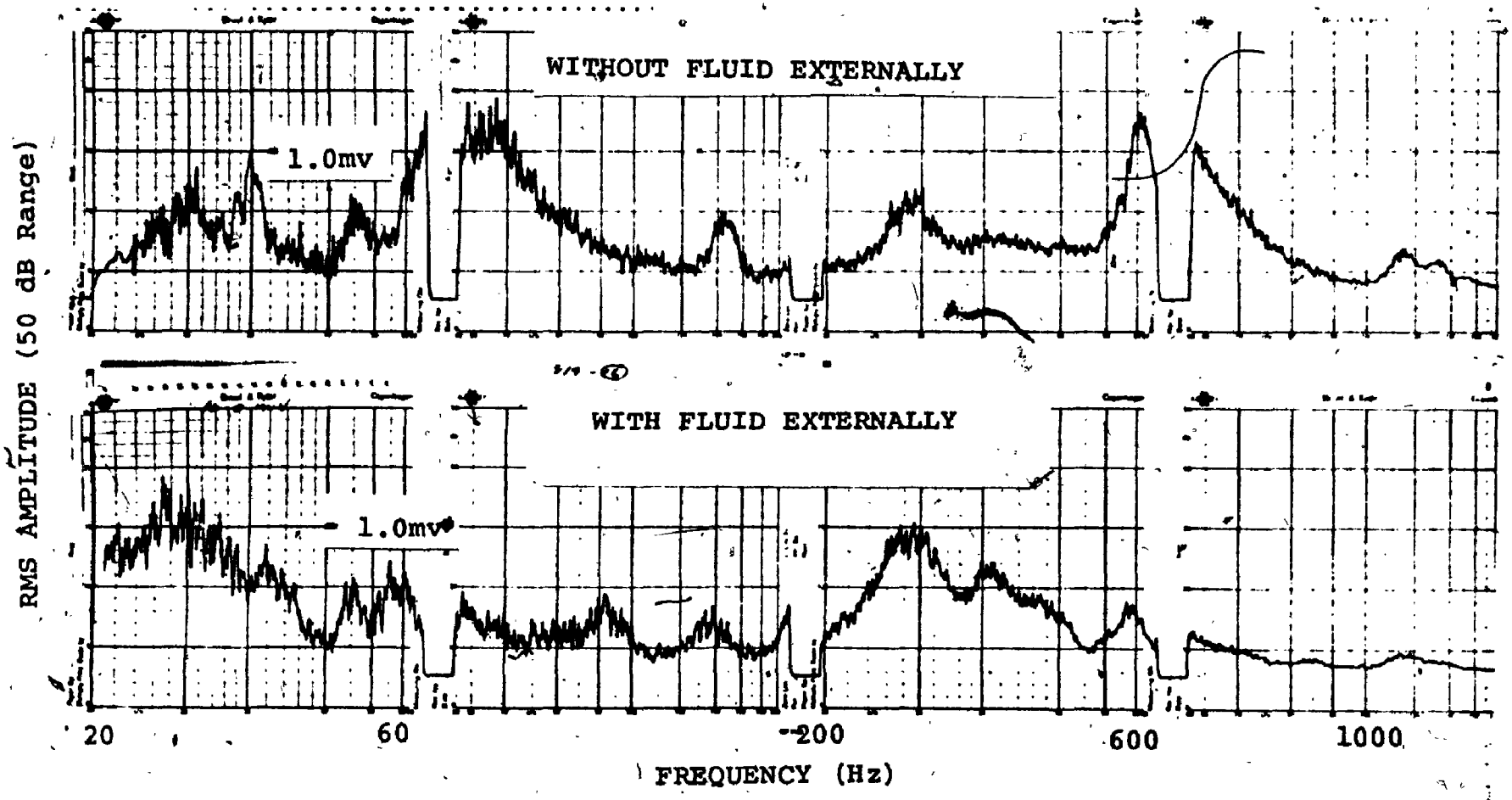
WITHOUT FLUID EXTERNALLY
1.0mv
WITH FLUID EXTERNALLY
1.0mv
RMS AMPLITUDE (50 dB Range)
20
60
200
600
1000
FREQUENCY (Hz)

As with acoustical stimulation, the high frequency circumferential mode n = 2 has fallen to about 40% of its initial value (from 600Hz to 245Hz). The main beam mode resonance has also fallen from about 68 Hz to 24Hz. The two smaller peaks at 145Hz and 240Hz appear to be the higher order beam modes m = 2 and m = 3 apparently dropping to 92 Hz and 135 Hz respectively.

The justification for the 245Hz peak in 25B being the pressure sensitive circumferential mode n = 2 is demonstrated in figure 26, which displays the wall vibration spectra under different pressures. The peak at 245Hz shifts to 205Hz and then to 150 Hz as the pressure is lowered, whereas the beam mode at 24Hz is noted to be insensitive to pressure, as expected. In figure 27, however, the longitudinal tension is lowered showing a decrease in the beam mode frequency off scale. The dominant circumferential mode is relatively insensitive to changes in longitudinal tension although two smaller peaks (at 205Hz and 290Hz in figure 27B) associated with this mode are not. Presumably they are higher order longitudinal modes m with n = 2.

This would seem to be confirmed in figures 28 and 29. Figure 28 shows the results of figure 26 plotted as a function of circumferential tension. The similarity of the two slopes (only the major circumferential peak and the

FIGURE 26

Effect of pressure on the wall displacement spectra with external fluid while the length and flow are constant at 10.6 cm (6% strain) and 1000 cc/min., respectively.

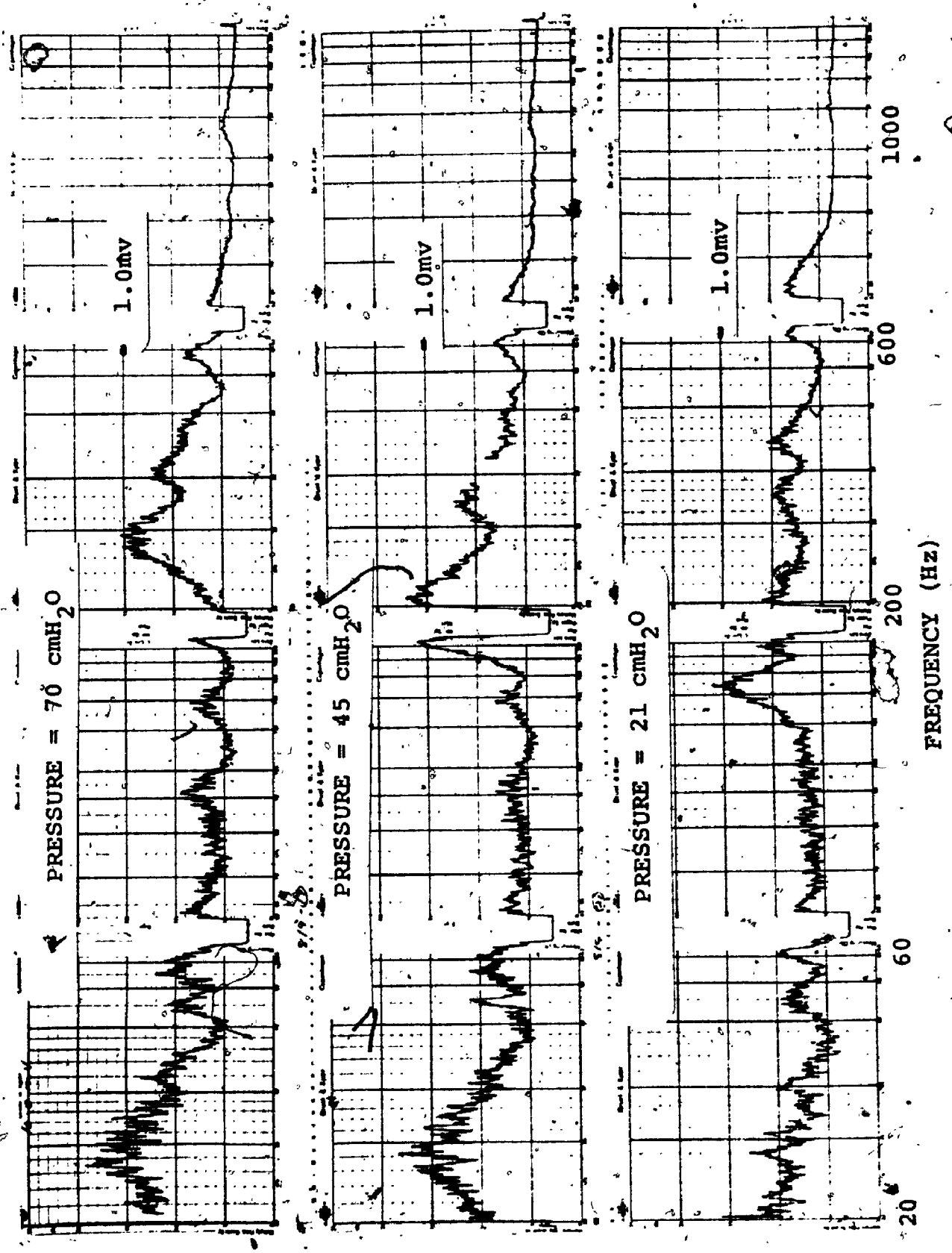
PRESSURE = 70 cmH2O
PRESSURE = 45 cmH2O
PRESSURE = 21 cmH2O
1.0mv
1.0mv
1.0mv
20
60
200
600
1000
FREQUENCY (Hz)
RMS AMPLITUDE (50 db Range)

FIGURE 27

Effect of longitudinal tension on the wall displacement spectra with external fluid while the pressure and flow are constant at 70cm H_2O and 1000 cc/min. respectively.

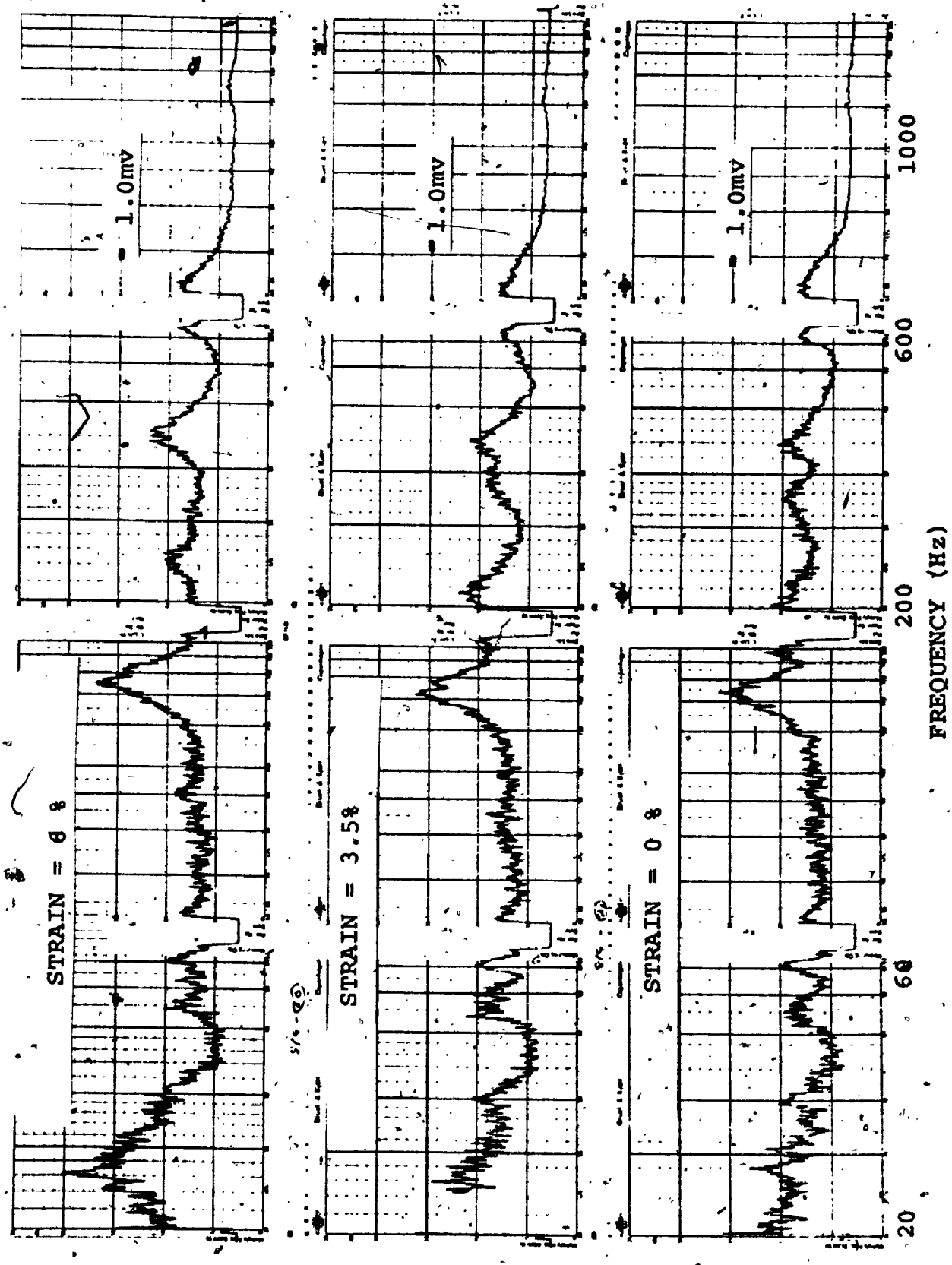
STRAIN = 0 %
STRAIN = 3.5%
STRAIN = 6 %
= 1.0mv
= 1.0mv
= 1.0mv
20
60
200
600
1000
FREQUENCY (Hz)
RMS AMPLITUDE (50 dB Range)

FIGURE 28

A plot of f^2 versus T_c' for the resonant peaks in figure 26.

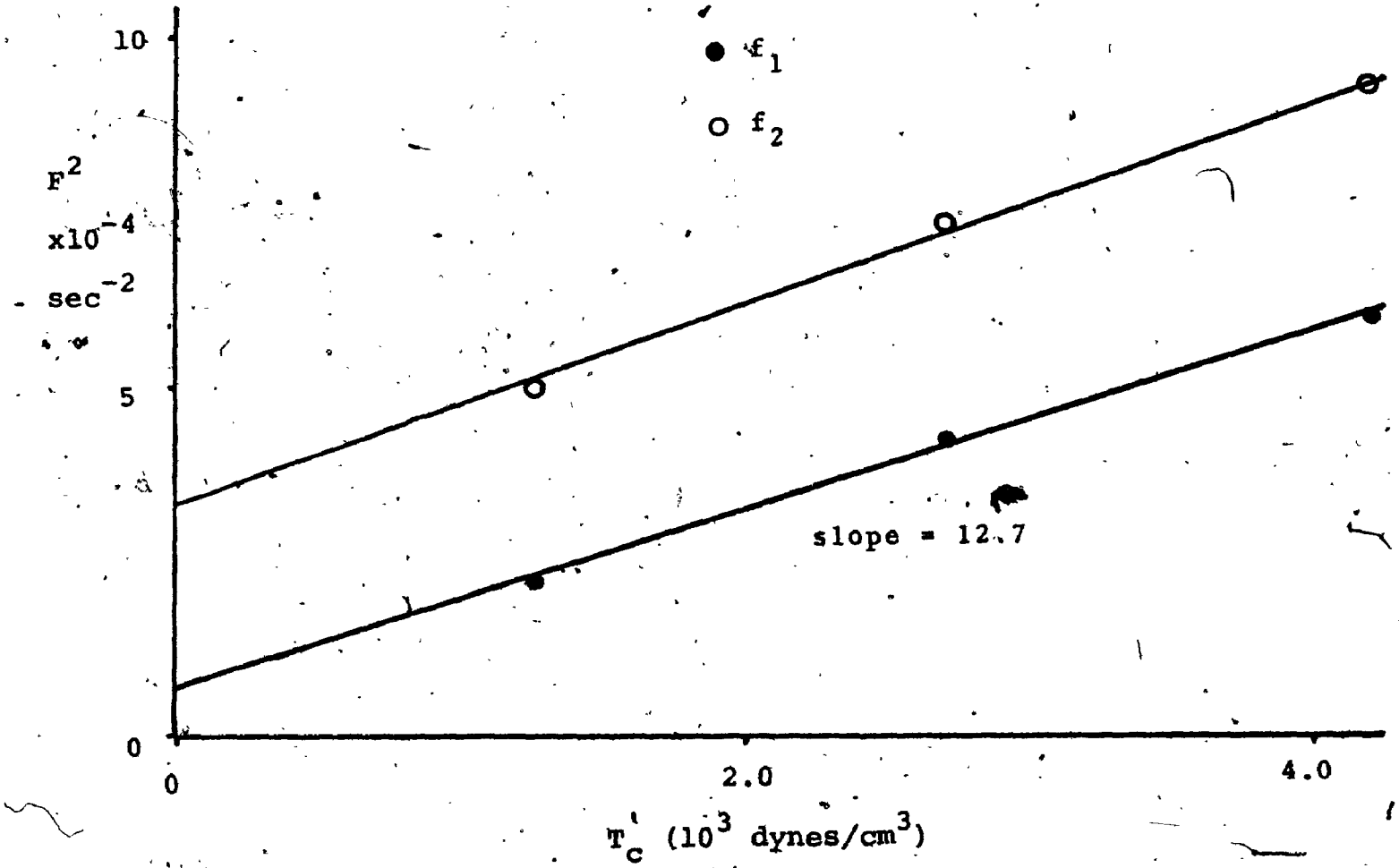
10
5
0
F^2
$x10^{-4}$
sec^{-2}
f_1
f_2
slope = 12.7
0
2.0
4.0
T_c' (10^3 dynes/cm^3)

FIGURE 29

A plot of f^2 versus the longitudinal strain term for the pressure sensitive resonant peaks associated with the n=2 circumferential mode in figure 27.

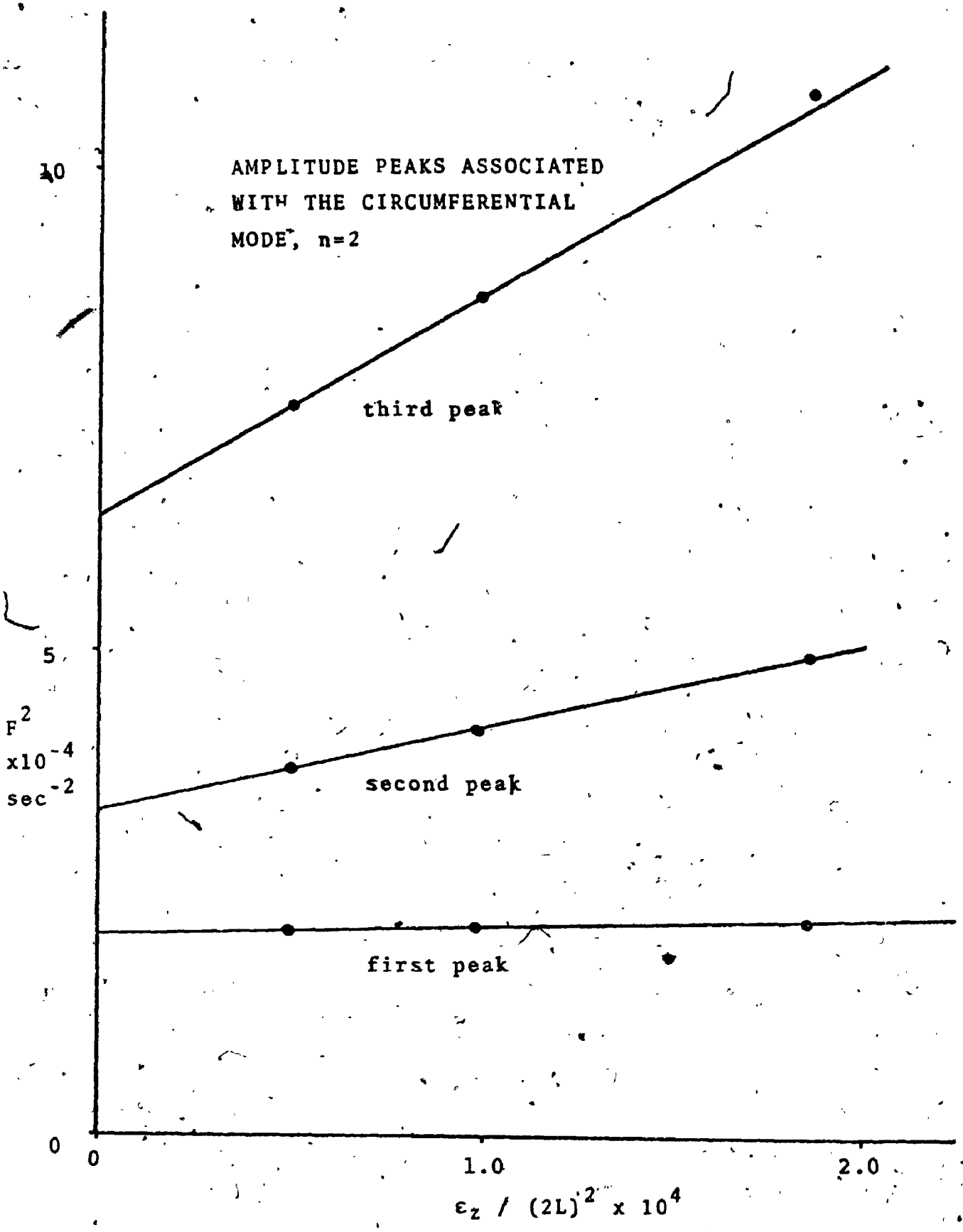
AMPLITUDE PEAKS ASSOCIATED WITH THE CIRCUMFERENTIAL MODE, n=2
third peak
second peak
first peak
10
5
0
F^2 x10^{-4} sec^{-2}
0
1.0
2.0
$\epsilon_z / (2L)^2 \times 10^4$

following smaller one were distinct in figure 26 and thereby used) confirms that they are of the same circumferential mode, n. The value of the slope (12.7) provides a more accurate description of $\rho_e h$ = 0.236 in comparison to the measured value of 0.23, stated previously. The difference between this result and that obtained under acoustical stimulation (10.5) may be due to an error in the frequency calibration of the latter system. Also the frequency resolution obtainable from charts as in figure 23 is poor.

Figure 29 shows the two higher order longitudinal modes of n = 2 plotted against $\varepsilon_z(2L)^{-2}$ along with the dominant circumferntial resonance which shows little change. The highest order mode plotted in figure 29 appears to merge with the peak at 330 to 350 Hz in figure 27A and was arbitrarily chosen as occurring at 330 Hz (this provides a better fit with the data). The expected straight line relations appear to be confirmed in this plot suggesting that there two higher frequency modes correspond to large mode values m. When m was estimated from the slopes $(m^2 \frac{Eh}{\rho_e h})$ values of m=6 and m=10 were calculated for the two slopes. Why these particular values are dominant is puzzling. These values of m, however, are quite high and out of the range considered in the theoretical development $(\frac{m\pi}{L} \leq 1)$.

Discussion

The results presented with this series of tests revealed the same dependence of the resonant frequencies on the state of prestress and geometry as was found previously. For the case of an external media of fluid rather than air, however, the model predicted a significant alteration in the resonant frequencies due to the additional loading of the fluid. This inertial dominance by the surrounding media was confirmed under both acoustical stimulation and exposure to disturbed flow (see figure 24 and 28) providing justification of the inertial term $\rho_w h + \frac{\rho_f a}{n}$.

The disturbed flow studies again revealed that the dominant resonant modes of vibration were the beam mode (n=1) and the circumferential mode (n=2).

(v) Vibrations in Fluid: Internally and Externally Method

The relative difficulty in obtaining acoustical stimulation with fluid coupling and the apparent success with turbulent flow in stimulating the modes of interest, suggested the use of the latter in this present study. Using the same experimental bath from the previous study the air line was replaced with one from a water reservoir whose height could be adjusted. With the adjustment of a clamp upstream and downstream of the sample, the pressure could be varied over the range of interest while maintaining a constant flow rate. A plug similar to the previous one

was placed in the upstream tubing creating a stenosis of 52% diameter. The same flow meter was used in the present tests although a different calibration curve was used for the water.

It was found during the tests that the flow rate could not be maintained at the higher pressures (greater than 65 cm H_2O) due to increasing pressure losses across the clamps. The result was a lowering of the Reynolds number and therefore the degree of turbulence. To maintain the flow rates at the higher pressures a pump was inserted for two series of tests. Its use, however, produced additional vibrations that were transmitted through the fluid to the sample. These were noted by varying the flow rate while maintaining the same prestress in the wall.

To consider the effects of geometrical changes a series of tests were performed on a smaller diameter (0.32 cm O.D. and 0.031 cm thickness) sample of the same penrose tubing. Samples of different resting lengths were also used to demonstrate this effect.

When a second photonic sensor became available it was possible to do space correlation studies by placing the two sensors at different locations. By filtering the two signals (two B & K 2107 Analyzers) at a resonance frequency of interest and then performing cross correlation (Random Signal Analyzer) on these

filtered signals, the respective phase shift between the two signals could be determined. By observing the relative phase changes longitudinally and circumferentially at several resonances the respective mode shapes could be confirmed.

Results

The additional inertial effect of the fluid internally is demonstrated in figure 30 where the two vessels are under the same prestress conditions. The resonance at 245Hz which was previously attributed to the second circumferential mode (n=2) appears to have decreased to 180 Hz as a result of the increased inertia. The smaller high frequency peak at 370Hz is probably the next order circumferential mode, n = 3. At first the beam mode might appear to have increased to 34-35Hz. However, as we shall see later this peak corresponds to the second order longitudinal beam mode, m = 2.

The sensitivity of the two high frequency peaks to changes in circumferential prestress is shown in figure 31, confirming that they are the higher order circumferential modes. The dominant high frequency mode changes from 150Hz to 200Hz to 225Hz while the second high frequency peak shifts from 310Hz to 390Hz to 450Hz as the pressure is raised. The smaller peak at 510Hz in figure 31b suggests an even higher order circumferential mode (n=4).

FIGURE 30

Comparison of the wall vibration spectra with and without fluid internally (in addition to external fluid). The samples are under the same pressure (70 cm H_2O) and length, 10.6 cm (strain =6%) but different flow rates of 1000 cc/min. (Re=300) and 520 cc/min. (Re=1180), respectively.

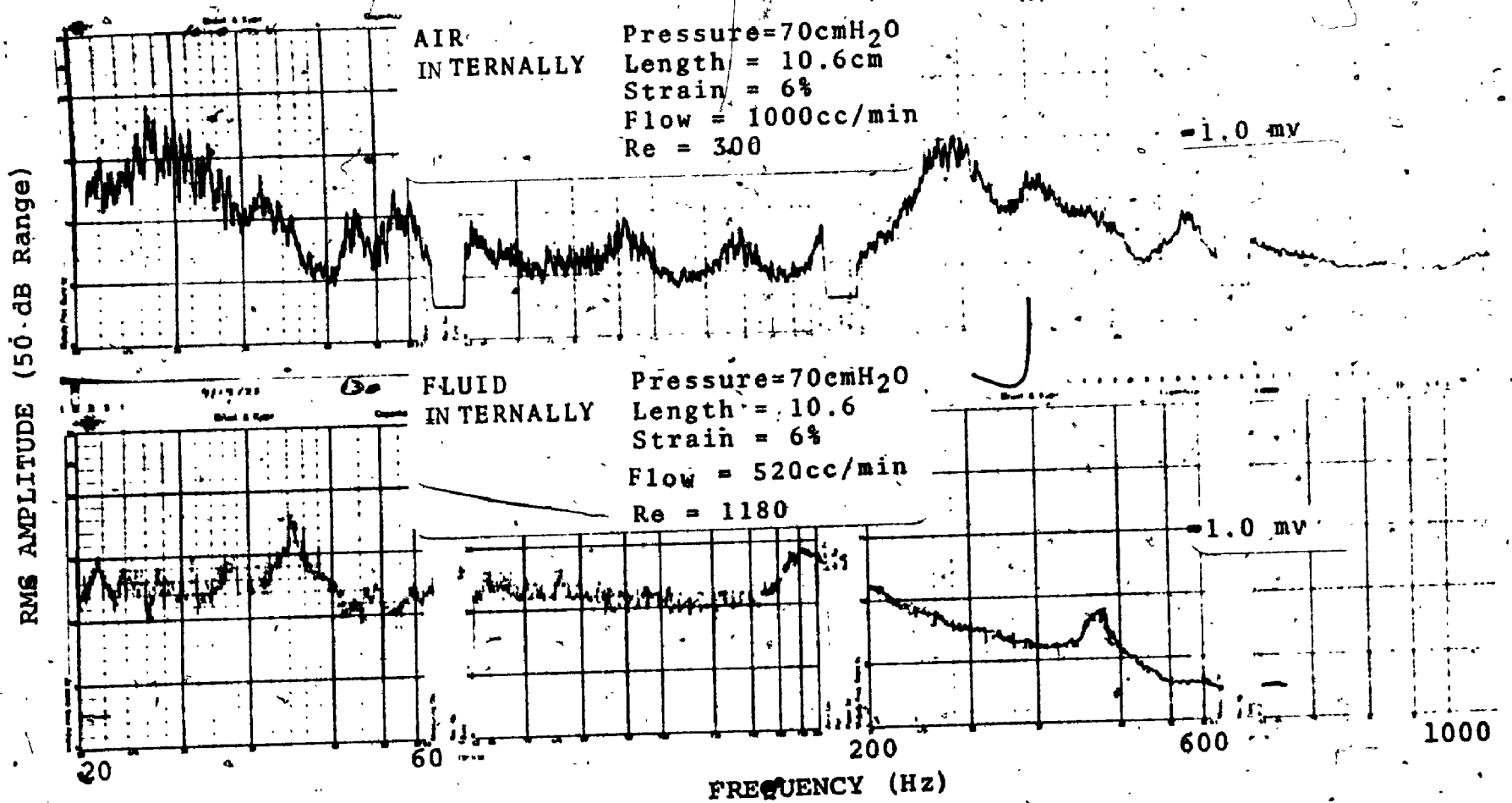
AIR
IN TERNALLY
Pressure=70cmH2O
Length = 10.6cm
Strain = 6%
Flow = 1000cc/min
Re = 300
1.0 mv
FLUID
IN TERNALLY
Pressure=70cmH2O
Length = 10.6
Strain = 6%
Flow = 520cc/min
Re = 1180
1.0 mv
RMS AMPLITUDE (50 dB Range)
20
60
200
600
1000
FREQUENCY (Hz)

FIGURE 31.

Effect of pressure on the wall vibration spectra with internal and external fluid under a constant longitudinal tension (length = 12.6cm). The flow rate could not be maintained constant

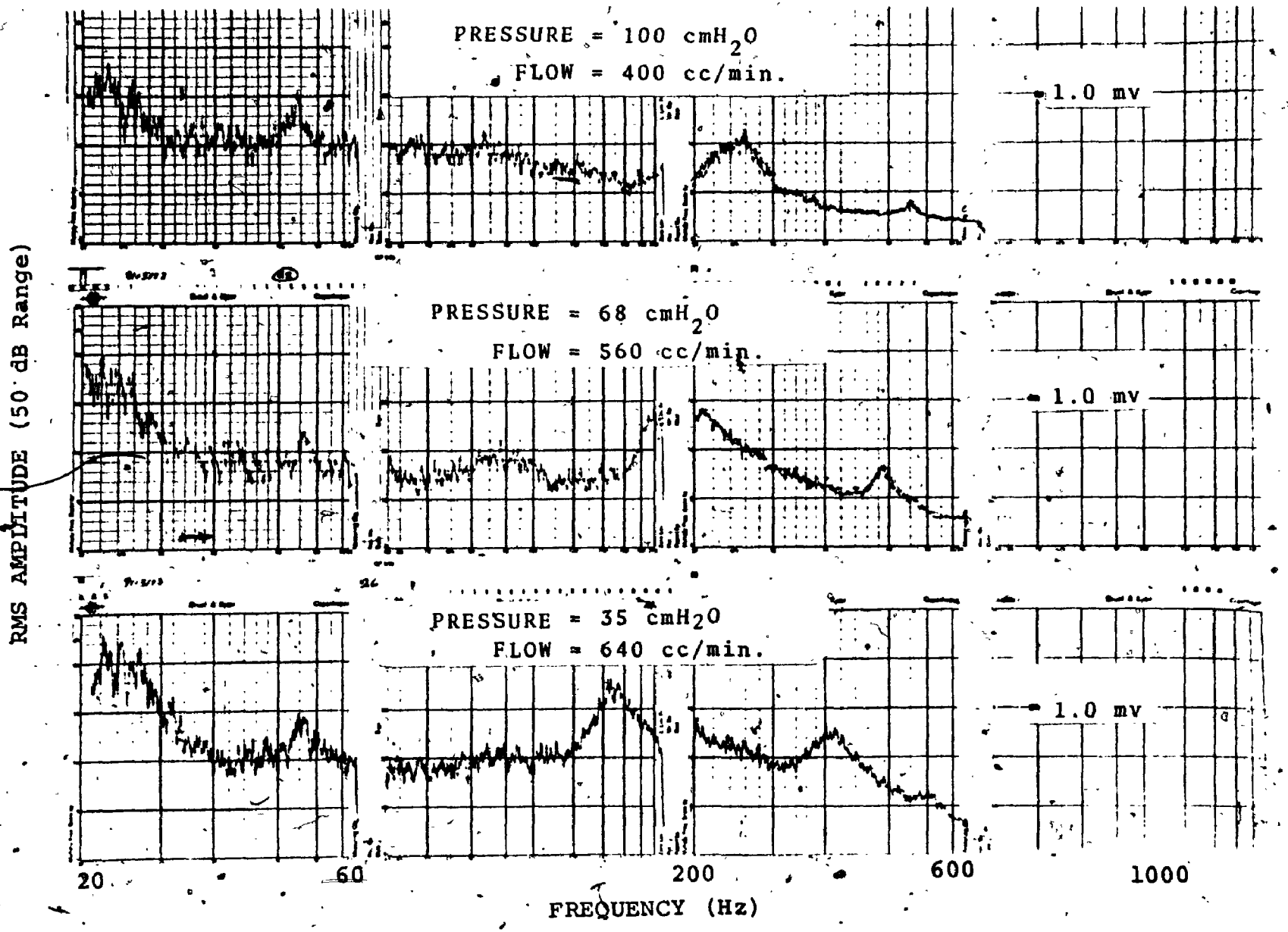
PRESSURE = 100 cmH2O
FLOW = 400 cc/min.
1.0 mv
PRESSURE = 68 cmH2O
FLOW = 560 cc/min.
1.0 mv
PRESSURE = 35 cmH2O
FLOW = 640 cc/min.
1.0 mv
RMS AMPLITUDE (50 dB Range)
20
60
200
600
1000
FREQUENCY (Hz)

FIGURE 32

Effect of longitudinal tension at constant pressure (70 cmH_2O) on the wall displacement spectra with internal and external fluid loading. The flow rate was constant at 550 cc/min.

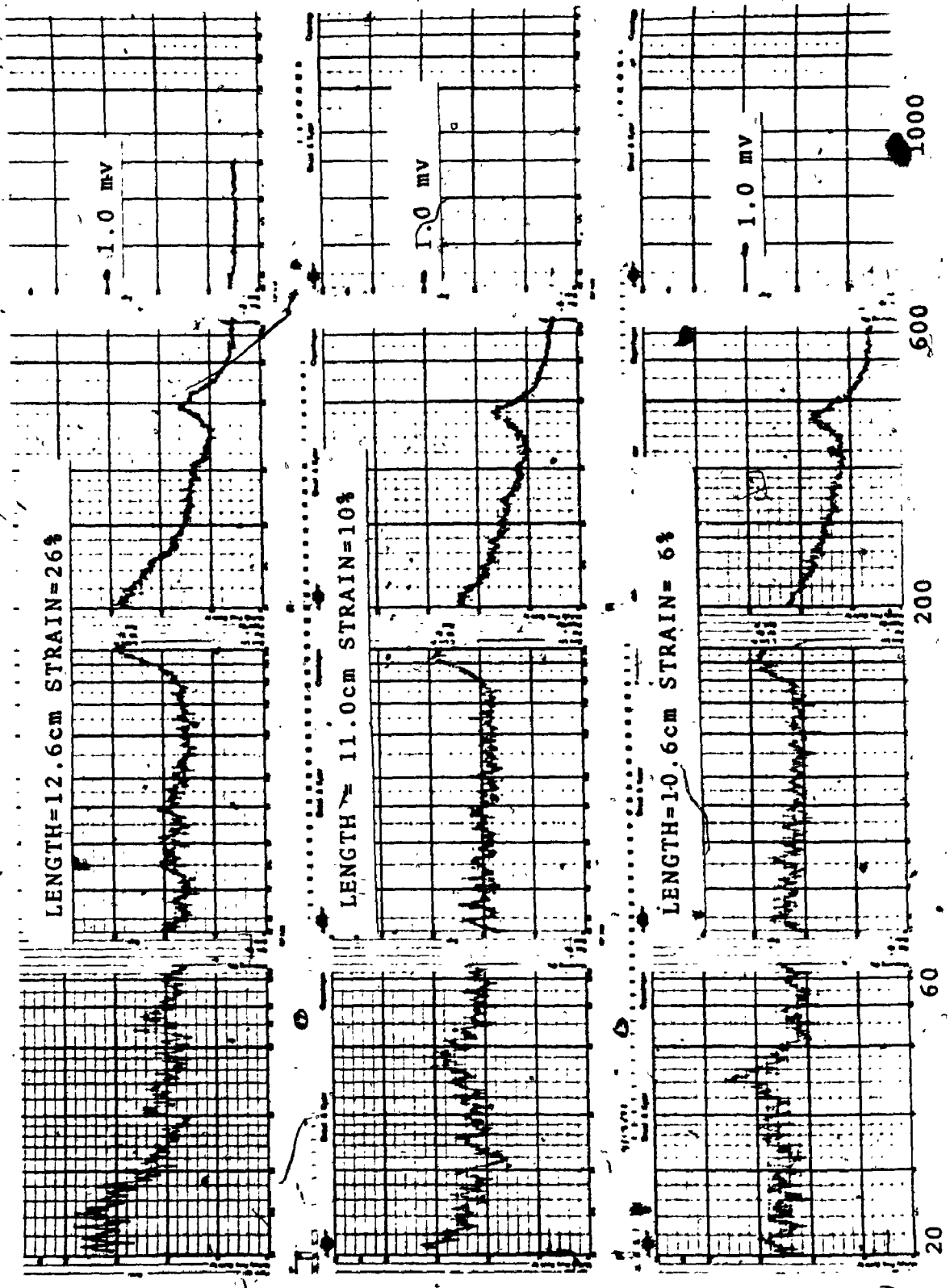
LENGTH=12.6cm STRAIN=26%
LENGTH= 11.0cm STRAIN=10%
LENGTH=10.6cm STRAIN= 6%
1.0 mv
1.0 mv
1.0 mv
1000
600
200
60
20
FREQUENCY (Hz)
RMS AMPLITUDE (50 dB Range)

The effect of increasing the longitudinal tension is shown in figure 32. The change in the dominant circumferential mode is even more pronounced than in the previous test due to the change in tension being considerably more. Much of this change is due to a narrowing of the vessel (smaller radius) as the sample is extended. The change in the beam mode from 35Hz is not obvious in this figure. However, at a higher flow rate and lower pressure as in figure 31 the change becomes more evident. This mode corresponds to the second low frequency peak and has increased to 46 Hz. The fundamental beam mode was off scale in figure 30B but occurs in figure 32C at 22-23 Hz.

Following the procedure established before, the effect of circumferential prestress on the high frequency peaks are shown in figures 33 and 34. The results for the n=2 mode with air internally (given in figure 31) are also displayed in figure 33 for comparison. If the resonance displayed in figure 33 corresponds to n=2 then the slope should be

$$\frac{n^2-1}{\rho_w h+2\rho_f a/n} = \frac{3}{0.43} = 7.0$$

which agrees very well with the observed slope of 7.2. Similarly, we would expect the slope for n=3 to be 26.5 which also agrees with that measured at 26.0.

Since the contribution of the longitudinal mode factor is small ($C_z^2/(2L)^2 \simeq 0.05 \times 10^4$ for $f_{1,1} \simeq 24$Hz) we may approximate the frequency for the higher order circumferential

FIGURE 33

A plot of f^2 versus T_c' for the dominant high frequency peak under internal and external fluid loading. The response with air internally is shown for comparison as the dotted line. The results for the two different lengths are at strains of 6% and 26%.

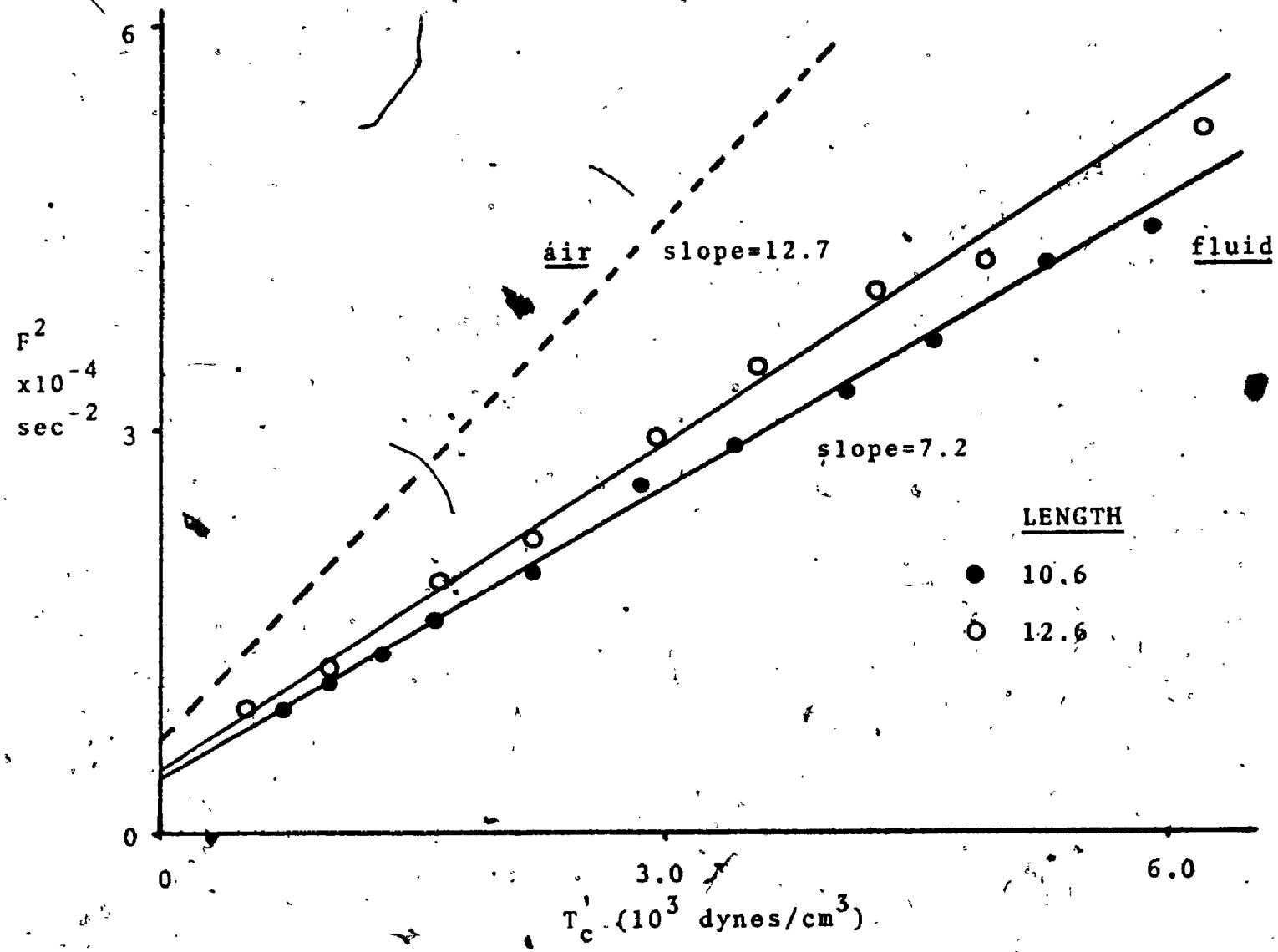
6
3
0
F^2
$x10^{-4}$
sec^{-2}
air
slope=12.7
fluid
slope=7.2
LENGTH
10.6
12.6
0
3.0
6.0
T_c' (10^3 dynes/cm^3)

FIGURE 34

A plot of f^2 versus T_c for the higher frequency peak corresponding to the circumferential mode n=3.

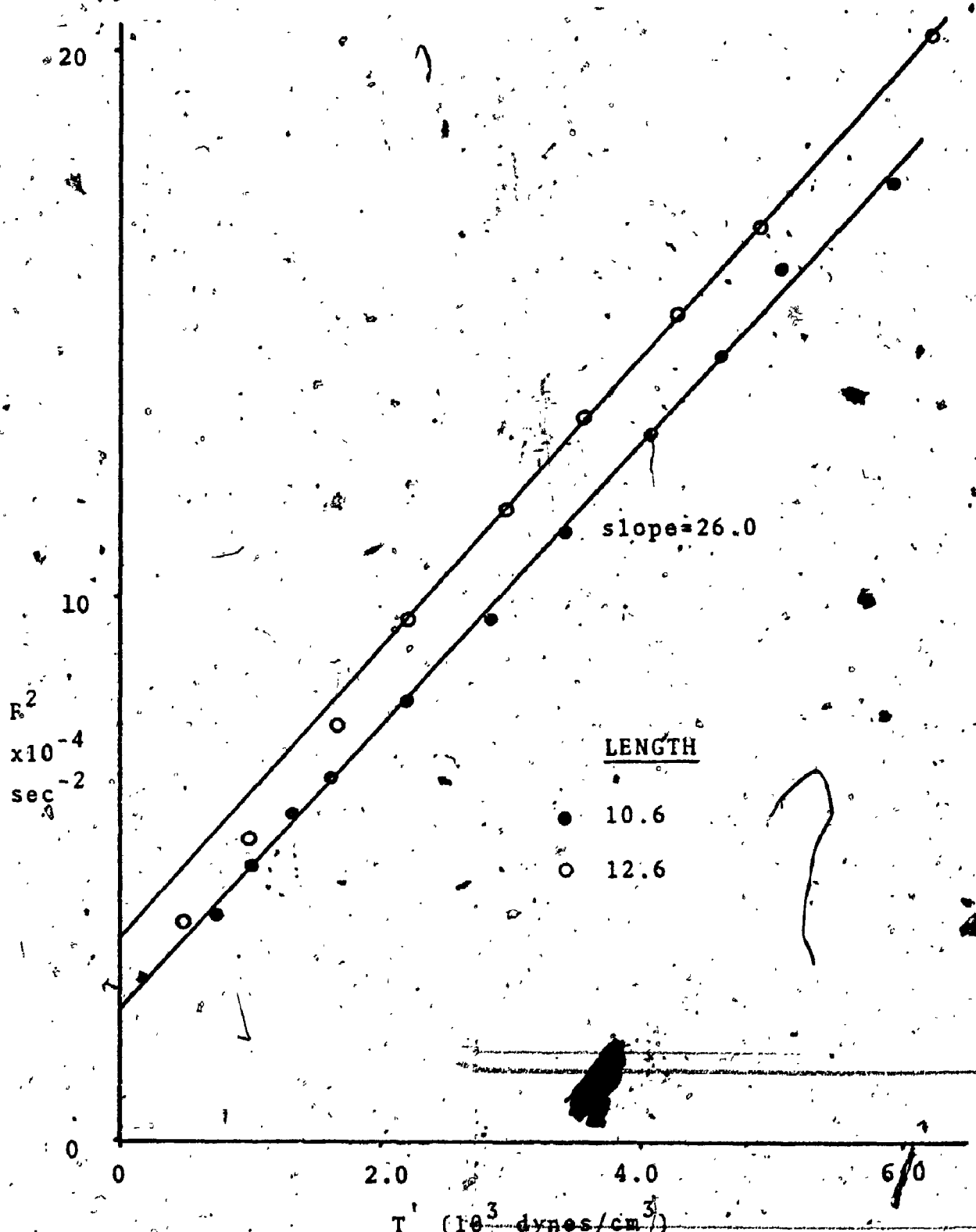
20
10
0
R^2 x10^{-4} sec^{-2}
slope=26.0
LENGTH
10.6
12.6
0
2.0
4.0
6.0
T_c' (10^3 dynes/cm^3)

modes as

$$f_{1,n}^2 \simeq \frac{n^2-1}{\rho_e h} \cdot \frac{T_o^o + n^2 \gamma A_1}{(2\pi a)^2} \qquad (27)$$

so that the intercepts are approximated by

$$\frac{n^2-1}{\rho_e h} \cdot \frac{n^2 \gamma A_1}{(2\pi a)^2}$$

Hence the ratio of intercepts between figure 33 and 34 for n=2 and n=3 should be $3^2/2^2$ x ratio of the slopes. This gives an intercept ratio of 8.5 which is significantly higher than the observed value of 6.3. However, the source of error is large here with a small change in the intercept for n=2 causing considerable change in the ratio.

Using the intercept of 2.5×10^4 for n=3 this gives a value of $\gamma A_1/(2\pi a)^2 = 107$ ($\gamma A_1 \simeq 750$) which agrees reasonably well with that obtained under vibration in air ($A_1 = 790$). Substituting this value into equation 27 along with $T_o^o/(2\pi a)^2 = 2.5 \times 10^3$ for the prestressed condition in chart 31C and using $\rho_e h = \rho_w h + 2\rho_f a/n = 0.24$ for n=4 then $f_4^2 = 26.3 \times 10^4$ or $f_4 = 512$ Hz. As is obvious from figure 31C this calculated resonance coincides with the small peak suggested earlier as the higher order circumferential mode n=4.

The decrease in high frequency vibration as the pressure was increased in figure 31 was due to a decrease in flow rate (640 to 400 cc/min) with a corresponding

decrease in Reynolds number (1450 to 900). As mentioned in the previous section this problem was eliminated by using a pump.

The effect of increasing longitudinal tension on the fundamental beam mode, m=1, which was obscured in figure 32 because of the low frequency (off scale), is shown in figure 35 where a sample of shorter length was used ($f^2_{m,1} \propto 1/L^2$). As done previously the results are plotted in terms of f^2 or $C_z^2/(2L)^2$ versus $\epsilon_z/(2L)^2$. Considering the errors involved in resolution here, with the frequency changing only from 21 Hz to 26.5 Hz, the resulting straight line appears to be a reasonable fit. Since we have $f^2_{m,1} = m^2 \frac{(T^o_z+\gamma A_2)}{\rho_e h\ (2L)^2} = \frac{m^2}{\rho_e h}\{E_z h\epsilon_z/(2L)^2+\frac{\gamma A_2}{(2L)^2}\}$ then the slope of f^2 versus $\epsilon_z/(2L)^2$ should be m^2E_zh/ρ_eh. But for the beam mode (from equation 15b) $\rho_eh=\rho_wh+\rho_fa/n$ which equals 0.44 so that for m=1 and h=0.035 cm. we have $E_z = \rho_eh/h$ x slope. Since the measured slope from figure 35 is 1.2×10^6 we find $E_z=1.5\times10^7$ which agrees quite well with that obtained in air. However, the intercept gives $\gamma A_2=7.7\times10^4$ which is higher than the previous result (6.4×10^4). Considering the errors inherent in the approximation of length, thickness and diameter, however, the results seem quite reasonable.

Geometry

The effect of a decrease in radius under the same prestress conditions is illustrated in the figure 36.

FIGURE 35

A plot of f^2 versus the longitudinal strain factor for the beam mode n=1 under internal and external fluid loading.

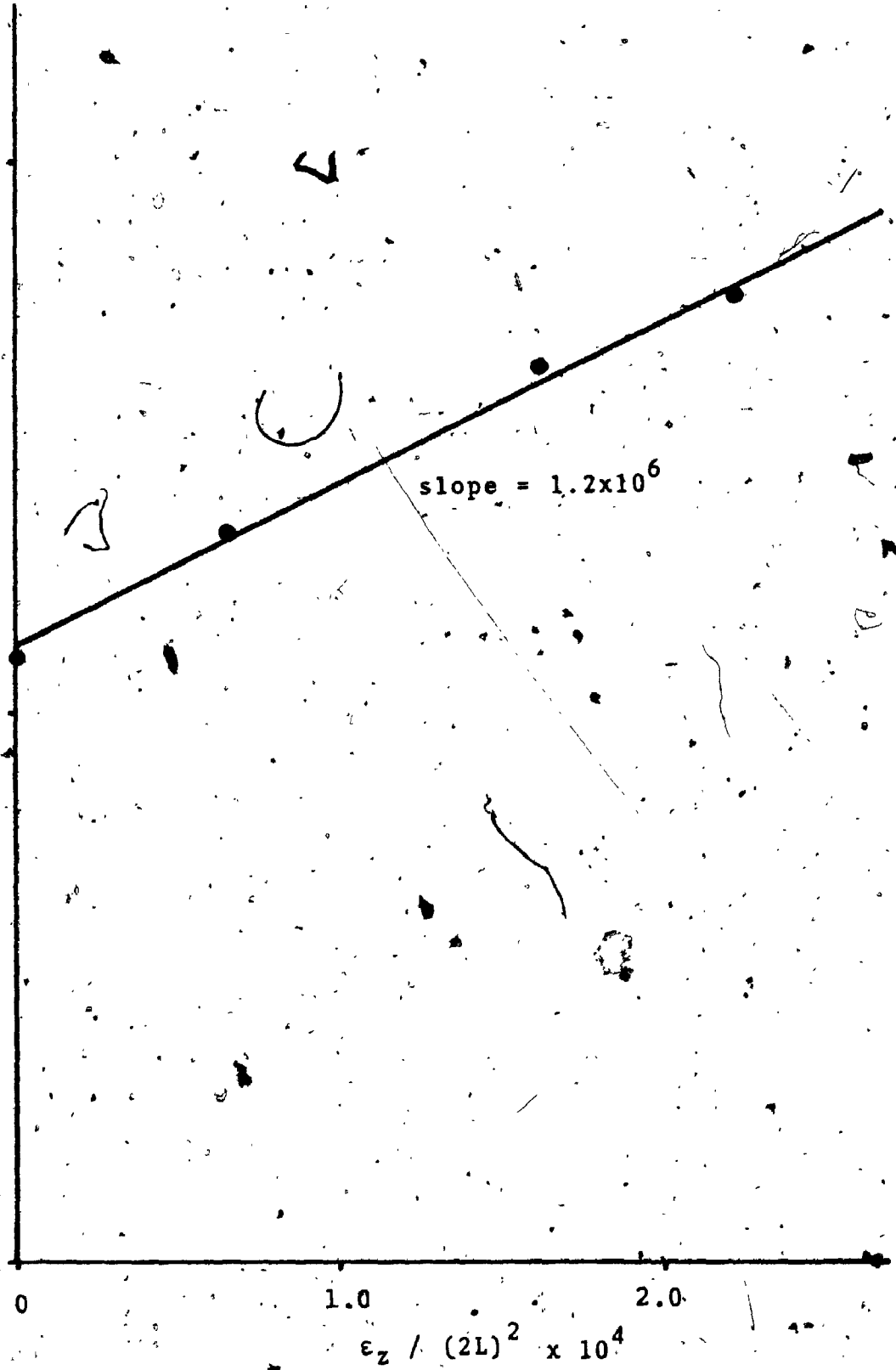
.08
.04
0
F^2
$x10^{-4}$
sec^{-2}
slope = $1.2x10^6$
0
1.0
2.0
$\varepsilon_z / (2L)^2 \times 10^4$

FIGURE 36

Wall vibration spectra under disturbed flow for the large and small penrose tubing. The pressures are 96 cmH_2O and 92.5 cmH_2O and the lengths are 8.1 cm (4.5% strain) and 7.4 cm (5% strain), respectively. The flow rate was constant at 900 cc/min. giving Reynolds numbers of 2150 and 2850, respectively.

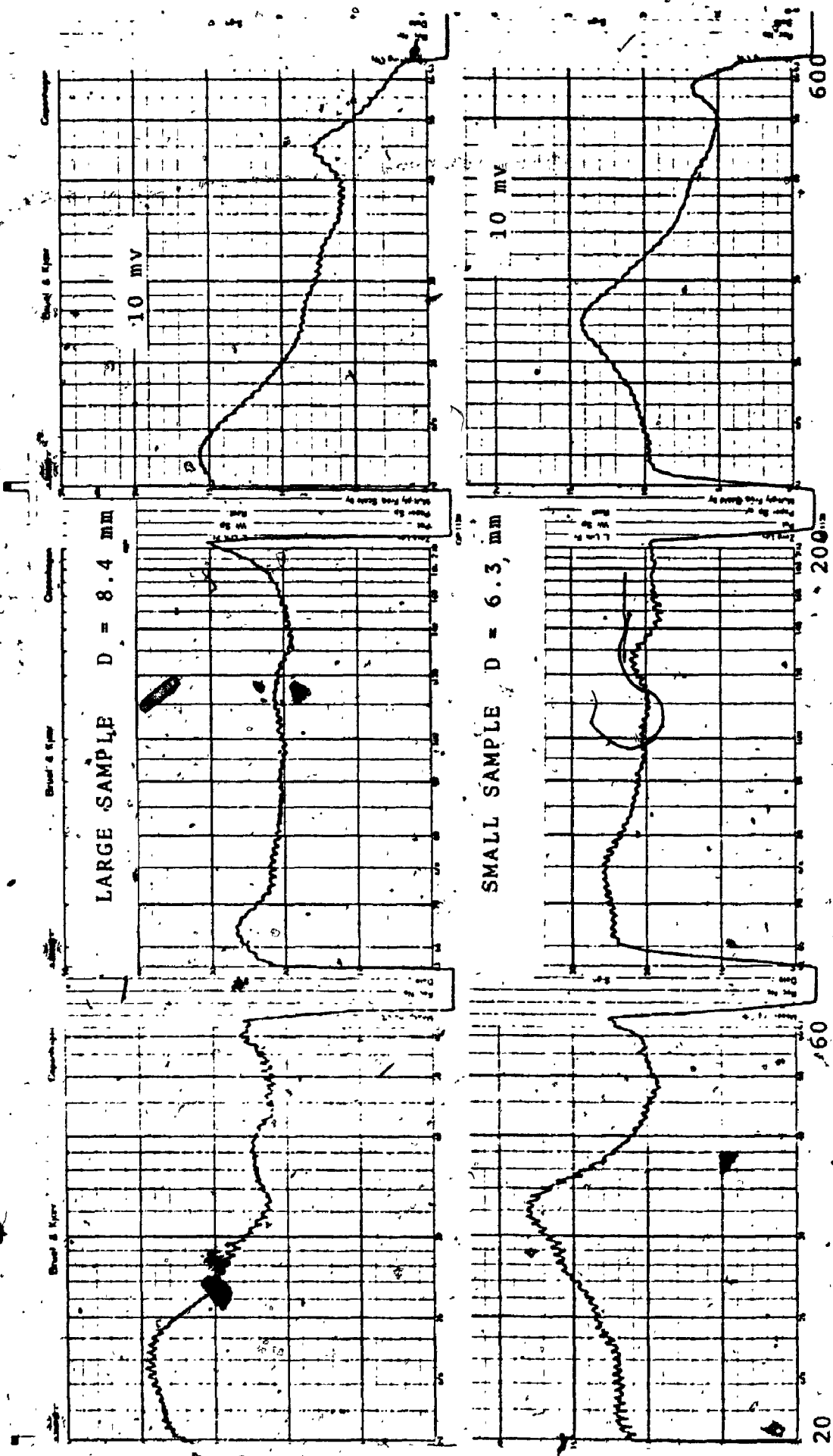
LARGE SAMPLE D = 8.4 mm
10 mv
SMALL SAMPLE D = 6.3 mm
10 mv
RMS AMPLITUDE (50 dB Range)
FREQUENCY (Hz)
20
60
200
600

As expected the higher order circumferential modes n = 2 and n = 3 increase in frequency from 210Hz to 270Hz and 450Hz to 570Hz respectively. The results of a test done on the smaller sample at different pressures is shown in figure 37 with the previous results (figure 33) for the large sample included for comparison. The frequency information is plotted as a function of pressure rather than Tc to accentuate this geometrical difference ($T_c' \propto \frac{P}{a}$).

The expected slope of f^2 versus P would be $\frac{n^2-1}{\rho_e h} \frac{1}{4\pi^2 a}$. For P in cmH_20, a = 0.32cm, h = 0.03cm and n=2 we find the expected slope to be 6.7×10^2 which is not substantially different from the measured slope of 6.2×10^2. However, the intercepts, which should be in the same ratio as the slopes (if m is the same and the term is small enough to be negligible), are significantly different, giving a ratio of 3.5 rather than 1.5 as expected. This result suggested that the longitudinal mode for the results on the small tube was greater than m = 1. This suggestion was confirmed when the results of a longitudinal scan were plotted (see figure 38). The amplitude distribution suggests that the mode shape corresponds to m = 2.

The reason for the dominance of the m=2 peak is probably related to the poor resolution between the different longitudinal mode shapes for the higher frequency circumferential modes. That is the term

FIGURE 37

A plot of f^2 versus Pressure for the small sample with the results on the large sample included for comparison.

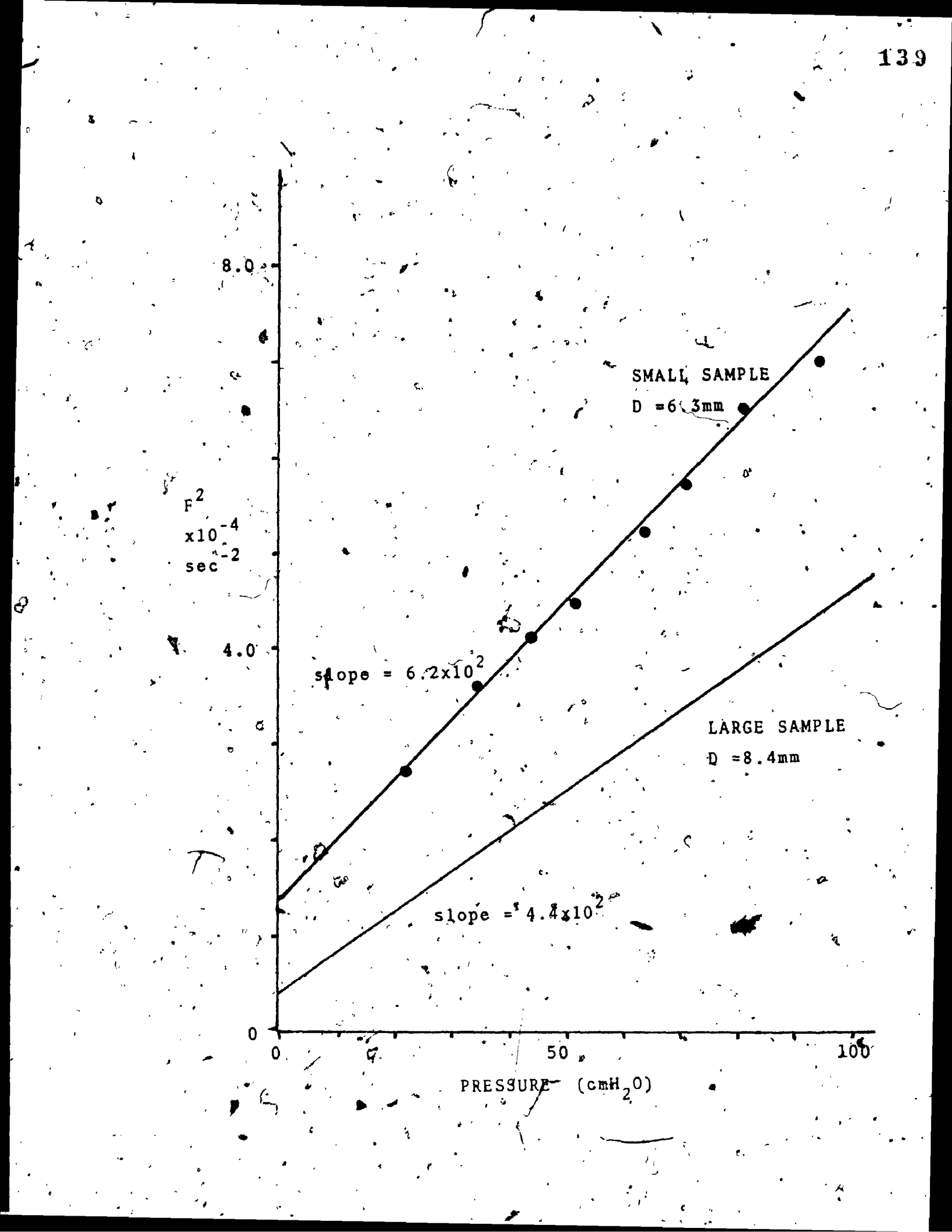
8.0
4.0
0
0
50
100
F^2 x10^{-4} sec^{-2}
PRESSURE (cmH_2O)
SMALL SAMPLE
D = 6.3mm
LARGE SAMPLE
D = 8.4mm
slope = 6.2×10^2
slope = 4.4×10^2

WALL DISPLACEMENT SPECTRA
USING
HP 3580A SPECTRUM ANALYZER

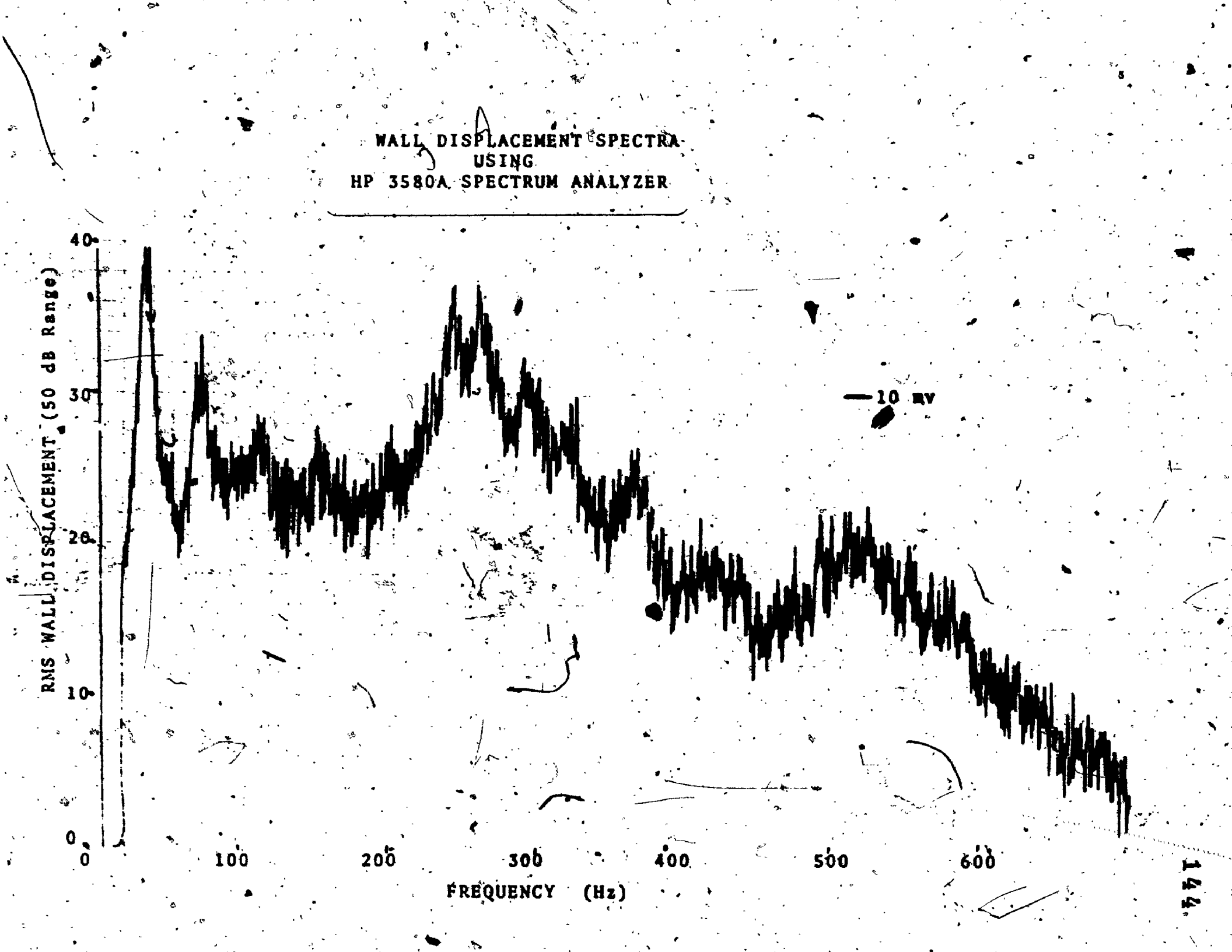

3 4

OF/DE

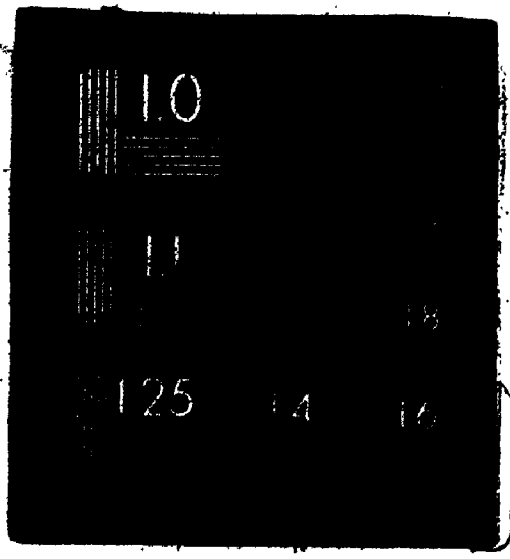

FIGURE 38

A plot of amplitude versus axial position for the peak at 235 Hz under disturbed flow with internal and external fluid loading suggesting an axial mode shape of m=2.

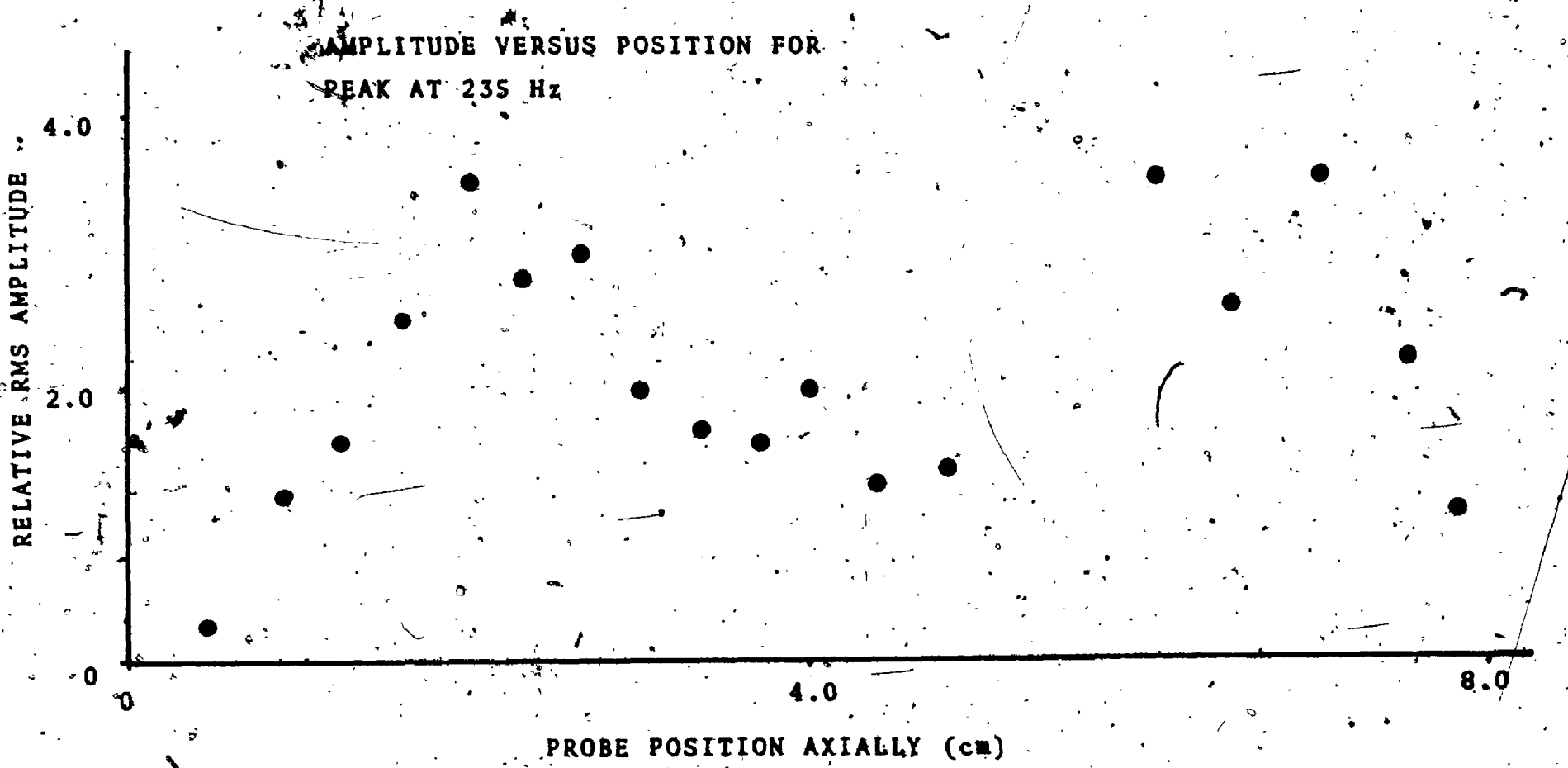
AMPLITUDE VERSUS POSITION FOR
PEAK AT 235 Hz
RELATIVE RMS AMPLITUDE
4.0
2.0
0
0
4.0
8.0
PROBE POSITION AXIALLY (cm)

$C_s^2/(2L)^2$ is small relative to the one related to circumferential prestress which when coupled with the decreasing resolution of the constant percentage bandwidth analyzer (15HzBW at 250Hz) prevents proper discrimination of the lower order modes. Greater frequency discrimination of the signal was obtained when a constant bandwidth analyzer (as low as 1HzBW) became available. The result of its use is shown in figure 39 which indicates more clearly the different longitudinal modes associated with a particular circumferential mode, n.

The results for the n=2 mode of the small sample under different circumferential prestress are shown in figure 40 using this improved resolution. The lower intercept associated with the smallest peak observed in these results confirms what was previously suggested. That is, the ratio of intercepts for the n=2, m=1 mode between the small and large tubing should be approximately 1.5, which this latter result confirms.

By plotting the intercepts in figure 40 versus the value m^2 corresponding to the expected longitudinal mode shape, the result shown in the upper part of figure 40 was obtained. The slope of this plot is equal to $C_s^2/(2L)^2$ which can be compared with the expected value. Using $E = 1.6 \times 10^7$, h=0.03, the imposed strain

3 4

OF/DE

FIGURE 39

Wall vibration spectra using the HP3580A spectrum analyzer for the small sample under internal and external fluid loading at a pressure of 67 cmH_2O and a length of 9.6 cm (strain = 20%).

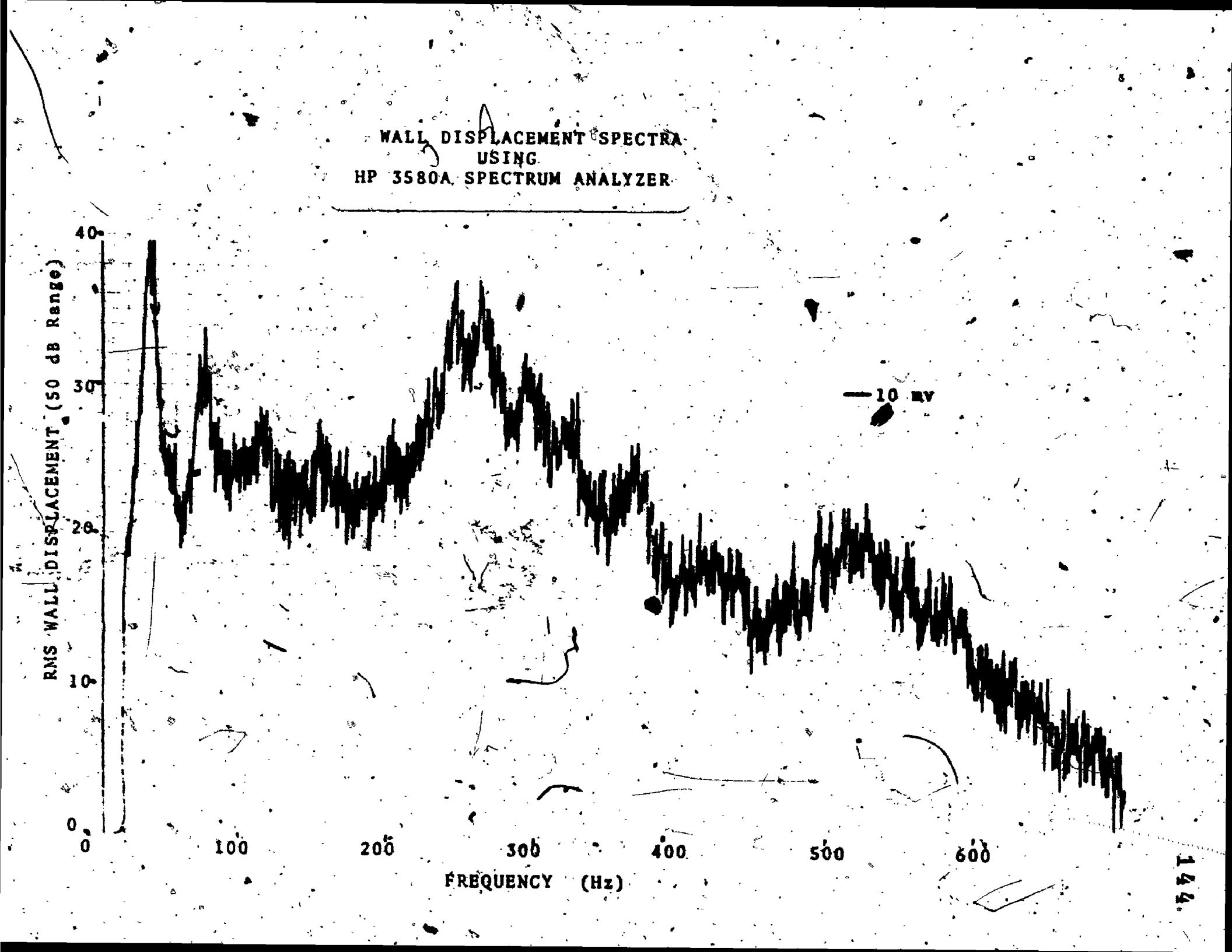
WALL DISPLACEMENT SPECTRA
USING
HP 3580A SPECTRUM ANALYZER
RMS WALL DISPLACEMENT (50 dB Range)
40
30
20
10
0
10 mV
0
100
200
300
400
500
600
FREQUENCY (Hz)

FIGURE 40

A plot of f^2 versus T_c for the results obtained similar to that in figure 39. The intercepts obtained from this plot are shown in the upper part of the figure plotted against m^2. The peaks have been assumed to correspond to m=1,2 and 3 for the circumferential resonances n=2.

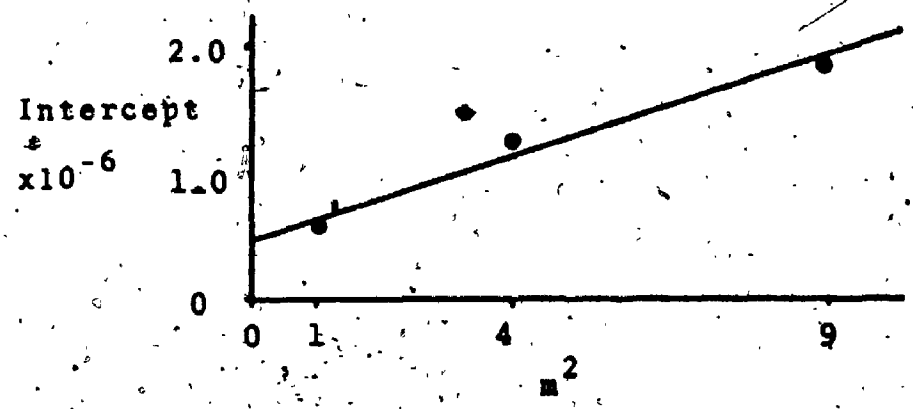
Intercept
x10^-6
2.0
1.0
0
0
1
4
9
m^2

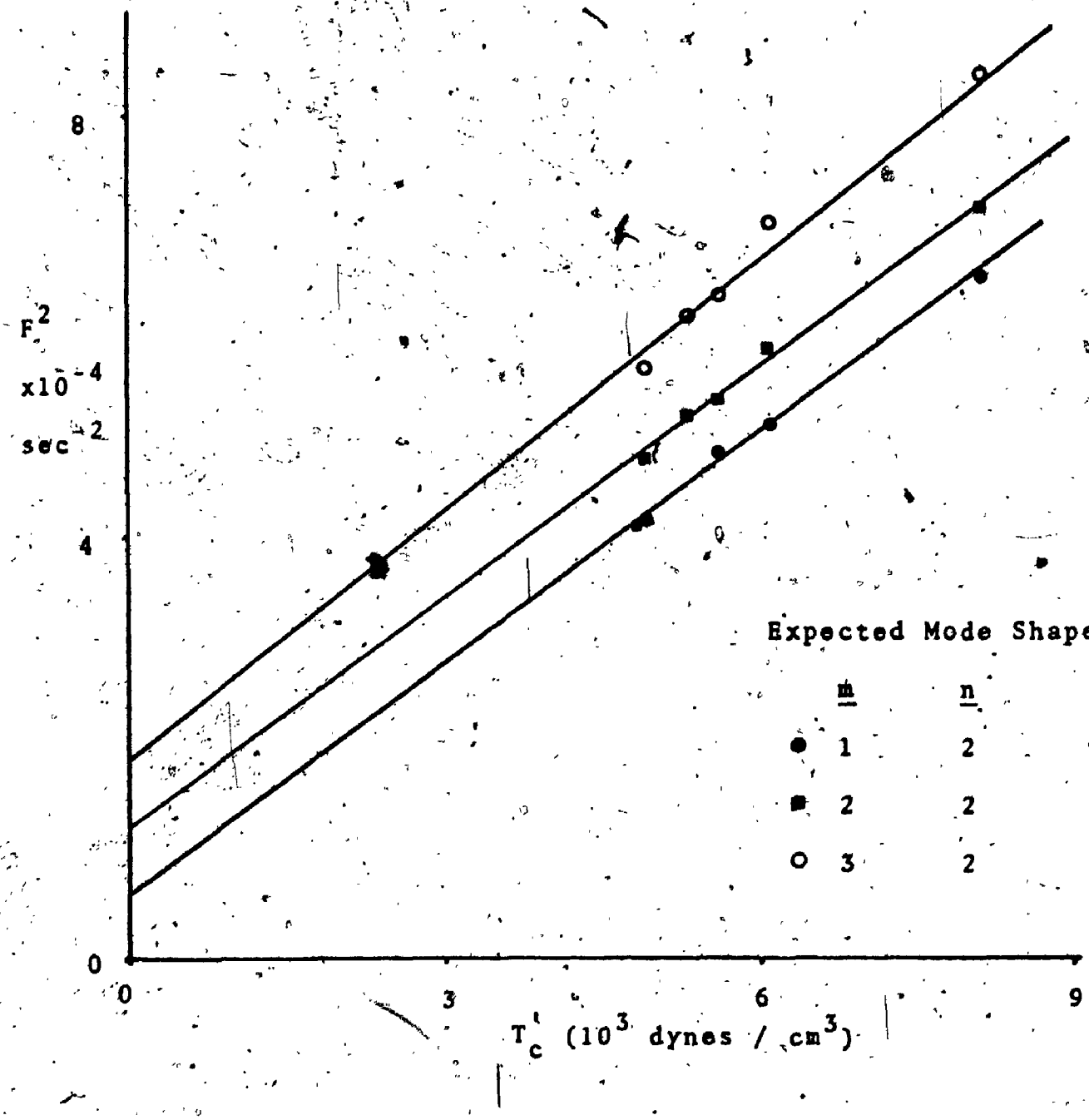
F^2
x10^-4
sec^-2
8
4
0
0
3
6
9
T'c (10^3 dynes / cm^3)
Expected Mode Shape
m
n
1
2
2
2
3
2

of 0.186 at L=9.1, and $\gamma A_2 = 6.4 \times 10^4$, then $(T_s^o + \gamma A_1)/(2L)^2$ = 465. But $\rho_e h_{n=2} = 0.33$ so that $C_s^2/(2L)^2 = 1.4 \times 10^3$. The observed slope was 1.7×10^3.

From the various tests it was also obvious that the beam mode resonance was inversely related to length. From the beam mode which is the most susceptible to changes in length we expect $f^2_{m,1} = m^2 C_s^2/(2L)^2$. Thus for two samples (smaller radius) of different lengths (9.1 and 4.5 cm) that were exposed to similar longitudinal strains (18%) a ratio of the frequencies for the dominant beam mode was found to be 35/75 or 0.48. From the lengths we would expect the inverse ratio of 4.5/9.1 or 0.495 which shows very good agreement with that observed.

Correlation Studies

When an additional photonic sensor become available cross correlation of the two signals was possible. With the two sensors located longitudinally at positions 17% and 84% (not specifically chosen) of the sample length, successive filtering at the resonant frequencies 35, 72, 114 (see figure 39) produced cross correlation signals that were alternatively in phase and out of phase (180^o) respectively. This is precisely what was expected with the three frequencies corresponding to the beam modes n = 1, m = 1, 2 and 3.

Unsatisfactory results were obtained when the filters were set around the different mode shapes m for the circumferential resonance, n = 2. This resulted from the fact that the bandwidth of the filters in this range was too large (15HzBW) to permit the discrimination between the different longitudinal modes. However, when the filters were set to one of the higher frequency longitudinal modes (of n=2) that was sufficiently distinct (the 370Hz peak in figure 39 for example) the results were more satisfactory. By moving the one probe longitudinally to four other locations, the respective alterations in phase from the cross correlograms permitted an evaluation of the 370Hz peak as m=6.

By locating the two probes at the same longitudinal point, but separating them circumferentially to a maximum of 120°, justification of the expected circumferential modal pattern was provided. For example, the auto and cross-correlation of the signals filtered at 260Hz and 550Hz for the sensors located 120° apart are shown in figure 41. As illustrated in this same figure, for a separation of 120° we would expect a phase change of 180°, for the n = 2 mode and a phase change of 0° for the n=3 mode. Both of these results were observed, as was an expected 180° phase change for the filter at the beam mode (n 1,m=1). When the probes were separated by 90° the 260Hz signal was still 180° out of phase but the 550Hz signal changed from 0° to 180°. Finally, at 60°

FIGURE 41

Correlation results upon filtering at the circumferential resonant frequencies corresponding to n=2 and n=3. The probes were separated by approximately 120%. The small phase shift observed is an artifact due to the instrumentation but was constant at 125 micro seconds.

AUTO AND CROSS CORRELATION OF FILTERED SIGNALS AT THE RESONANT FREQUENCIES 260 Hz AND 550 Hz

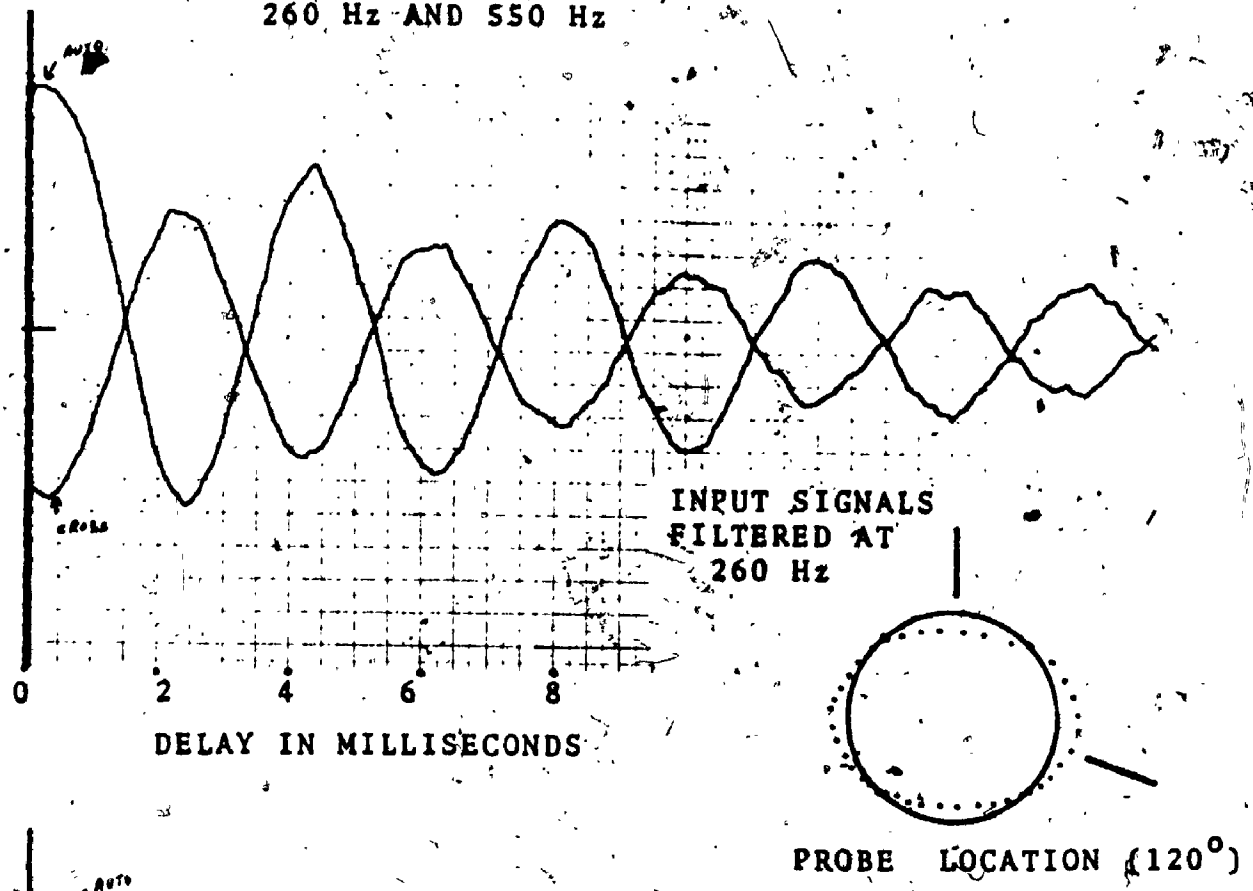

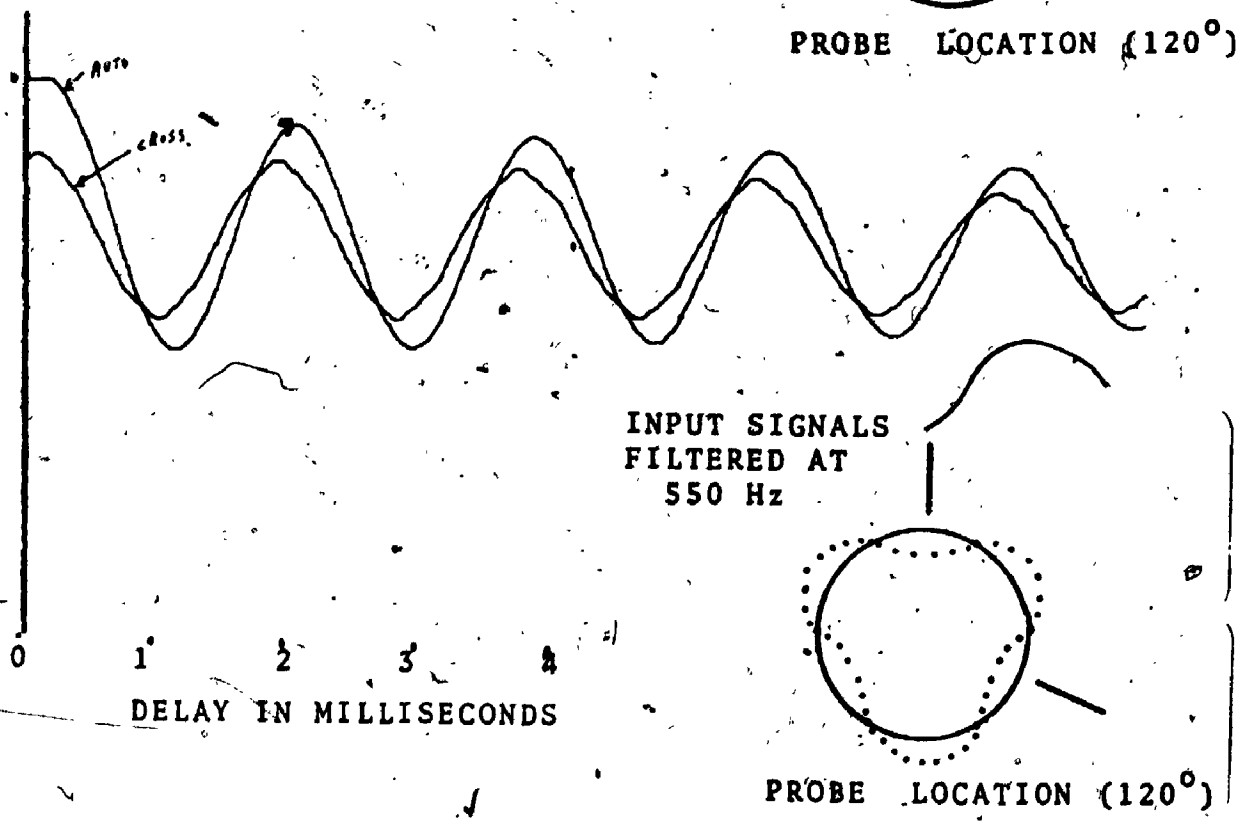

separation the respective phase changes were 0° and 180° confirming that the mode shapes were n=2 and n=3 respectively.

Discussion

The preceding experimental analysis has convincingly demonstrated the validity of the model presented in chapter III. The implications of these studies to biological material are that wall stress and geometry are the dominant factors governing the resonant frequency. By knowing just the pressure and radius of the vessel of interest, a good estimate of the dominant circumferential resonance can be obtained.

The results also confirm the importance of the acoustical media in determining the resonant frequency. This validity of the inertial term emphasizes the different response that would be expected between bronchi and arteries. In this regard the approach by Anliker & Maxwell (1966) with respect to wave propagation in arteries would seem to be in error. Their approach does not consider the additional inertial response of the external medium but only that of the internal fluid. As is obvious from the present results this would result in a significant error in the calculated wave propagation speeds.

The approach by Anliker & Maxwell would also lead to an additional term $\frac{E_e h}{\rho_e h (2\pi a)^2}$ on the right hand side of equation 26. The result would be an extremely large

intercept $\simeq 10^5$ sec^2 for the mode n=2, m=1, which is clearly not observed.

The additional description of the bending terms appears to adequately describe the non-zero intercepts of the frequency squared - stress relations, particularly that term for the circumferential component γA_1. This term was much easier to evaluate which may account for its successful description. The dominating effect of this term over the longitudinal term γA_2 may allow us to ignore the latter term. The observed results for this latter term appear to be higher than that expected and may reflect an additional term that has been overlooked. However the term is more complicated to evaluate and further comparison is avoided.

Seemingly only for the beam mode, the term $\frac{C_a^2}{(2L)^2}$ does not appear to be constant with the longitudinal mode shape factor, m. Thus, a plot of $f_{m,1}^2$ versus m^2 led to a non-linear response rather than a straight line. The results appeared to show dependence on a m^4 term, which does occur in the term γA_2. However, as will be discussed later, the beam mode does not appear to be an important one when considering the response physiologically.

The cross correlation results justify the assumption that the sample is being stimulated at its resonant modes when exposed to disturbed flow. By noting the respective phase relations between the sensors, the cross correlation provides evidence as to whether standing waves are being

set up. These results on disturbed flow indicate that the vessel wall is stimulated over a fairly large frequency range.

The adequate representation of the model

$$f^2_{m,n} = \frac{1}{\rho_e h}\ m^2\ \frac{T_s^o + \gamma A_2}{(2L)^2} + (n^2-1)\ \frac{T_e^o + n^2\ \gamma A_1}{(2\pi a)^2}$$

where $\rho_e h = \rho_w h$ in air, $\rho_e h = \rho_w h + \rho_f \frac{a}{n}$ with fluid externally, and $\rho_e h = \rho_w h + \frac{2\rho_f a}{n}$ for fluid internally as well as externally is summarized in figure 42. The results obtained under disturbed flow are used for the three types of experiment with the calculations based on $E=1.6\times10^7$, $\gamma A_2 = 6.4\times10^4$ and $\gamma A_1 = 790$.

The results summarized in figure 42 indicate that the model presented describes the higher frequency, asymmetrical, resonant modes of an elastic vessel, surrounded by and enclosing different acoustical media, quite well. Although no tests were conducted with fluid internally and air externally, which would be an approximation of the environment of the pulmonary artery, we would expect the inertial term, $\rho_e h = \rho_w h + \rho_f \frac{a}{n}$, to describe this situation. This suggests that we should be able to calculate the resonant frequencies of a biological vessel, knowing its wall stress, geometry, and environment.

(vi) Vibration of Arteries

Method

The left and right femoral and carotid arteries were removed from a 32 kg, male dog and stored in saline at 3°C until use. In each case the degree of retraction

FIGURE 42

Summary of the results obtained on synthetic tubing under disturbed flow. The calculated resonant frequency is plotted against the observed value for the three acoustic media tested.

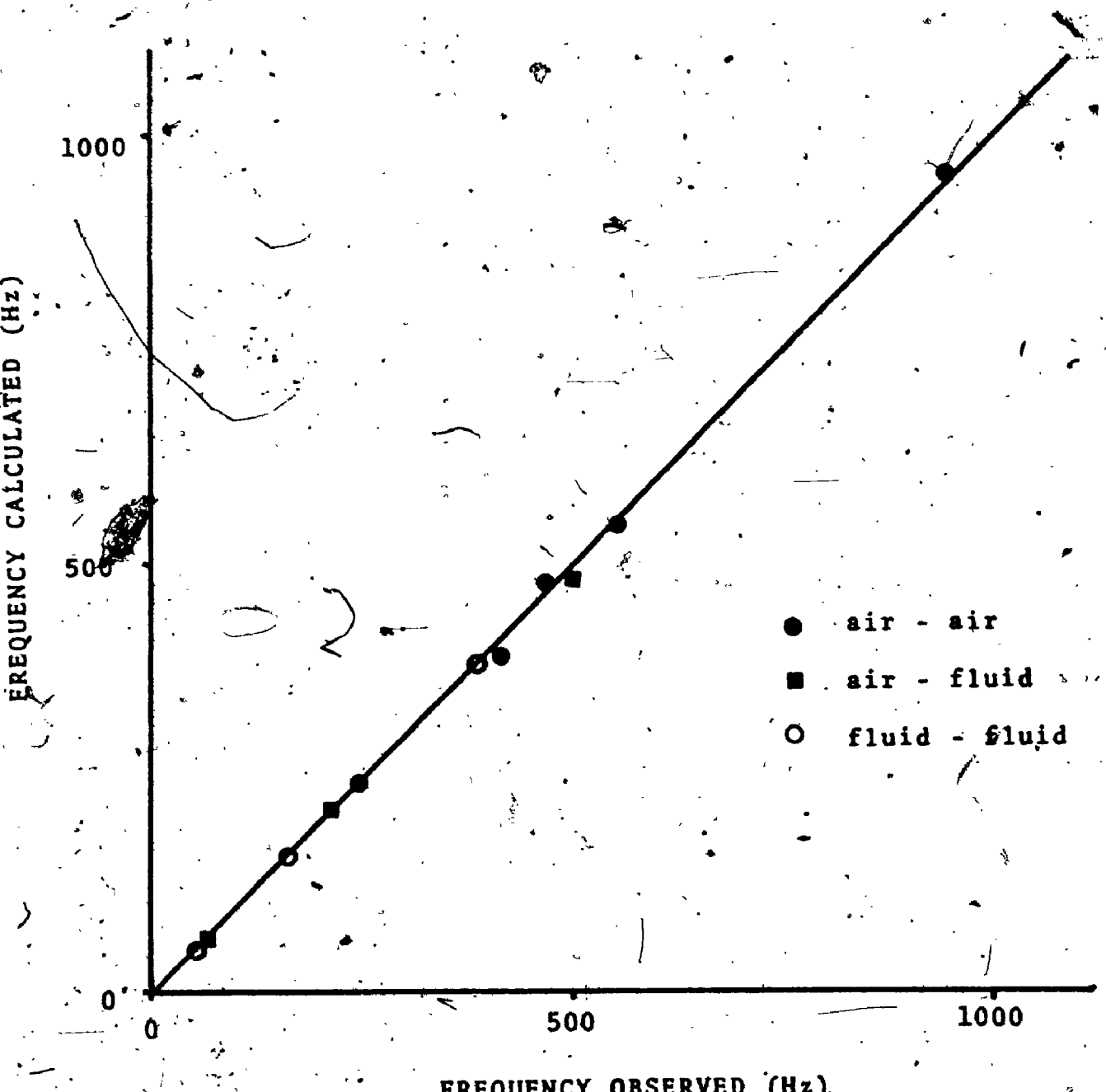
1000
500
0
0
500
1000
FREQUENCY CALCULATED (Hz)
FREQUENCY OBSERVED (Hz)
air - air
air - fluid
fluid - fluid

was noted by measuring the length between ties before removal (average about 40% based on resting length) so that the strain induced experimentally could be related to the in vivo values. The two carotids were separated into halves providing six samples for investigation. At least 24 hours elapsed before using the first sample while the final sample was examined 5 days post mortem.

The samples were mounted in a saline bath between two stainless steel tubes (3.9mm O.D.) with a plug (1.8mm I.D.) inserted at one end. This created an effective stenosis of 46% based on the outside diameter of the steel tubes. Two saline reservoirs were connected to the inflow and outflow tubes of the sample such that a constant pressure head (and hence flow rate) was maintained. By moving the two reservoirs together, vertically, the pressure in the sample could be varied (up to a maximum of 145 cm H_2O). As done previously the longitudinal prestress was varied by altering the length.

For the four carotid samples with no branches the pressure was measured at the end of the downstream stainless steel section. This meant that the pressure reading was in error by the respective pressure drop along this section. This pressure loss was estimated as 15 cm H_2O by measurements after the biological tests were conducted. The two femorals, however, had a large branch in the mid section of the sample which was used to

measure the pressure. A size 18 cannula was tied to these branches to obtain the pressure tap.

The wall thickness was measured in the relaxed state by cutting a thin section at one end of the sample and using a travelling microscope to measure the thickness. The resting wall thickness varied from the thin walled femorals (0.39 ± 0.01mm at 5.0 mm O.D.) to the thicker walled carotids (0.6 ± 0.01 mm at 4.8 mm O.D.). The thickness under prestressed conditions was estimated, as before, by using incompressibility ($h = h_o \frac{Ro}{R} \frac{Lo}{L}$). The outside diameter was obtained from calipers at several different pressures and lengths.

Following the procedure used previously, the surface reflectivity was increased by spraying a small aluminum spot at the point of interest. This was done while the sample was under the longitudinal prestress of interest and a pressure of approximately 90 cm H_2O. This was done because of the significant changes in geometry during variations in prestress (5.0 to 6.0mm O.D. variation at in vivo strain between 30 cm H_2O and 140 cm H_2O). This resulted in a buckling of the small aluminum coating at the lower pressures.

The photonic sensor was located at approximately ½ or 1/4 of the sample length and the signal was recorded on the Nagra tape recorder. Since there was a certain

amount of initial creep of the tissue a three minute stabilizing period was allowed at each new pressure and length studied. Later, a spectral analysis of an eight second tape loop was performed from each one minute record.

Results

The results obtained with biological tissue demonstrated that the dynamic response was the same as that with the synthetic material, with the dominance of the beam mode n=1 and the circumferential mode, n=2. Figures 43 and 44 show characteristic spectra under various pre stressed conditions. Figure 43 demonstrates the sensitivity of the circumferential modes to pressure with the dominant circumferential mode (n=2) changing from 265Hz at 60cm H_2O to 395Hz at 126cm H_2O, and the higher order peak from 550 Hz to 760 Hz. The additional distortion of the shoulder in figure 43A at 1200 Hz is probably the n=4 circumferential mode.

Figure 44 demonstrates the changes due to increasing longitudinal tension. The dominant low frequency peak which is probably the fundamental beam mode apparently changes from 63 Hz to 78 Hz. The smaller peak at 110 Hz in figure 44A also appears to be sensitive to longitudinal stress. It may arise from partial reflection from the branch which occurs at a shorter length. Note in figure 44 that the dominant low frequency peak which we are attributing to the fundamental beam mode, appears to be sensitive to pressure. This may be due to a change in

FIGURE 43

Effect of pressure on the wall displacement spectra of a femoral artery exposed to disturbed flow under constant tethering (strain = 46%) and constant flow rate, 290 cc/min. (Re=1100). Note that the input attenuator is adjusted in the higher frequency ranges to permit the spectrum to be displayed.

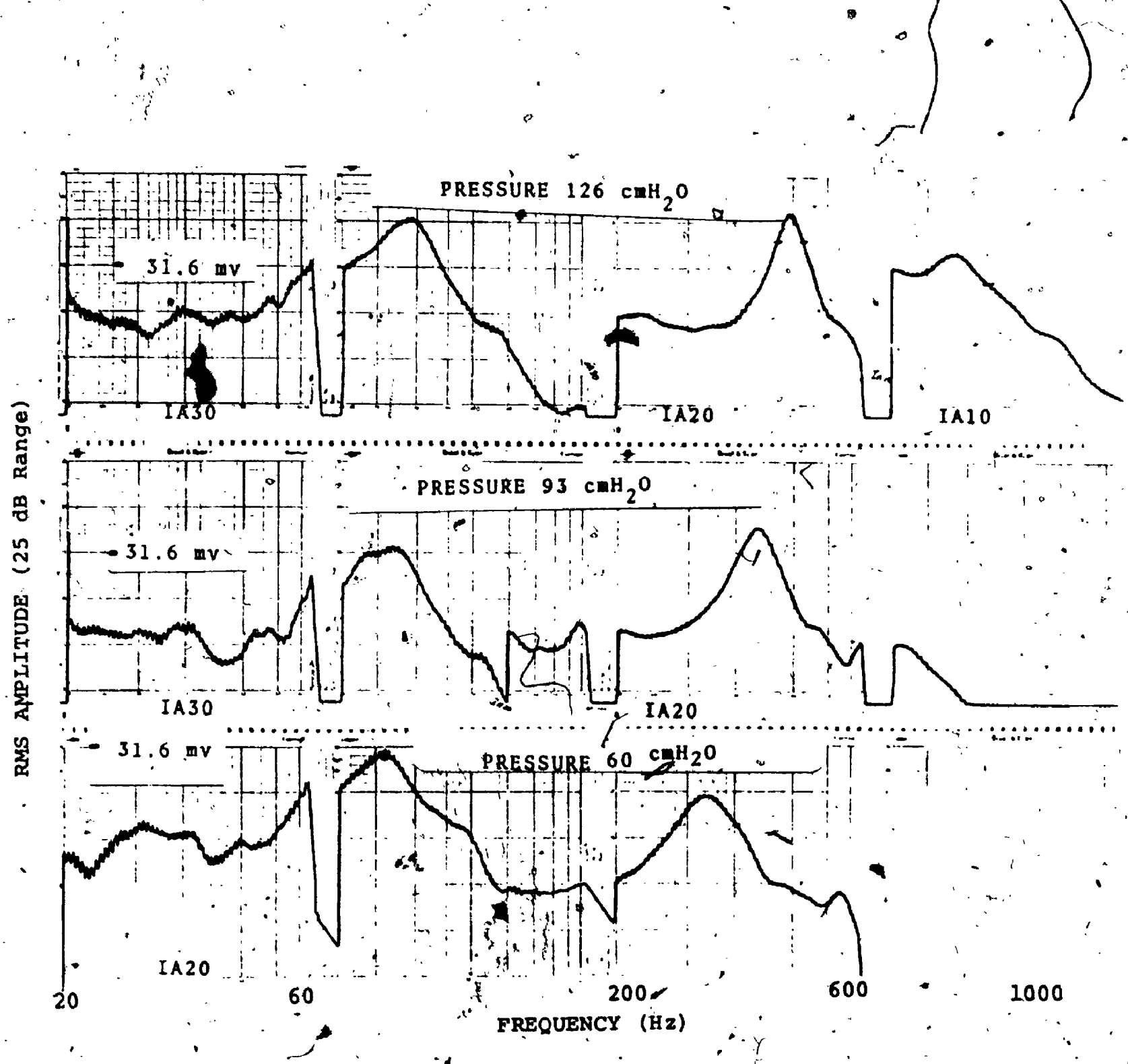
PRESSURE 126 cmH2O
31.6 mv
IA30
IA20
IA10
PRESSURE 93 cmH2O
31.6 mv
IA30
IA20
31.6 mv
PRESSURE 60 cmH2O
IA20
RMS AMPLITUDE (25 dB Range)
20
60
200
600
1000
FREQUENCY (Hz)

FIGURE 44

Effect of longitudinal tension on the wall displacement spectra of a femoral artery. The flow was constant at 290 cc/min. (Re=1100) but the pressure was not. Note the change in the input attenuator to permit the high frequency part of the spectra to be displayed.

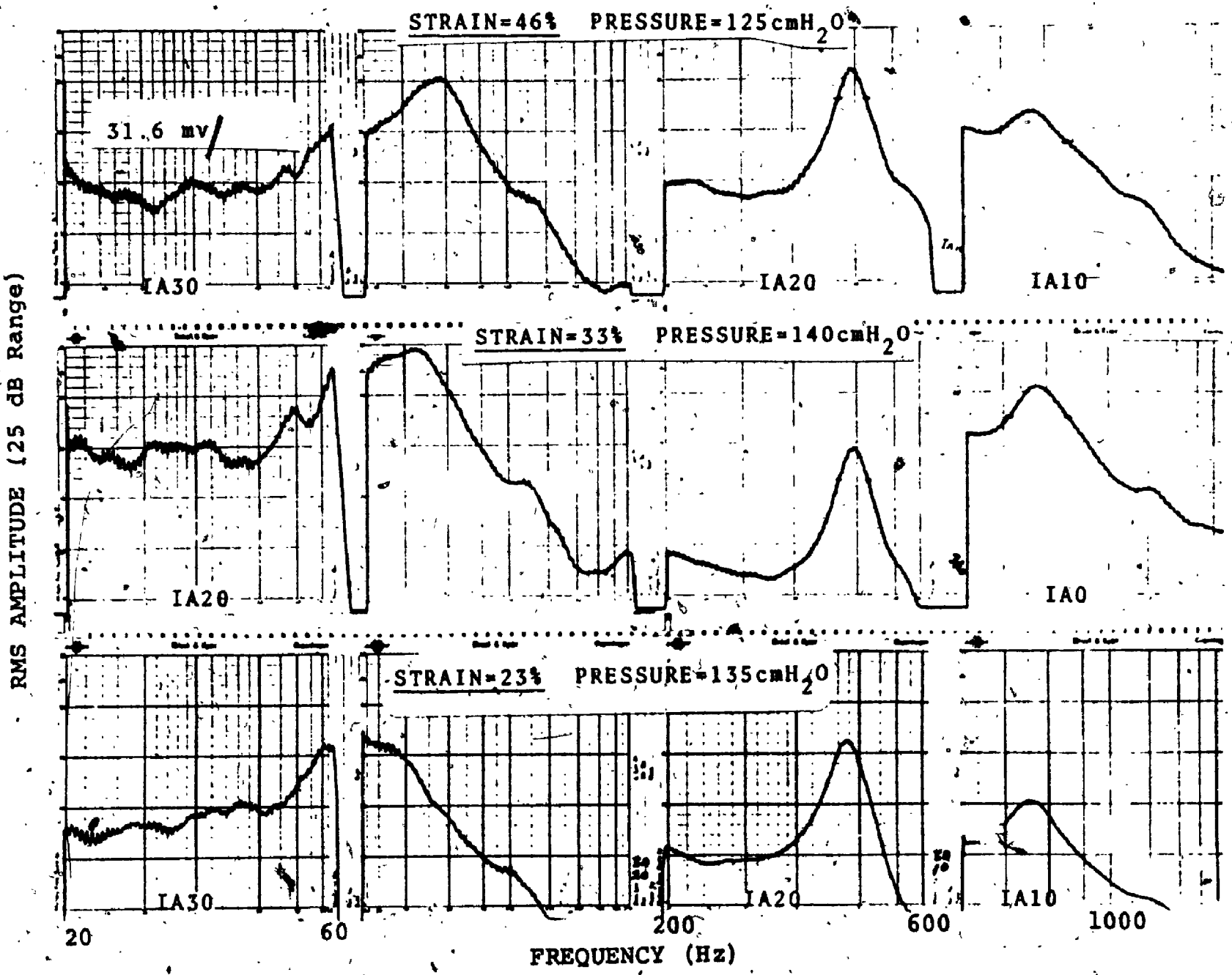
STRAIN=46% PRESSURE=125cmH2O
31.6 mv
IA30
IA20
IA10
STRAIN=33% PRESSURE=140cmH2O
IA20
IA0
STRAIN=23% PRESSURE=135cmH2O
IA30
IA20
IA10
RMS AMPLITUDE (25 dB Range)
20
60
200
600
1000
FREQUENCY (Hz)

increases with increasing pressure ($T_z = T_z^o + \nu T_c$), although no evidence of the latter was found with penrose tubing.

The frequency information for the circumferential modes in figure 43 is plotted in figure 45 and 46 for both high frequency peaks. The data provides a good fit to a straight line as in the previous tests. The results are also shown for a set done at a different longitudinal strain.

The expected slopes are given by $\frac{n^2-1}{(\rho_e h)n} = \frac{n^2-1}{\rho_w h + 2\rho_f \frac{a}{n}}$.

For the sample extended to 3.5cm (46% strain) with an outside diameter of 5.4 mm the estimated wall thickness was 0.24mm. Note that this gives an h/r ratio of less than 0.1. Using this wall thickness the mid surface radius is calculated as a = 2.58mm, so that.

$$(\rho_e h)_{n=2} = 0.282$$

$$(\rho_e h)_{n=3} = 0.196$$

Thus the expected slopes are 10.6 and 40.8. The first result shows excellent agreement with that observed while the latter appears to be about 10% high. This would not seem serious, however, in view of the approximation made.

The intercepts should provide information on the bending term γA_1 as was done previously. The intercept of the plots in figure 45 and 46 are given by

$$m^2 \frac{C_s^2}{(2L)^2} + \frac{(n^2-1)}{\rho_e h} n^2 \frac{\gamma A_1}{(2\pi a)^2}$$

FIGURE 45

A plot of f^2 versus T_c' for the dominant circumferential peak n=2 in figure 43 at two different lengths.

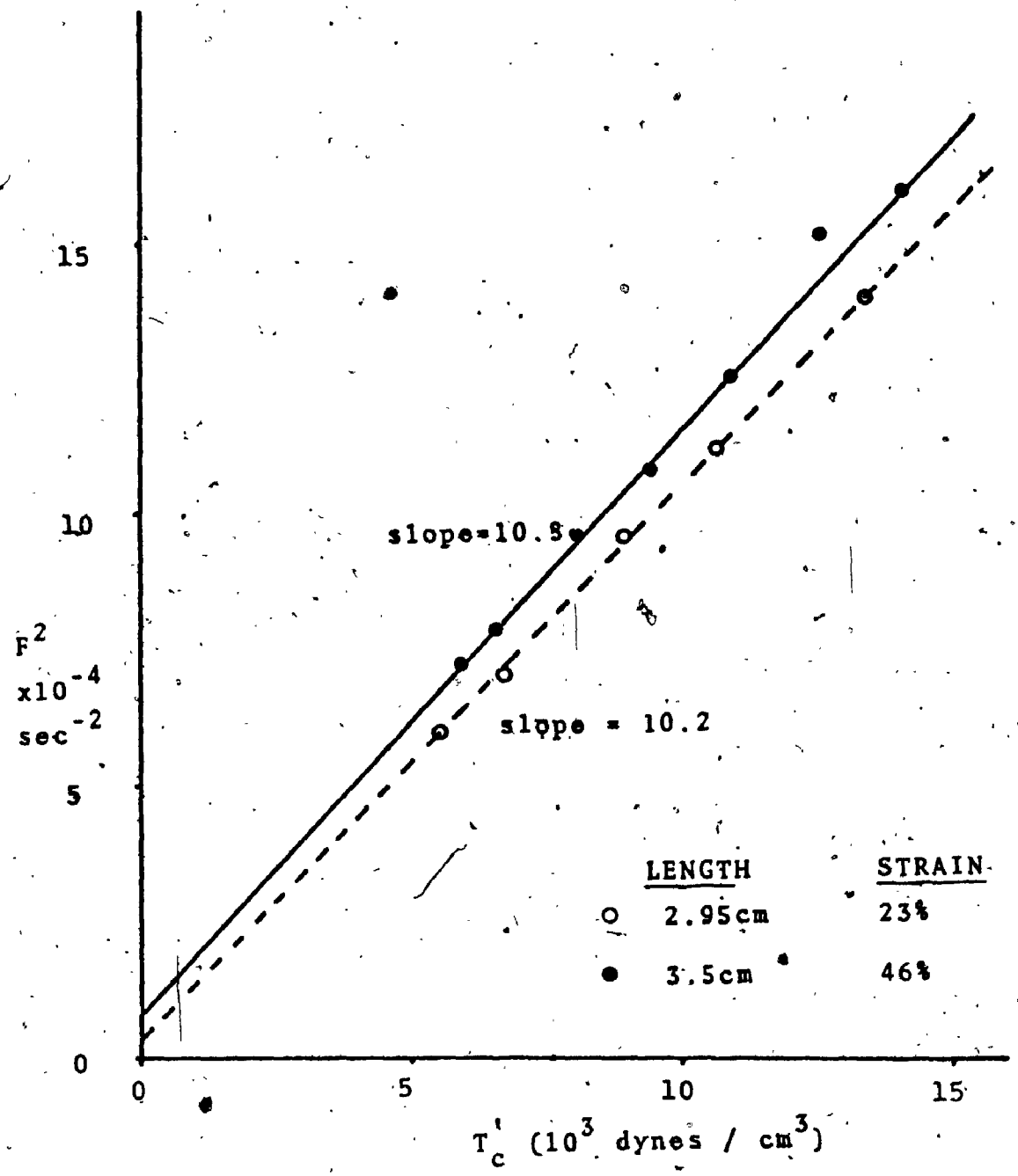
15
10
5
0
F^2 x10^{-4} sec^{-2}
slope=10.8
slope = 10.2
LENGTH
STRAIN
2.95cm
23%
3.5cm
46%
0
5
10
15
T_c' (10^3 dynes / cm^3)

FIGURE 46

A plot of f^2 versus T_c' for the higher frequency peak in figure 43 corresponding to n=3.

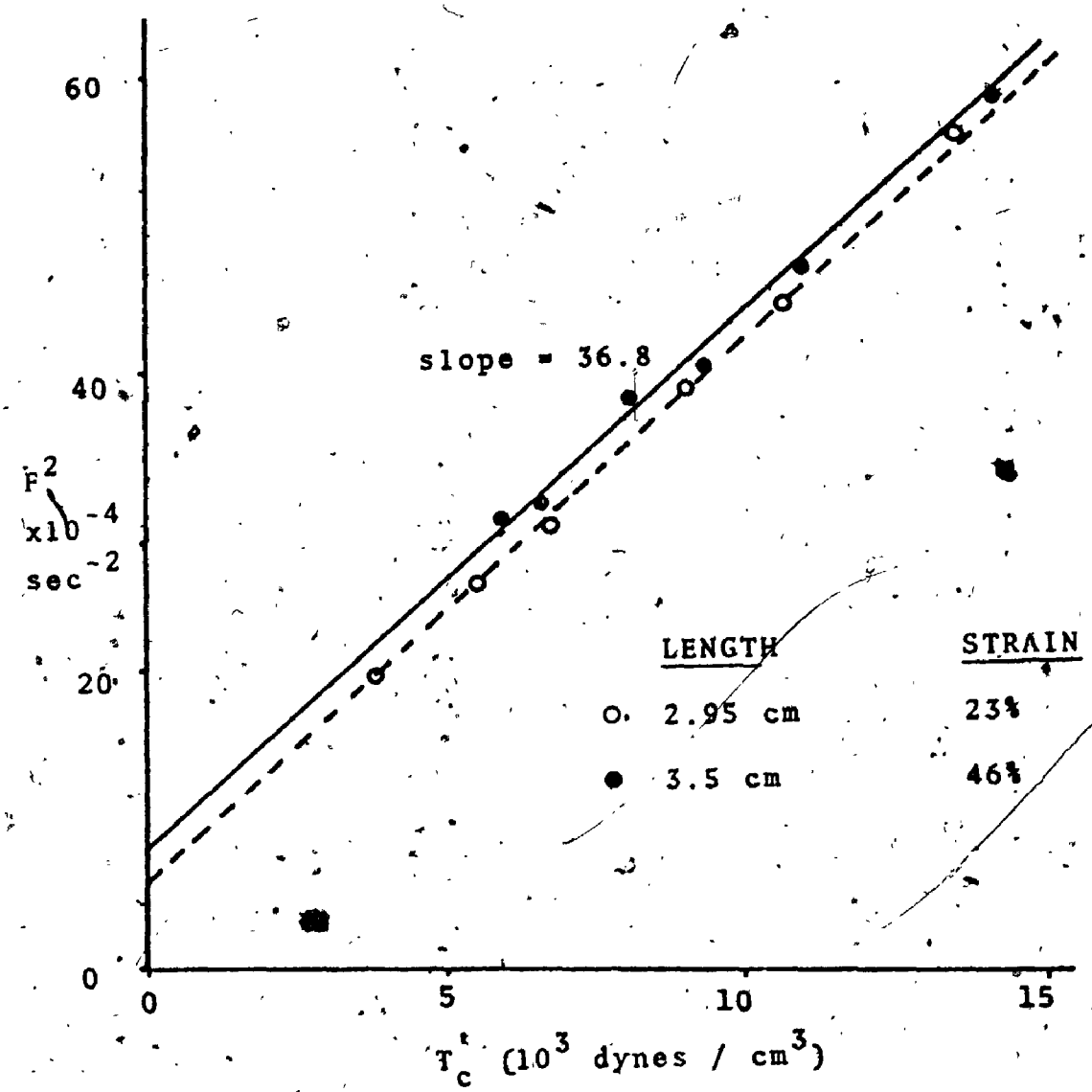
60
40
20
0
F^2 x10^{-4} sec^{-2}
slope = 36.8
LENGTH
STRAIN
○ 2.95 cm
23%
● 3.5 cm
46%
0
5
10
15
T_c^t (10^3 dynes / cm^3)

The term $\frac{C_s^2}{(2L)^2}$ is approximately 0.5×10^4 from interpretation of the beam mode so that for the intercept of figure 45 we have

$$\frac{n^2-1}{\rho_e h}\; n^2 \frac{\gamma A_1}{(2\pi a)^2} = 0.3\times10^4 \text{ or } \gamma A_1 = 1.88\times10^2.$$

Thus $A_1 \simeq 1.9\times10^6$ or $E_e \simeq 8\times10^6$ dynes/cm^2.

If we assume that the peak at 78Hs in figure 44c is the fundamental beam mode m=1, then we may plot this frequency information versus $C_s/(2L)^2$, as was done previously, to obtain an estimate of the longitudinal modulus. This result is shown in figure 47 for the information in figure 44. Because of the expected non linearily of the wall we cannot extrapolate the straight line fit of the three data points to obtain the intercept. However, at the large strains of the data points we can consider the modules to be approximately linear and use the resulting slope to calculate it. The slope in figure 47 is approximately 0.8×10^6. Since the expected slope is given by $\frac{E_s h}{\rho_e h} = 0.8\times10^6$ where $\rho_e h\big|_{n=1} = 0.282$ and h = .024cm then we find $E_s = 9.8\times10^6$. This value does not seem unreasonable, appearing to be the right order of magnitude.

The increasing importance of the bending terms in the thicker walled carotids is shown in figure 48 where they are exposed to the same flow rate. In both cases the longitudinal strain was 46% at a length of 3.5cm.

FIGURE 47

A plot of ξ^2 versus the longitudinal strain factor for the beam mode, $n=1$ of the femoral artery.

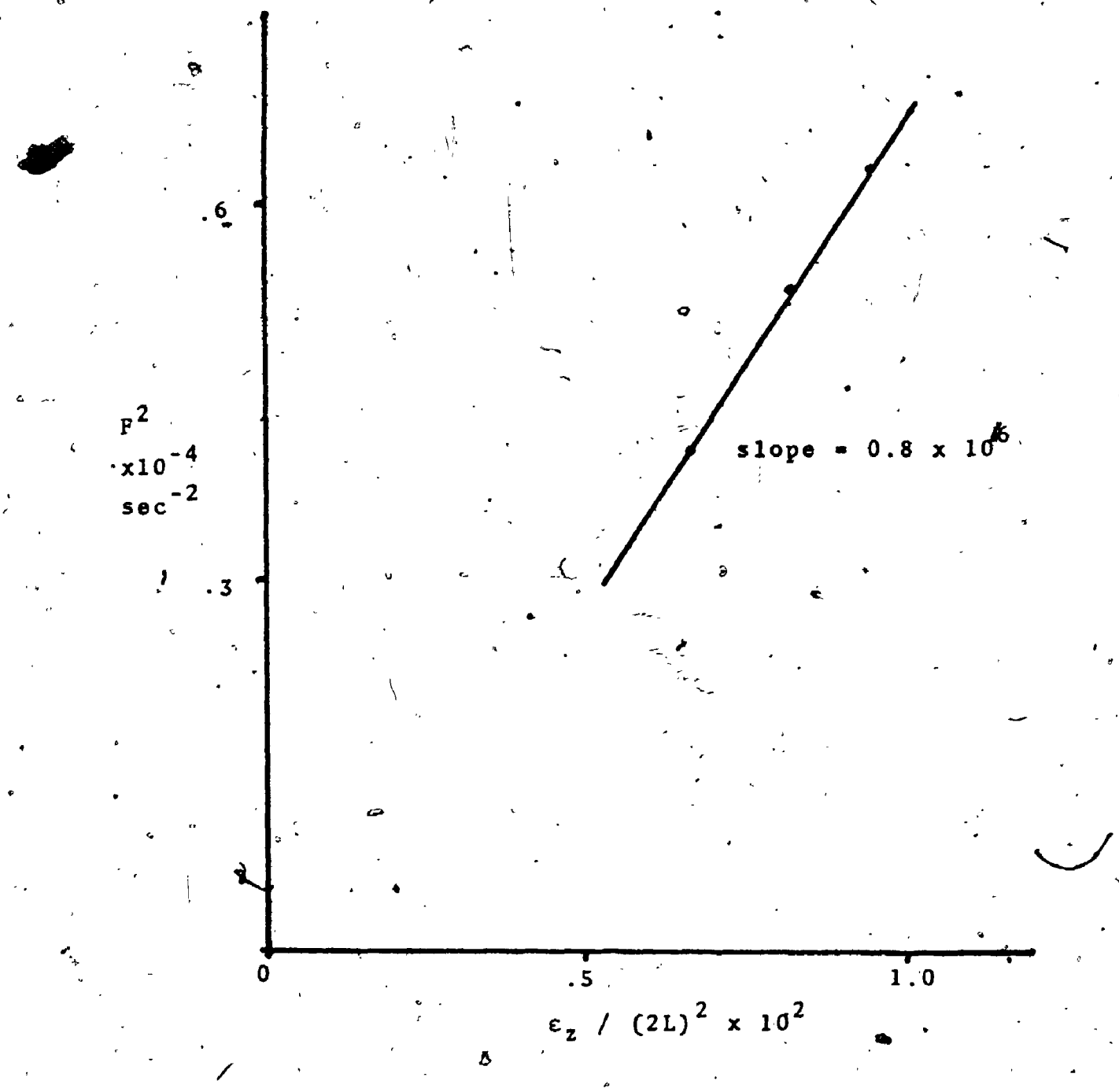
.6
.3
P^2
$\times 10^{-4}$
sec^{-2}
slope = 0.8×10^6
0
.5
1.0
$\varepsilon_z / (2L)^2 \times 10^2$

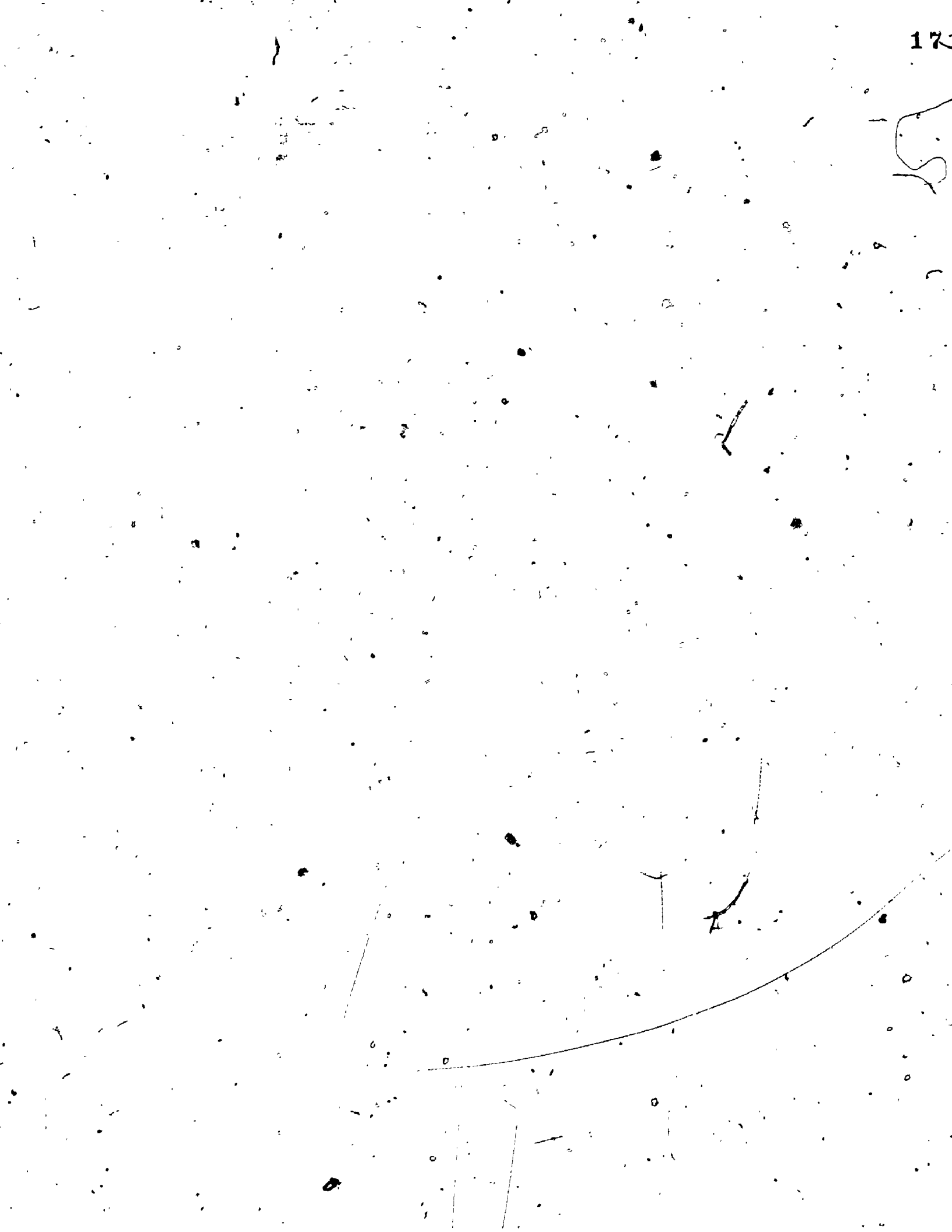

FIGURE 48

Wall vibration spectra of a carotid artery with a result from the femoral for comparison. The pressures and longitudinal strains are shown in the figure.

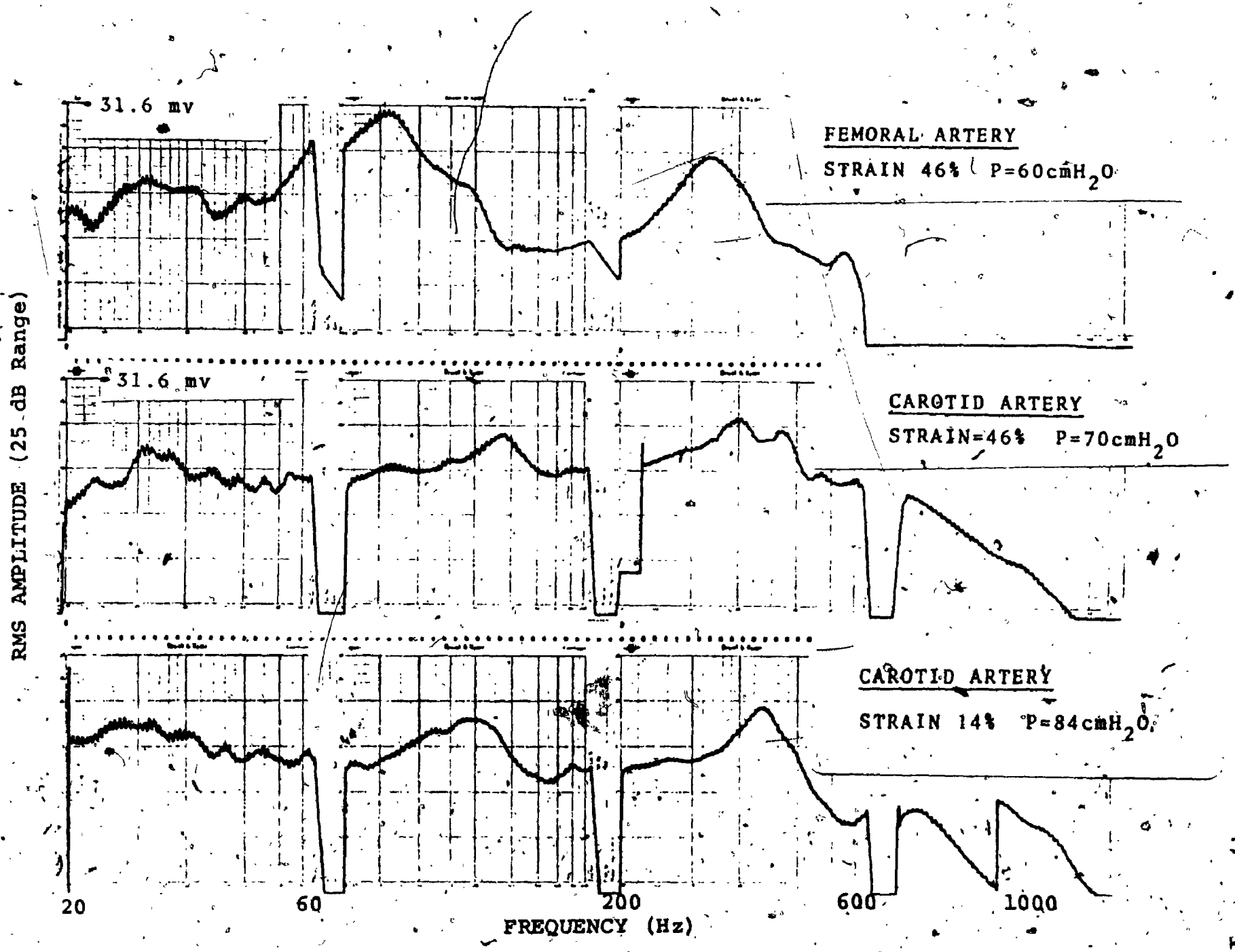
31.6 mv
FEMORAL ARTERY
STRAIN 46% P=60cmH2O
31.6 mv
CAROTID ARTERY
STRAIN=46% P=70cmH2O
CAROTID ARTERY
STRAIN 14% P=84cmH2O
RMS AMPLITUDE (25 dB Range)
20
60
200
600
1000
FREQUENCY (Hz)

However, the pressures and diameters are slightly different resulting in different circumferential prestress. In spite of this, the increasing importance of the term describing the contribution from the longitudinal mode is clear. This is obvious from not only the higher frequency for the apparent beam mode (at 115Hz in 48B) but also the separation of the individual longitudinal modes associated withthe dominant circumferential mode. That the three peaks at 300Hz, 370Hz and 460Hz are due to the longitudinal strain is obvious by comparison with figure 48C, which shows the same carotid artery at a longitudinal strain of only 14%. Although figure 48C is under a slightly higher circumferential pre stress the effect of decreasing tension is clear.

We can determine if the three peaks in figure 48B are the first three longitudinal mode value (m=1,2,3) associated with n=2 by plotting f^2 versus m^2 as in figure 49. The resulting fit seems quite good giving a slope $\left(\frac{Cs}{(2L)}\right)^2 = 1.54 \times 10^4$. Since the inertial term for the beam mode and that for n=2 are approximately the same, (see equation 15b), this result may be compared with the beam mode. The value given from the beam mode is $f^2/m^2 = 1.32 \times 10^4$ which is not substantially different. The dotted line in figure 49 represents the results from the same carotid artery at a different pressure. The third line represents the results at the same pressure as the dotted line but at a lower longitudinal strain (33%). The resulting slope

FIGURE 49

A plot of f^2 versus m^2 for the three dominant modes associated with n=2 in the carotid artery at different pressures and longitudinal strains.

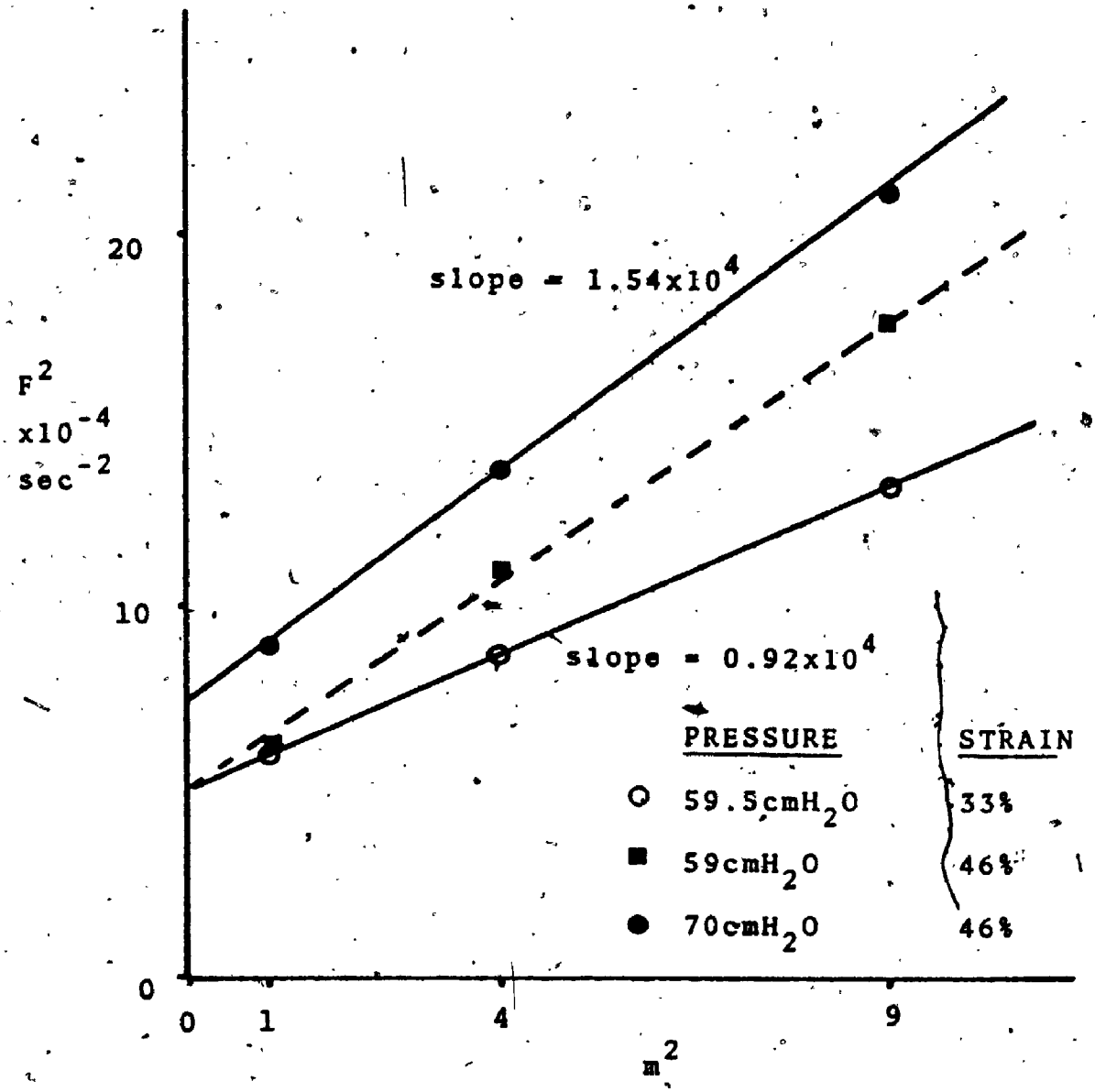
20
10
0
F^2
$x10^{-4}$
sec^{-2}
slope = $1.54x10^4$
slope = $0.92x10^4$
PRESSURE
STRAIN
$59.5cmH_2O$
33%
$59cmH_2O$
46%
$70cmH_2O$
46%
0
1
4
9
m^2

of $0.92x10^4$ shows excellent agreement with the expected comparison of the beam mode at 95Hz ($0.9x10^4$).

The vibration of the first two peaks (m=1,2 for n=2) with circumferential prestress are shown in figure 50. Recall that with the carotid samples the pressure reading was approximately 15cm H_2O in error. This is the reason for the relatively large intercept observed in figure 50 which was typical of the carotid results. The dotted line shows the corrected form adding this correction of 15 cm H_2O to the pressures.

Since the relative pressures are accurate, however, the slope in figure 50 can be used to evaluate the theoretical prediction as in the past. For the range of pressures used (>50 cm H_2O) the outside diameter was approximately constant at 5.9mm under a longitudinal strain of 46%. Using these values the wall thickness was calculated as 0.38mm which gives an h/r ratio of 0.15, considerably larger than the equivalent value for the femoral discussed. For the n=2 circumferential mode, then, the expected slope is calculated as 10.2 which is higher than the observed value of 9.0. However the results on the other carotid values under similar plots produced slopes of 10.1, 9.8 and 9.2.

The frequency information on the higher order circumferential mode (n=3) for the same sample is shown in figure 51, along with the estimated result when corrected by 15 cm H_2O. Using the same parameters as above the expected slope is 38.0 which is higher than

FIGURE 50

A plot of f^2 versus T_c' for the two dominant modes associated with n=2 in the carotid artery. The dotted line shows the corrected value for pressure.

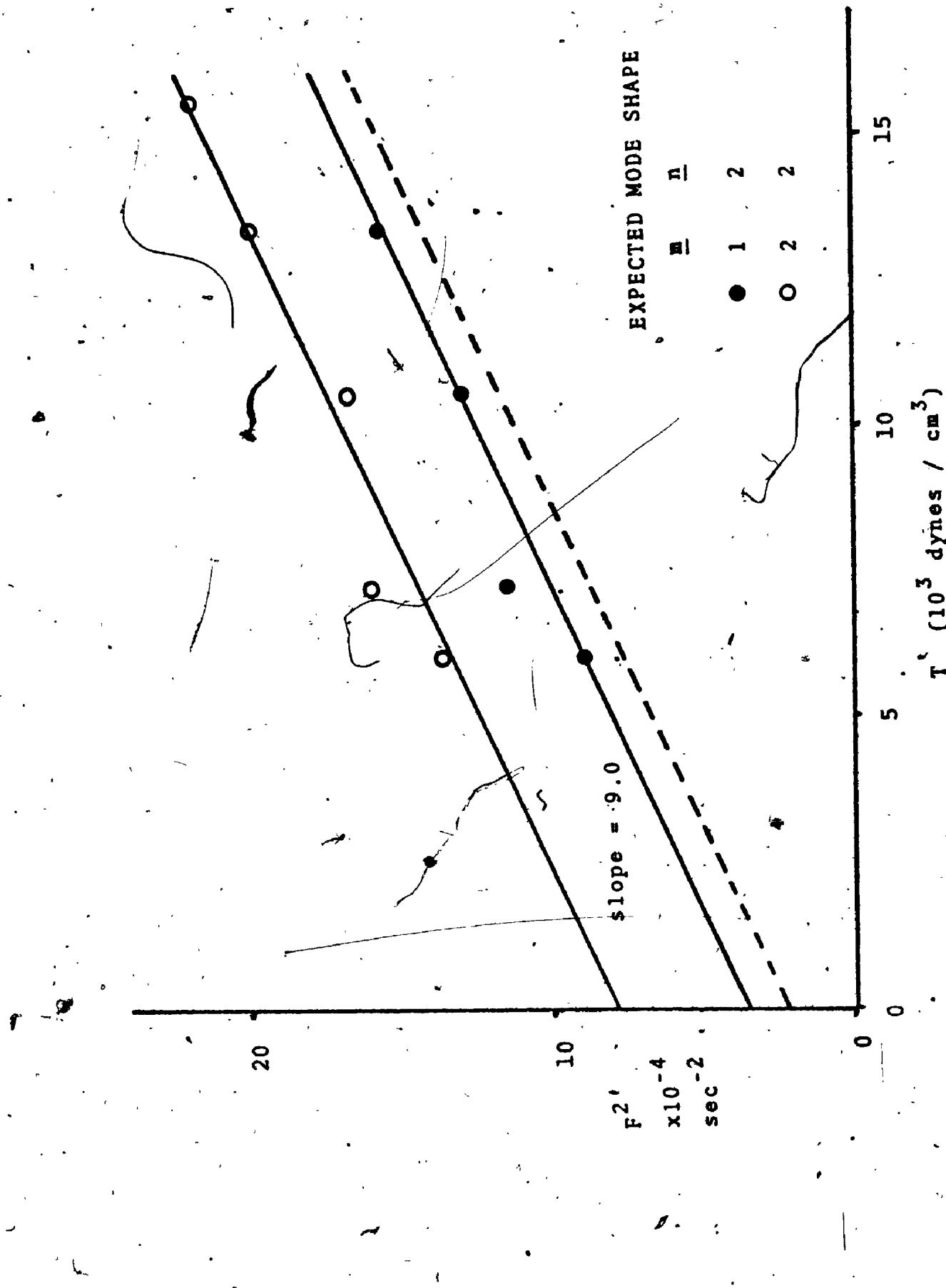
EXPECTED MODE SHAPE
m n
1 2
2 2
slope = 9.0
$F^{2'}$ x10^{-4} sec^{-2}
T_c' (10^3 dynes / cm^3)
0
5
10
15
20

FIGURE 51

A plot of f^2 versus T_c' for the n=3 circumferential mode in the carotid artery results. The dotted line shows the corrected value for pressure.

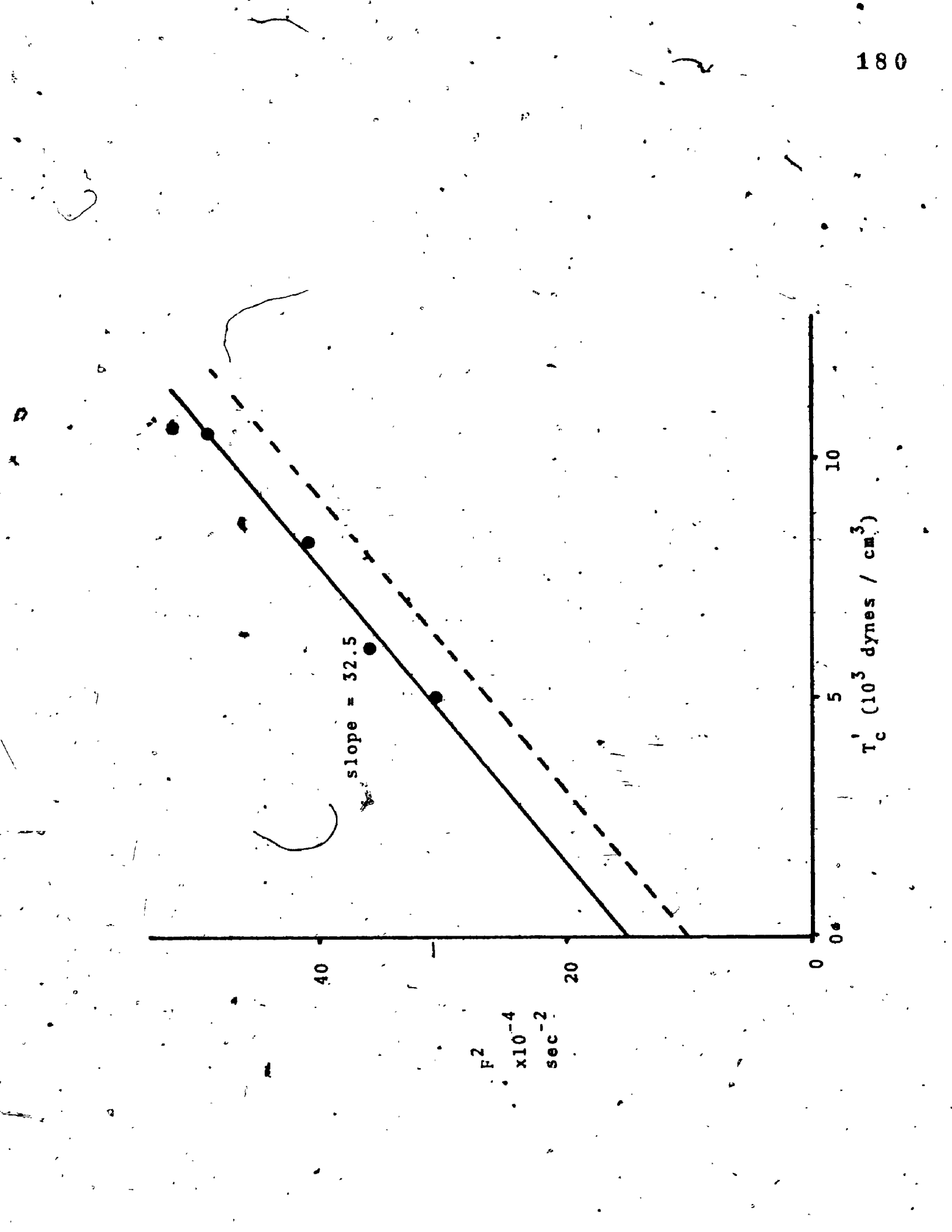
slope = 32.5
40
20
0
0
5
10
T_c' (10^3 dynes / cm^3)
F^2 x10^{-4} sec^{-2}

the observed result of 32.5.

If we assume that the corrected intercept in figure 50 for n=2 is 2.2×10^4 then we may estimate the bending term for the carotid sample. Using the longitudinal term $Cs^2/(2L)^2$ obtained as 1.54×10^4 then $\frac{n^2-1}{\rho_e h} \; n^2 \frac{\gamma A_1}{(2\pi a)^2} = 0.7 \times 10^4$ which gives $\gamma A_1 = 520$. This value is higher than that obtained on the femoral (190) which would be expected just from the higher value of γ, if the moduli were similar. Using the value of h/r calculated at 0.15 this gives $\gamma = 2.8 \times 10^{-4}$ so that $Ee = 7 \times 10^6$ which is not substantially different from the modulus obtained on the femoral.

Discussion

The present results confirm that the resonant modes of a biological vessel can be adequately described by the model. These results emphasize that the principal factors governing the resonance are the wall stress and geometry. The success of this model in describing the resonant frequencies is shown in figure 52, which summarized the test results obtained on the six samples. For each artery studied, the spectra taken nearest 100 cm H_2O and at the maximum longitudinal strain was used. Since the beam mode could not be calculated for the biological data its value was used to determine the term $\frac{Ta^o + \gamma A_2}{(2L)^2}$ so that the calculation of the contribution to the higher circumferential modes could be done. The values obtained,

FIGURE 52

A plot of the calculated resonant frequencies versus the observed values for the six biological samples tested.

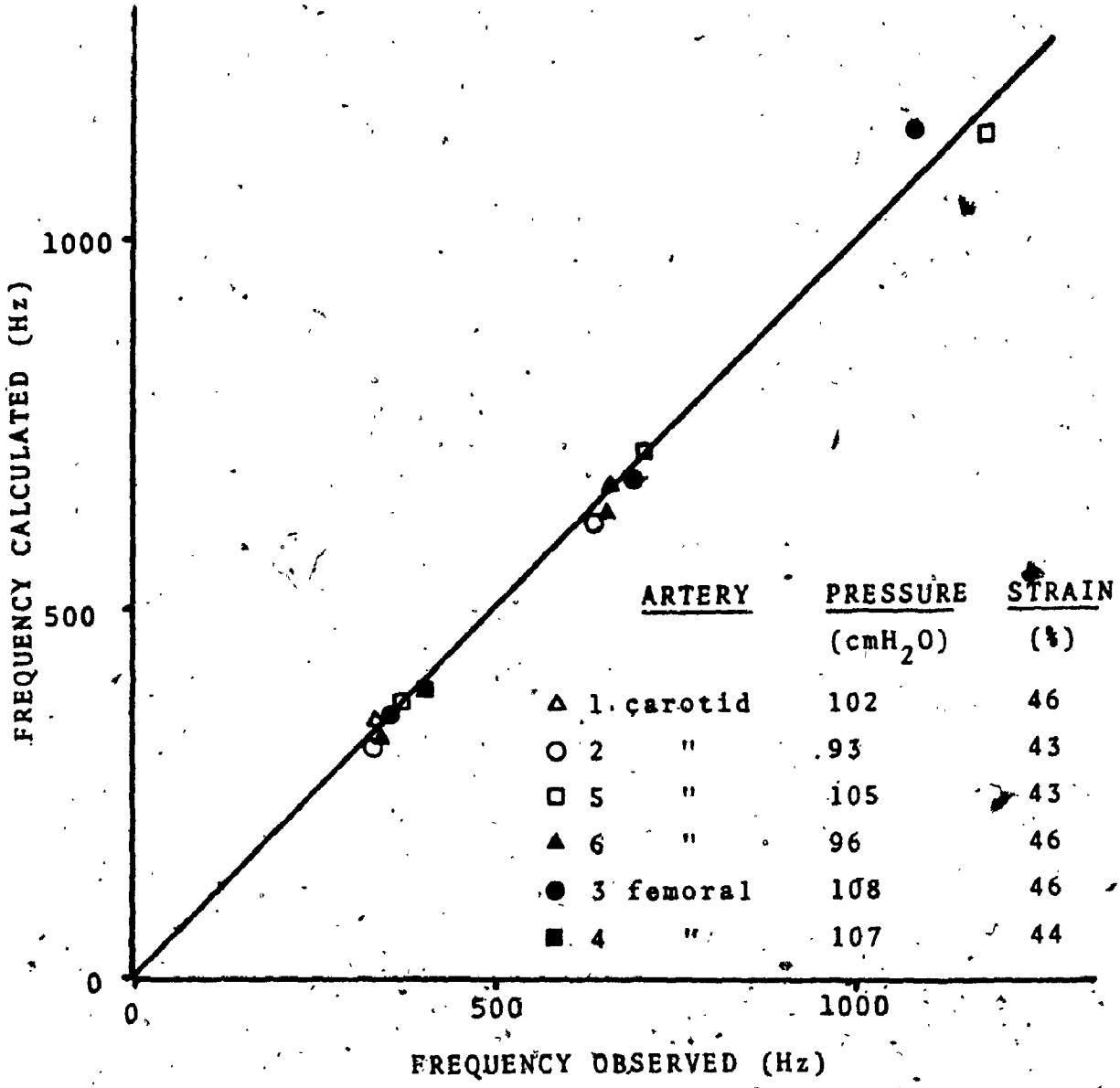
FREQUENCY CALCULATED (Hz)
1000
500
0
0
500
1000
FREQUENCY OBSERVED (Hz)
ARTERY
PRESSURE (cmH_2O)
STRAIN (%)
△ 1 carotid 102 46
○ 2 " 93 43
□ 5 " 105 43
▲ 6 " 96 46
● 3 femoral 108 46
■ 4 " 107 44

previously, for the bending term γA_1 for the femorals (190) and carotids (520) were used in the calculation. Finally, the pressure readings for all the carotid samples were augmented by 15 cm H_2O to account for the pressure error. The resulting fit is quite encouraging.

We may extend this success in describing the resonant frequencies by examining the original data from Foreman and Hutchison's study.[1] The major peaks observed in their wall vibration spectra exposed to disturbed flow (created by a stenosis), similar to the result shown in figure 4, were tabulated (see table I). The internal geometry of these samples was obtained from latex casts and is recorded in table I. Their results are similar to the present study, with a low frequency peak that probably corresponds to the beam mode and two or three high frequency peaks that would appear to be the higher order circumferential modes. It is immediately apparent from the table that the smaller the radius the higher the circumferential resonant frequency. For example the peak corresponding to the dominant circumferential mode n=2 varies from 305 Hz at 8.3 mm I.D. to 560 Hz at 4.3 mm I.D., as would be expected.

The use of a capacitive transducer in their experiments meant that the vessel could not be fully covered with saline.

---

[1] Obtained with permission from Professor J.E.K. Foreman.

TABLE I

A summary of the data from Foreman and Hutchison's study (1970b) on the wall vibration spectra distal to an artificial stenosis, in vitro. The dominant low frequency peak was in the range expected for the beam mode and referred to as f_1. The remaining amplitude peaks fell within the range expected for the circumferential modes n=2,3 and 4 and referred to as f_2, f_3, and f_4, respectively.

ARTERY	FLOW (cc/min)	LENGTH (mm)	INTERNAL DIAMETER (mm)	AMPLITUDE PEAKS (Hz) f_1	f_2	f_3	f_4
5-External Iliac(H)	440	20.9	6.0	145	450	820	
6- " "		23.5	7.8	130	310	550	820
7- " "	1000	19.4	8.3	128	305	560	
8- " "	500	19	7.6		340		
9-Common Iliac(H).	900	11.5	8.0		325		
2-Common Iliac(D)	250	14.3	4.3	180	500	1050	

This result would be expected to complicate the response, particularly with respect to the inertial term. We might expect the inertial response to be some value between $\rho_w h + \frac{2\rho_f a}{n}$ and $\rho_w h + \frac{\rho_f a}{n}$. However calculations quickly revealed that the latter result provided the best description.

Using the inertial term $\rho_w h + \frac{\rho_f a}{n}$ and considering $h/r = 0.1$ (since no value of h was reported), for all the samples based on the internal diameter the resonant modes could be calculated. The effect of the different radii were evaluated in the following manner.

Since $f^2 = m^2 \frac{Cs^2}{(2L)^2} + \frac{(n^2-1)}{\rho_e h} \cdot \frac{Te^o + n^2 \gamma A}{(2\pi a)^2}$

and $\rho_e h \simeq \frac{\rho a}{n} (1 + n \frac{h}{a}) = \rho_f \frac{a}{n} (1 + \frac{n}{10})$

then $f^2 = m^2 B + n \frac{(n^2-1)}{(1+\frac{n}{10})} \cdot \frac{Te^o + n^2 \gamma A}{\rho_f \frac{a}{n} (2\pi a)^2}$

Thus by plotting f^2 versus $\frac{n(n^2-1)}{(1+\frac{n}{10})}$

we can obtain the slope $\frac{Te^o + n^2 \gamma A_1}{4\pi^2 a^3}$

This result is shown in figure 53 which demonstrates a good fit for the data available and clearly indicates the effect of different radii at the same pressure. If we can assume that the term $n^2 \gamma A_1$ is small compared to Te^o then we can rewrite the slope as $\frac{P}{4\pi^2 \rho} \frac{1}{a^2}$.

The slopes from figure 53 are plotted against the factor $1/a^2$ for the three samples used (allowing for wall thickness, $h = 0.1R$) in the upper corner of figure 53.

FIGURE 53

A plot of f^2 versus the circumferential mode factor, $n(n^2-1) / (1+n/10)$, for the results of Foreman and Hutchison's study. The slopes obtained from this result are plotted in the upper part against the corresponding inverse radius squared. For the three extremes in data used the pressure remained constant at 100 mmHg.

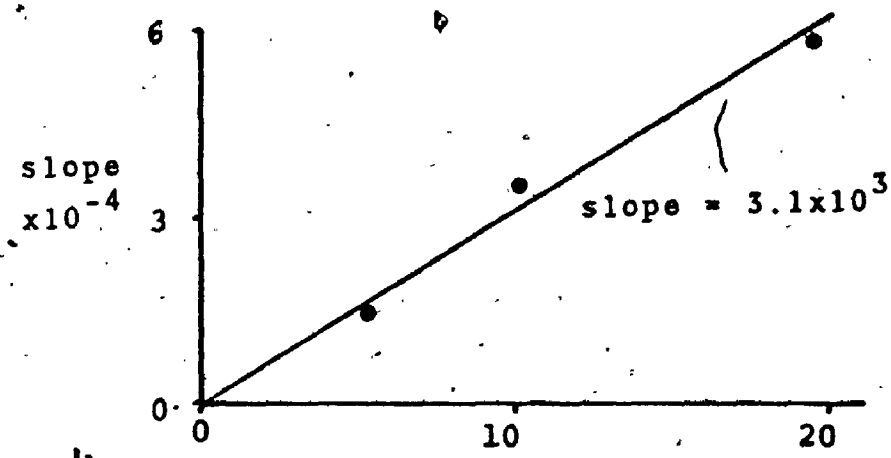
6
3
0
slope
x10^-4
slope = 3.1x10^3
0
10
20
1/a^2 cm^-2

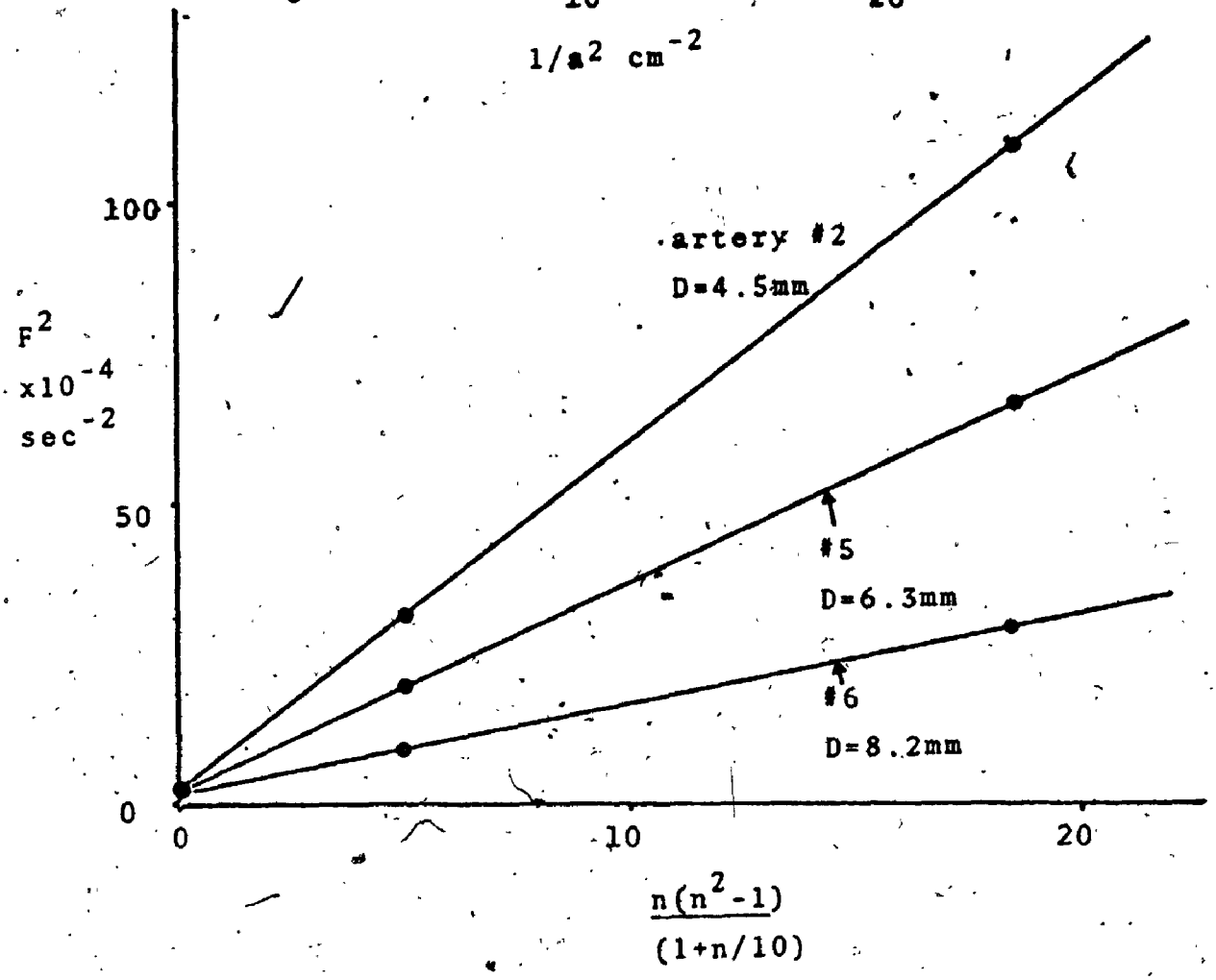
100
50
0
F^2
x10^-4
sec^-2
artery #2
D=4.5mm
#5
D=6.3mm
#6
D=8.2mm
0
10
20
n(n^2-1)
(1+n/10)

The result should give the slope $\frac{p}{4\pi^2\rho_f} = 3.26\times10^3$ which agrees very well with the observed result of 3.1×10^3.

The results for the five human and one dog iliac arteries are summarized in figure 54. The same assumption of wall thickness was used (since h was not available) and the results from the beam mode used to calculate the longitudinal term. The resulting fit would appear to be quite good, considering the approximations made and the errors possible in the calculation.

FIGURE 54

A plot of the calculated resonant frequencies versus the observed values for the six samples in Foreman and Hutchison's study.

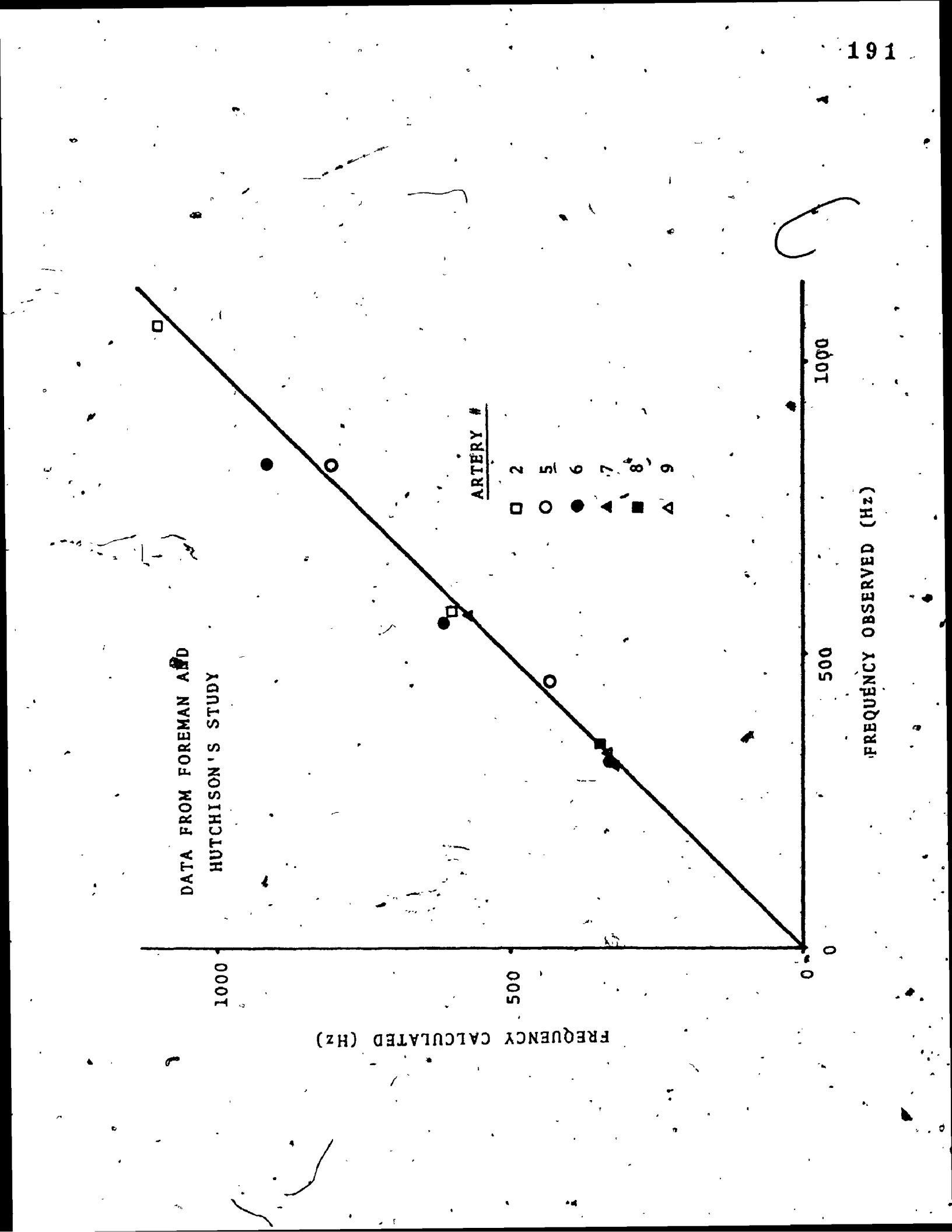
DATA FROM FOREMAN AND
HUTCHISON'S STUDY
ARTERY #
2
5
6
7
8
9
FREQUENCY CALCULATED (Hz)
FREQUENCY OBSERVED (Hz)
0
500
1000
0
500
1000

V GENERAL DISCUSSION

(i) Evaluation of Model

The objective of this study was to determine the resonant modes of transverse or radial vibration of biological vessels. Chapter III presented a theoretical model to describe the resonant frequencies involved while chapter IV presented experimental justification of that description. The model suggested that prestress and geometry were the most important factors involved and the experimental evidence confirmed it.

By varying the prestressed values of longitudinal tension (changing the length) and circumferential tension (changing the pressure) the predicted response of each mode shape was evaluated. Indeed, it was possible to determine each mode shape (m,n), except for the symmetrical ones (n=0), by their different response to variations in prestress. The mode shape could also be confirmed by noting the spatial variation in amplitude and phase. The absence of the lower order symmetrical modes from the experimental results was to be expected from the relatively large circumferential prestress. The lack of evidence of the higher order longitudinal modes (m) associated with this

symmetrical mode n=0 is not clear. Their absence in the studies on disturbed flow may be a reflection of the type of stimulation, with asymmetric modes preferred.

Since the state of prestress governs the propagation speeds of the disturbance, the importance of geometry in determining the distance that must be travelled is obvious. The predicted increases in resonant frequencies due to a smaller geometry was confirmed by the use of samples, both biological and synthetic, of smaller diameter and length.

The inertial term predicted a response that was dependent both on the acoustical media in contact with the wall and the circumferential mode shape, n. This complicated response was evaluated on synthetic tubing by tests in three different acoustic media: in air-air, air-fluid and fluid-fluid. The results provided excellent agreement with that predicted in the three types of acoustical media and that due to the different mode shapes, n.

It was seen that the resonant response of the wall could be estimated quite well from just a knowledge of the prestress; however, considerable improvement was noted upon inclusion of the bending terms, particularly the

circumferential one. The evaluation of the circumferential bending term $n^2 \gamma A_1$, seemed to agree quite well with the value expected. The longitudinal bending term, γA_2, on the other hand, was more difficult to analyze and did not yield the same success. Estimates of its value were substantially lower than the results observed and suggested that an additional term not accounted for may be involved.

In summary, the description by equation 26 has adequately described the resonant modes of radial vibration of an elastic vessel subjected to a constant wall stress, in vitro. Although the in vivo situation is one of constantly changing geometry and wall stress, this description is probably still valid. This would seem true because the changing conditions are quite slow compared to the high frequency vibrations of interest. The cardiac cycle, for example, has a period of approximately 1 second while the respiratory cycle is even greater. Clearly, these changes are negligible compared to the high frequency vibrations of the circumferential resonant modes, with periods less than 5 microseconds. Thus we would expect equation 26 to describe the changing resonant vibrations of biological tissue when the dynamic values of stress and geometry are included.

(ii) Dynamic Response to Disturbed Flow

If an elastic system is exposed to a randomly fluctuating force with a frequency content that includes some of its resonant modes, then it will vibrate with an energy contant confined to a narrow region around those resonances. In the present situation the number of resonant modes occurring within the frequency range of stimulation was considerable as is obvious from spectra such as figure 39. In every case the response was dominated by the beam mode (n=1) and the higher order circumferential mode (n=2).

In evaluating the theoretical model we have been primarily concerned with information on the frequency of vibration; however, the actual amplitude levels of the vibration are an important consideration in the problem of fatigue and murmur production. For a simple linear system, (with damping) that is exposed to a random force, the amplitude levels at resonance are given by $\overline{w^2} = \frac{\pi}{2} S_f(\omega_r) \frac{\omega_r}{k^2 \xi}$ (Mead, 1968), where S_f is the power spectral density of the force ($S_f = p^2/\Delta f$), ξ is the damping ratio and k is the stiffness constant. This can be rewritten in the present form to give the root mean square amplitude as $(\overline{w^2}/p^2)^{\frac{1}{2}} \propto 1/[\Delta f \cdot f_n (\rho_e h)_n]$, where Δf is the half power bandwidth. Thus the levels of vibration will be related not only to the root mean square pressure fluctuations but inversely related to the resonant frequency (for a particular circumferential mode).

This inverse relation to frequency of the resonant amplitude was noted in both the biological and synthetic samples during a constant flow rate when the transmural pressure was varied. Figure 55 demonstrates this response by plotting the amplitude of the n=2 mode against $1/f_n$ for the same femoral artery as in figure 43. The results seem quite good giving vibration levels of $\frac{w}{a} \approx 2 \times 10^{-4}$. Although the bandwidth, Δf, is obscure due to the presence of more than one resonant mode its value was constant throughout this range. With increasing circumferential order, n, the bandwidth increased which probably contributes to the decreasing amplitude with increasing mode number, n.

As expected, the increasing turbulent pressure fluctuations due to an increase in the flow rates (with a stenosis) produced a greater level of vibration, particularly at the high frequency end. This was evident from the wall vibration spectra in figure 21 for the results in air. Figure 56 displays the change in amplitude of the resonant peaks n = 2 and n = 3 under different flow rates for the synthetic material (smaller smaple) with fluid internally and externally.

Thus, the results seem to confirm that the vessel responds like a simple elastic system exposed to a randomly fluctuating force (provided by the disturbed nature of the flow). We would therefore expect that the in vivo response will be one of fluctuating frequency

FIGURE 55

A plot of the RMS amplitude ratio w/a versus the inverse of the resonant frequency for the dominant circumferential mode n=2 on the femoral artery (in figure 43). The longitudinal strain remained constant at 46% (length = 3.5cm) and the flow at 290 cc/min. (Re=1100).

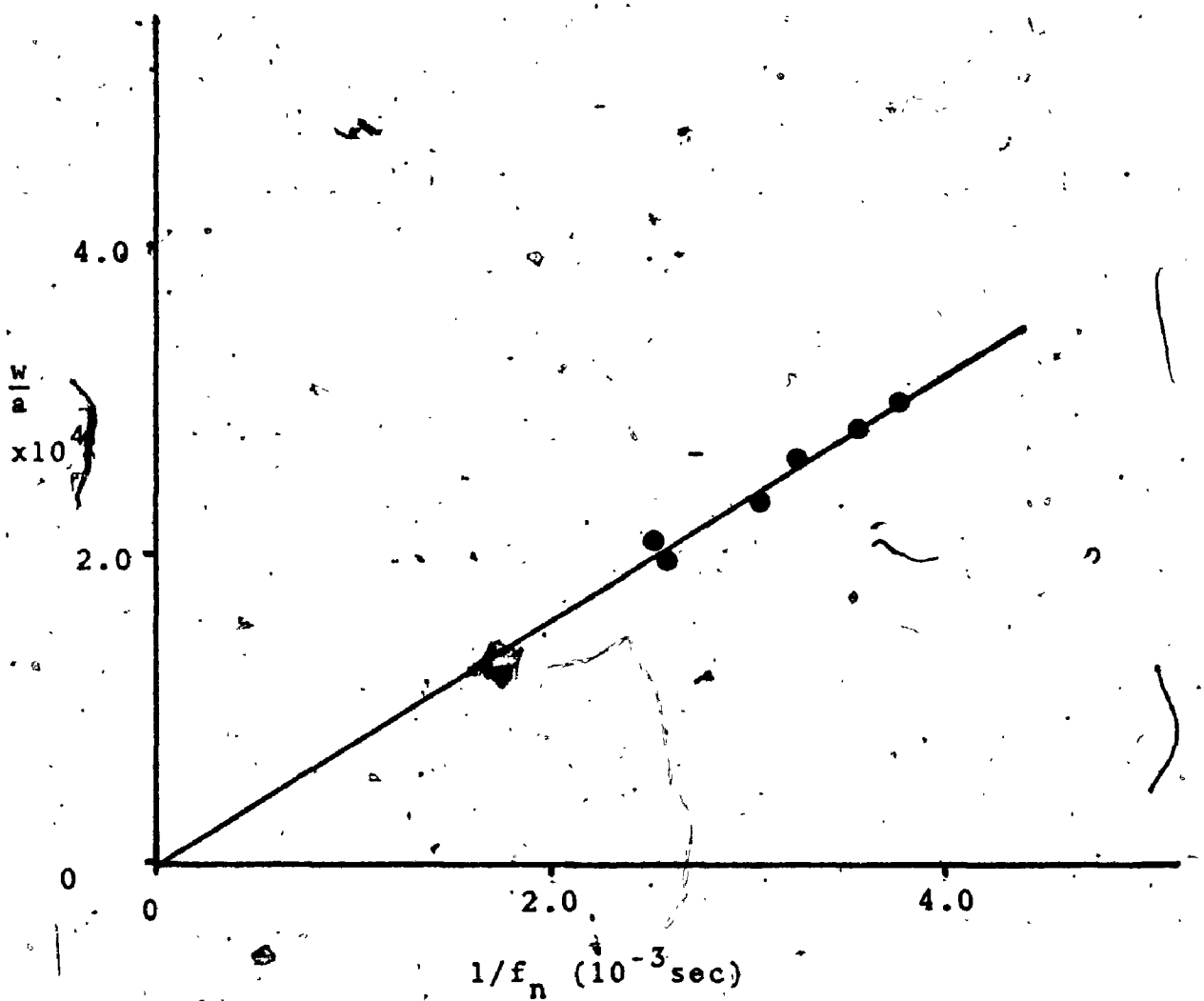
4.0
2.0
0
0
2.0
4.0
a/w
x10
1/f_n (10^-3 sec)

FIGURE 56

A plot of the RMS amplitude of wall displacement versus the flow rate at constant pressure (96 cmH_2O) and length (8.35cm, strain = 20%) for the small diameter (0.32cm) penrose tubing. The calcualted Reynolds numbers are also shown.

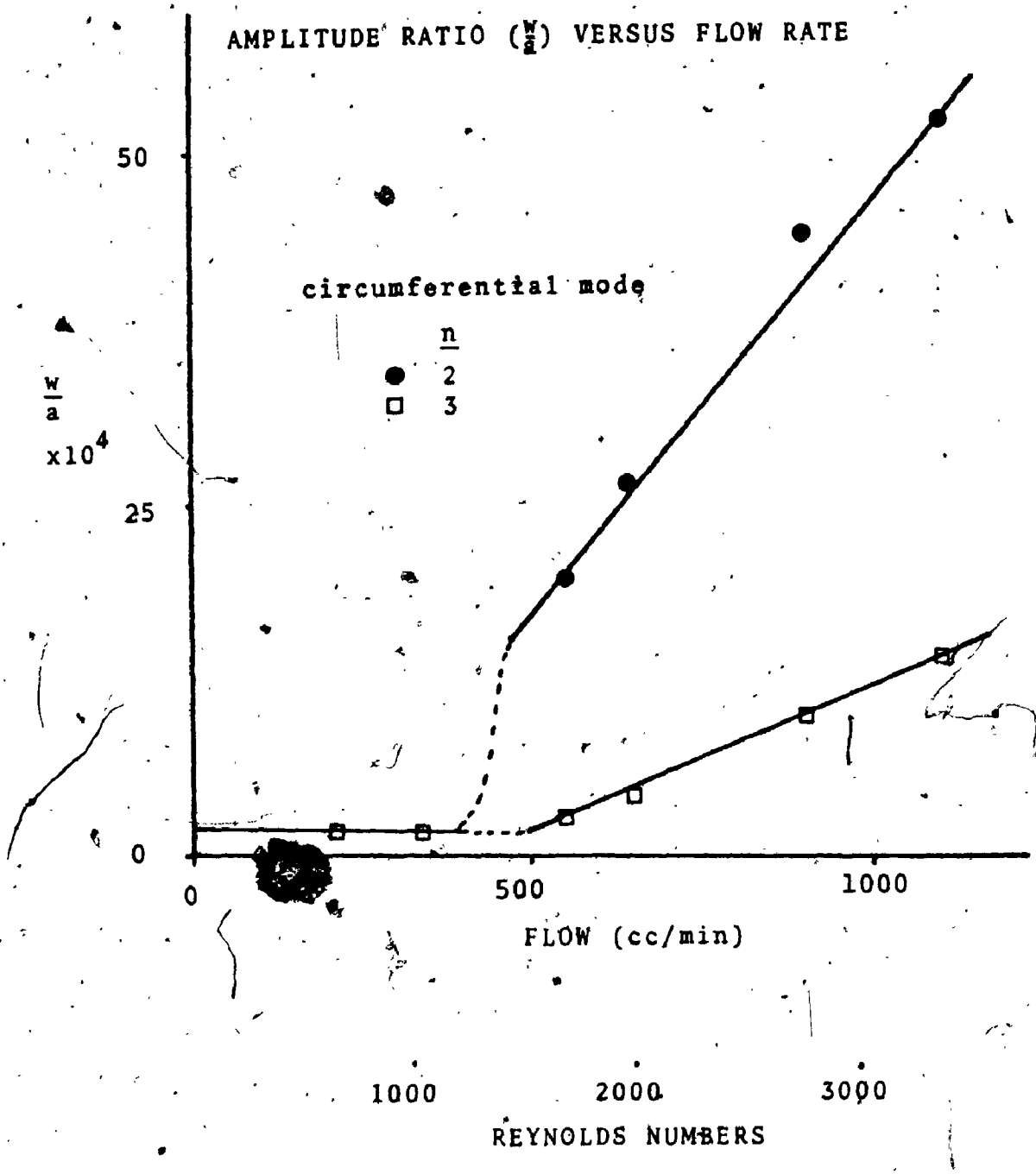
AMPLITUDE RATIO ($\frac{w}{a}$) VERSUS FLOW RATE
50
25
0
$\frac{w}{a}$
x10^4
circumferential mode
n
2
3
0
500
1000
FLOW (cc/min)
1000
2000
3000
REYNOLDS NUMBERS

and amplitude of vibrations. The resonant frequencies will change due to the variations in wall stress discussed in the previous section while the amplitude of vibration will change due to the variation in frequency and the changing spectral content of the flow throughout the cardiac cycle. As Sacks, Tickner and MacDonald (1971) noted, the length of time that a murmur occurred (evidence of wall vibrations) was related to the time that the flow exceeded the critical value.

One other important aspect of the dynamic response, in vivo, that should be considered is the viscoelastic nature of the wall. Anliker (1972) has shown, for example, that small axi-symmetric pressure or radial disturbances are attenuated by the viscoelastic elements of the wall according to the relation $A/A_o = e^{-1.1 \frac{\Delta x}{\lambda}}$. Thus, with increasing frequency or decreasing wavelength the disturbance will be attenuated more rapidly with axial distance. With respect to the high frequency resonant modes (n=2 and above) stimulated locally by a stenosis, therefore, we may expect the amplitude of vibration to be localized. This would seem to agree with the localized nature of both poststenotic dilatation and murmurs.

One final aspect of the dynamic response of the vessel wall that can occur, in vivo, and was observed in

the present study is the condition of 'flittering' (Rodbard, 1957). With the pressure head maintained constant during the biological tests and the pressure lowered there was an increase in vibration levels, as discussed above. Eventually, a low value of pressure was reached at which an instability occurred and large scale vibrations of the wall resulted. Unfortunately, these levels were out of the range of the photonic sensor and could not be measured. However, the impression received was that a vibration mode similar to n=2 was occurring with the large vibrations allowing the walls to touch each other. Such an instability is sometimes thought to be the mechanism in bronchial asthma (McKusick, 1958). The large dynamic stresses occurring with this type of condition would seem to be quite important from the aspect of fatigue (Sinclair, 1972).

(iii) Fatigue

The vibrations arising from disturbed flow produce dynamic stresses within the wall of the vessel that can lead to structural degeneration as in post-stenotic dilatation. Since the stresses are related to the vibration amplitude, the resultant increase in vibrational energy content due to stimulation of several resonant modes may be the most significant factor in this problem. The observation by Roach and Harvey (1964) that moderate stenoses were required to produce a dilatation may

be a reflection of the need to have sufficient high frequency energy content in the pressure fluctuation. This would certainly occur with increasing severity of occlusion.

The fatigue studies of Boughner (1971), when coupled with the present study, seem to suggest that stimulation at resonance was a necessary factor in the observed fatigue.

Recall from chapter II that Boughner (1971) found the dilational response of arteries to be frequency dependent, seemingly related to age. Figure 57 is a reproduction from his thesis, showing the frequencies producing a dilatation versus their length. The interesting feature to note here is that the frequencies appear to fall within three discrete frequency bands, suggesting possibly three resonant modes. However, this experiment was not designed to weight all frequencies evenly[1] so that such a conclusion can not be made based on this data. Nevertheless, in view of the present studies we would expect the resonant frequencies of these iliac arteries (similar to Foreman and Hutchison's data) to correspond to the range observed.

The relative insensitivity to length for the 300Hz group might suggest that it corresponds to the

---

[1] personal communication

FIGURE 57

A plot of the length versus the corresponding frequency producing a dilatation. Reproduced from Boughner (1971) with permission.

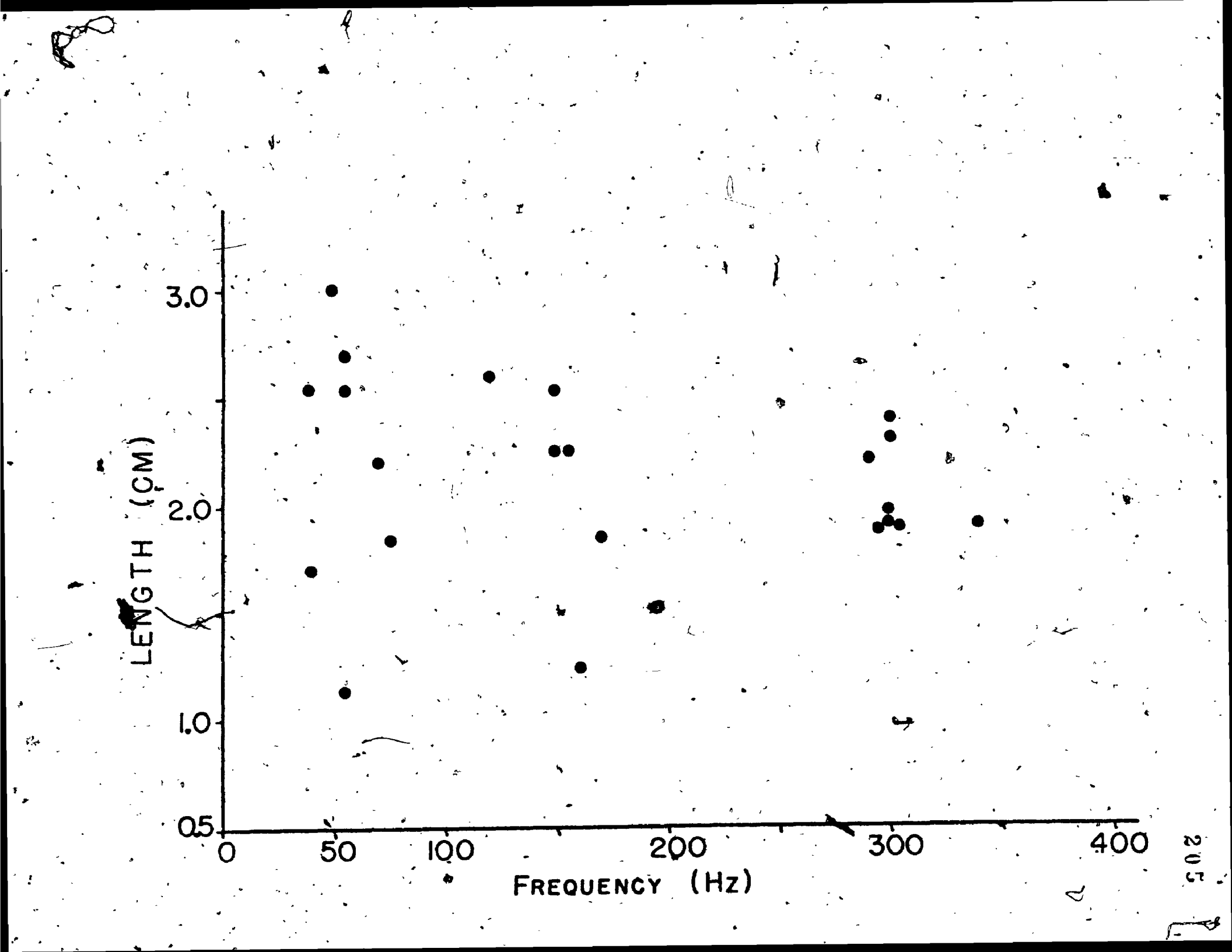
LENGTH (CM)
3.0
2.0
1.0
0.5
0
50
100
200
300
400
FREQUENCY (Hz)

dominant circumferential mode n=2 since the longitudinal term $\frac{C_z^2}{(2L)}^2$ is small relative to the circumferential term. If we consider the bending term and longitudinal term negligible, we can write $f_n^2 \simeq \frac{n(n^2-1)}{(1+\frac{nh}{2a})} \frac{P}{8\pi^2\rho a^2}$ for the case of external and internal fluid media. Thus taking n = 2, $\frac{h}{a}$ = 0.1; P = 1.33×10^3 dynes/cm^2 and f_2^2 = 9×10^4 then we can write a^2 = 0.1 or a = 3.18 mm. Although the radii of the samples used by Boughner are not reported we can see from Foreman and Hutchisons results that the external iliacs ranged from 3.0mm to 4.15mm internal diameter.

The two other groupings around 50Hz and 150Hz have considerably more scatter although they too appear to fall within a specific frequency range. We might expect that the 150Hz signal corresponds to a beam mode (n=1) based on our present results. However, we might expect more dependence on length, since $f_{m,1}^2 = m^2 \frac{C_B^2}{(2L)}^2$ (i.e. frequency is inversely related to length). Without control of the tension or longitudinal stress, however, this could lead to changes in C_B^2. Also changes in radii affect the term C_B^2. If we ignore the data point corresponding to the shortest length then the remaining points do appear to be inversely related to length. Taking the extreme of length of these remaining points we find a length ratio of approximately 2.6/1.8 = 1.45, while the corresponding frequencies are in a ratio of 170/120 = 1.4.

Thus if the geometry and stress values of these data points were known it seems possible they may lead to the conclusion of stimulation occurring at a beam mode resonance. The lower grouping may correspond to a lower order beam mode (i.e. m = 1) such that if the geometry and prestress were known the results may show the length dependence expected. The significant relation to age that Boughner noted presents an interesting idea in relation to the type of dynamic stress experienced. The beam mode and higher order circumferential mode would result in different dynamic stresses. The beam mode, for example, may be expected to produce predominantly longitudinal stresses, since there is no effective change in circumference. The circumferential mode, n = 2, on the other hand would experience significant circumferential stresses. The relationship to age, therefore, may be a reflection of a difference in the anisotropic properties with age. Roach and Burton (1957), for example, have shown that the structural properties of iliac arteries are related to age.

If there is a change in the longitudinal properties with age such that the vessels have increased in length or 'yield' as far as they can go, then it seems possible that the dynamic stresses longitudinally (as from the beam mode) would have little effect. In this regard it is interesting to note that Boughner (1971) reports a retraction

of only 1 or 2% for the iliac arteries he studied whereas Bergel (1972) reports a value of 40% in the dog.

In the circumferential direction, however, the vessels may 'yield' or dilate when exposed to circumferential stresses. Thus the circumferential resonance (n=2) would be expected to cause a dilatation of the vessels whereas the beam mode would have no effect.

With the younger arteries, on the other hand, a 'yielding' longitudinally may be permissable. Indeed, the apparent preference of the youngest arteries for the beam mode may suggest that a 'yielding' or structural alteration in this direction is the dominating one.

These suggestions are, naturally, speculative, since a complete understanding of the effect of dynamic stresses on biological tissue requires a proper experimental evaluation with the complex anisotropic properties of that tissue in mind. Nevertheless, the results of Boughner (1971), and those of Roach and Harvey, (1964) suggests that the relatively large amplitudes associated with stimulation near resonance may be the dominant factor involved. In this regard, the observation by Roach that a moderate stenosis (with a higher spectral content of pressure fluctuations) was required to produce a dilatation may indicate that stimulation of the high frequency circumferential resonance (n=2), or above, is necessary.

(iv) Murmurs

Perhaps the most significant aspect of this work is the realization that the frequency content associated with many murmurs (up to 1000 Hz) includes several resonant modes of the artery wall. This implies that the wall should be responding in a similar manner to the present studies, although the cyclic nature of the pressure and flow would produce a similar modulation. The important point, however, is that the increased amplitude of vibration due to stimulation near several resonances would be a dominant factor in producing the sound that is heard. Recall from the introduction that a rigid tube with the same state of disturbed flow did not produce an audible murmur.

The description of the external sound field (equation 12b) gives the magnitude of the pressure field at the wall as $|P_e'| = \rho\omega^2 \frac{a}{n} Wo$ or $\rho \frac{(2\pi a)^2}{n} \left(\frac{Wo}{a}\right) (f^2)$, which indicates the importance of both amplitude of vibration and frequency. For example, if we consider the results of the biological tests where $\frac{Wo}{a} \sim 2\times10^{-4}$, for the dominant circumferential resonance, n = 2, a = ¼cm and f=330 Hz, then $|P_e'|$ is calculated as 20 dynes/cm^2. This corresponds to a sound pressure level of approximately 100 dB, which is a considerable sound source. Thus a level of vibration which appears insignificant is in fact very significant when coupled with a relatively high frequency.

An estimate of the importance of stimulation near resonance can be obtained from the magnification factor, Q, which is a ratio of the amplitude at resonance to that under static conditions for the same driving force. Related to the damping ratio, it is obtained from the half power bandwidth, $Q = f_r/\Delta f$. Although measurement of Δf was partially obscured by the presence of more than one resonant mode, an estimate of $Q = 10$ at physiological stresses was obtained, using the finer resolution of the constant bandwidth analyzer (HP 3580A). This would provide a significant 20dB increase in the sound source over the corresponding level in the absence of a resonance. Clearly, even with an elastic structure whose flexibility alone can be responsible for a significant sound field (when exposed to disturbed flow), the stimulation near a resonant mode can become the dominant factor in the resulting sound field.

Except for musical murmurs, which are rare, the analysis of murmurs by spectral phonocardiography does not reveal the dominant peaks we might expect due to resonance. Most murmurs are characterized as noisy with a spectral content that appears continuous, as shown in plate 1A. The possible diagnostic usefulness of the frequency content has therefore been lost, with timing, duration and relative intensity being the quantities of interest to the physician.

PLATE I

A) Example of spectral phonocardiography on a noisy murmur due to rheumatic aotic stenosis recorded at the base (left) and the apex (right). Reproduced from figure 247 in McKusick (1958) with permission.

B) Example of a contour plot in spectral phonocardiography on a noisy murmur due to aortic stenosis. Reproduced from Rushmer and Morgan (1968) with permission.

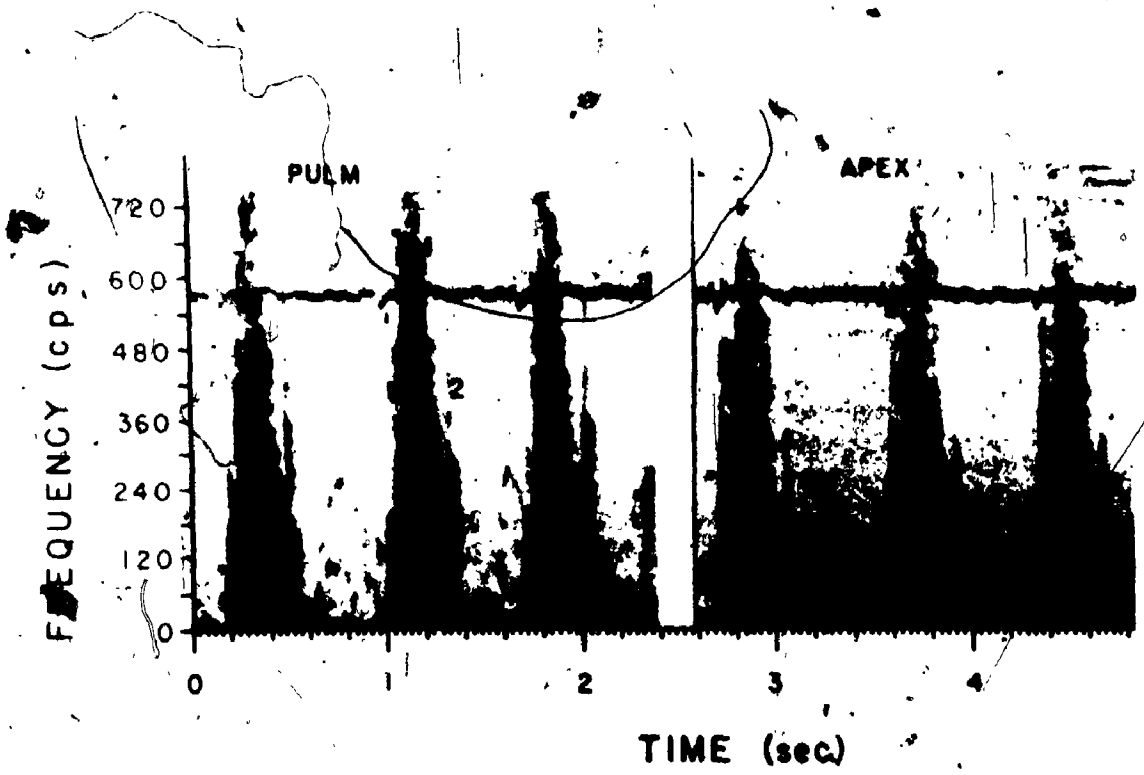
PULM
APEX
720
600
480
360
240
120
0
FREQUENCY (cps)
0
1
2
3
4
TIME (sec)

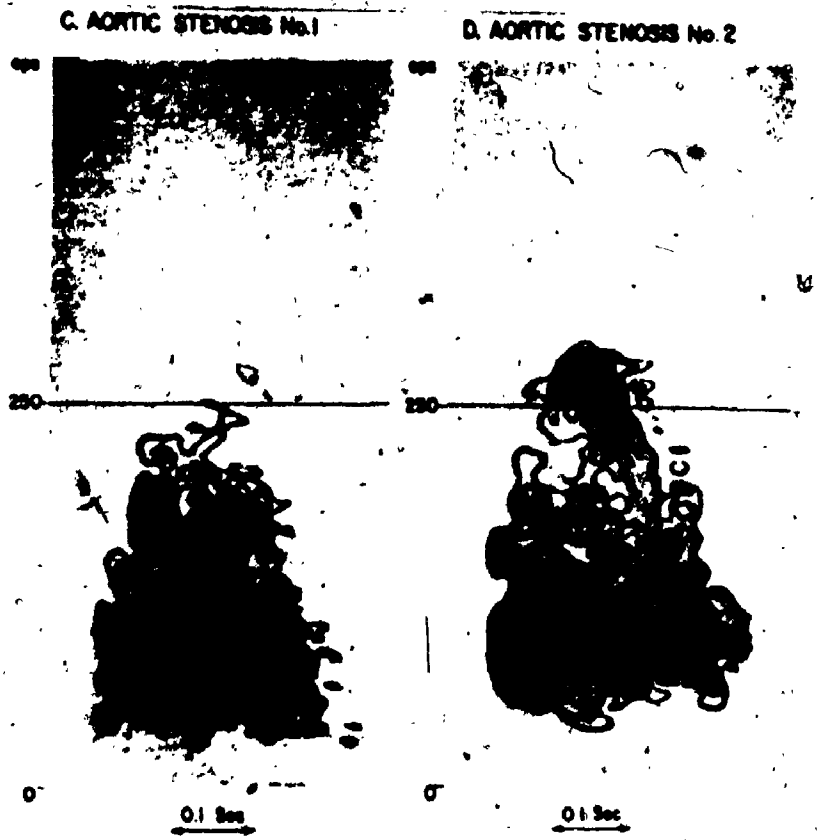
C. AORTIC STENOSIS No.1
D. AORTIC STENOSIS No. 2
250
250
0.1 Sec
0.1 Sec

There are several probable reasons for the absence of distinct peaks in spectral phonocardiograms. Probably the most significant factor is the poor resolution of the equipment used, both with respect to frequency and intensity. The records displayed by McKusick (1959), for example, use a filter bandwidth of 23 Hz, which in the present studies would not be able to discriminate between the different longitudinal components of the second order circumferential mode. Furthermore, the use of different shadings to represent intensity is at best qualitative. The 15 dB dynamic range of the electro sensitive paper does not permit a large enough dynamic range to be evaluated whereas the larger dynamic range permissible with photographic displays requires too great a variation in intensity. However, the use of contour plots of the spectrograms (see plate 1B) improves this technique considerably (Prestigiacomo, 1962).

The relatively large spectral content of pressure fluctuations at the lower frequencies, particularly with minor stenoses or lower Reynolds numbers, would favour the lower modes.

The dominant circumferential mode (n=2), for example, was seen to occur primarily above 200 Hz. The beam modes (n=1) on the other hand are probably less important in

the physiological state. In the present investigation long samples were used, tethered only at their ends. This freedom permitted relatively large transverse movements for the beam mode that would seem unlikely in the physiological state with the restraining tissue externally. For example, when the edge of a small plate (2cm long) was placed along the sample, 90° to the probe, to constrain it, the spectra revealed little change in the circumferential mode (n=2) but a complete disappearance of the beam mode (n=1) into the background levels (14dB lower).

In the physiological state, single abrupt discontinuities are replaced with tapering, curvature and numerous branches which tend to complicate the response longitudinally. When this is coupled with the considerable attenuation of a disturbance, axially, the absence of discrete peaks of the lower order circumferential modes (n=0,1) seems likely.

All these factors, along with the apparent selective attenuation of murmurs through the body tissue (Boughner, 1971), are probably involved in the lack of discrete peaks in spectral phonocardiography.

An example of a musical murmur combined with a noisy murmur is shown in plate 2A (McKusick, 1958) resulting from a partial occlusion of the left carotid bifurcation. As noted by McKusick the frequency of the musical murmur appears to follow the arterial pulse

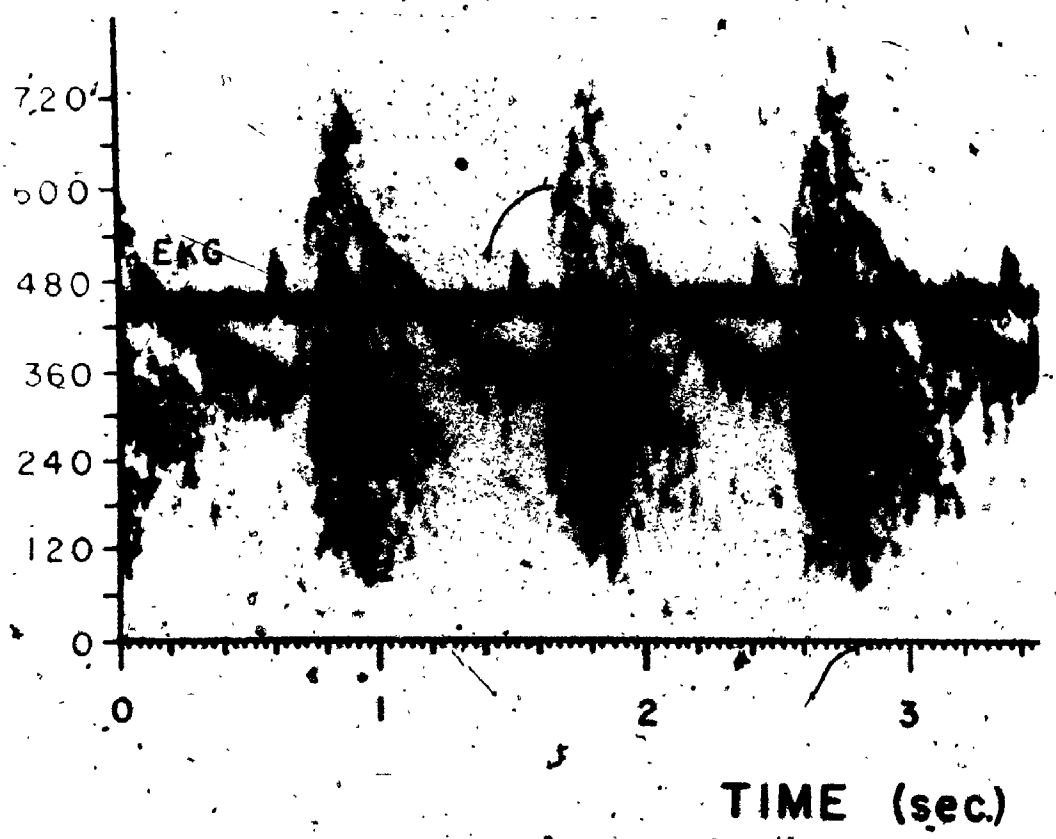
720
600
480
360
240
120
0
EKG
0
1
2
3
TIME (sec.)

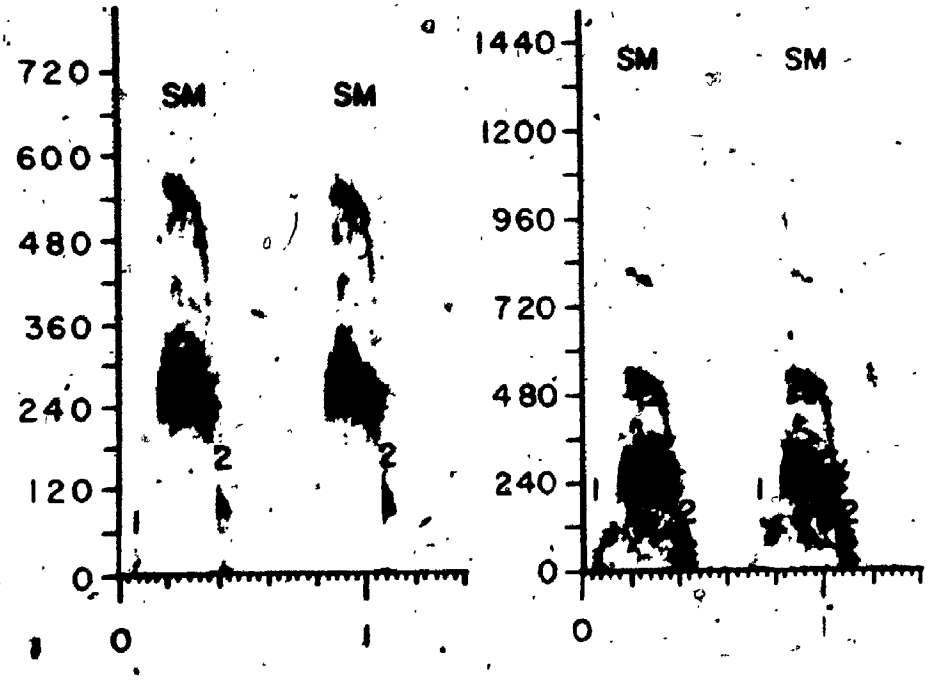
720
600
480
360
240
120
0
SM
SM
1
2
2
0
1
1440
1200
960
720
480
240
0
SM
SM
1
2
1
2
0

4 4

OF/DE

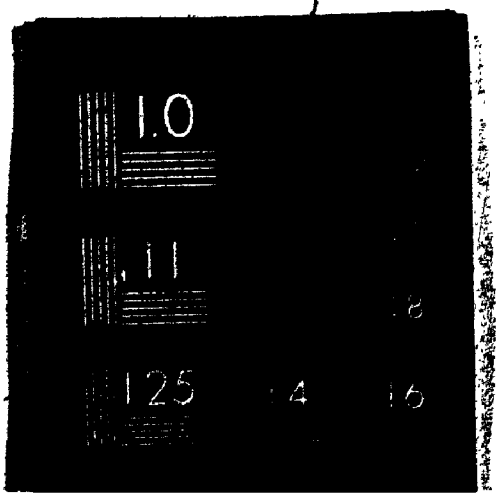

PLATE 2

A) Example of a musical murmur due to partial arterial occlusion recorded over the left carotid bifurcation. As in plate 1A the ordinate is frequency. Reproduced from figure 201 in McKusick (1958) with permission.

B) Example of a musical systolic murmur in calcific aortic valve disease. Reproduced from figure 175 in MuKusick (1958) with permission.

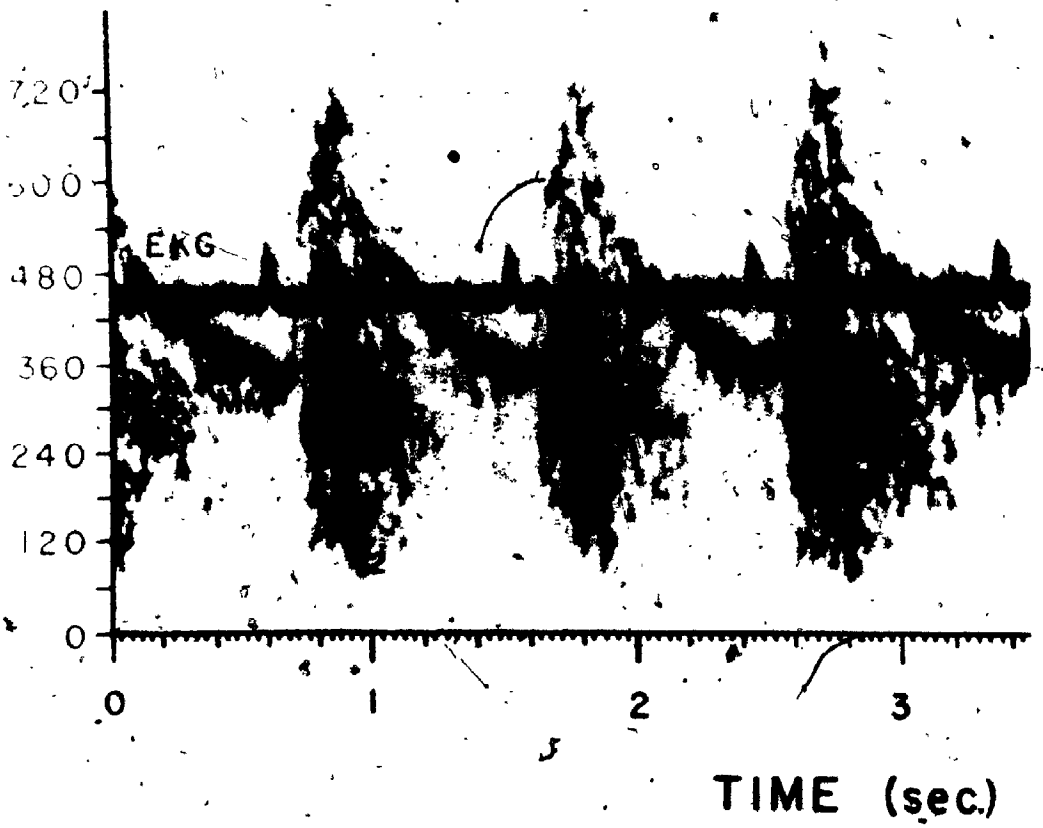
720
600
480
360
240
120
0
EKG
0
1
2
3
TIME (sec.)

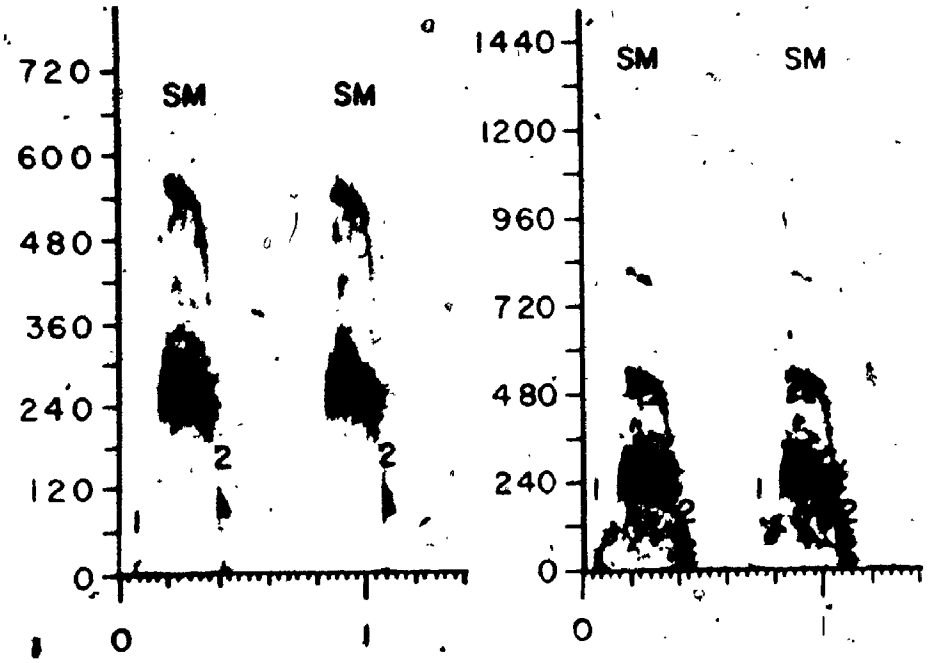
720
600
480
360
240
120
0
SM
SM
1
2
2
0
1
1440
1200
960
720
480
240
0
SM
SM
1
2
1
2
0
1

pressure, a factor which appears to be common to almost all musical murmurs. As explained by McKusick the continuous nature of the murmur probably arises from the fact that the large pressure drop across the occlusion results in the proximal pressure always exceeding the distal pressure. However, the musical nature was more difficult to understand with the suggestion that a mechanism comparable to bronchial asthma was involved.

In view of the present study the musical nature of the murmur may not be difficult to understand. We would expect that the sound may be due to a stimulation of the circumferential resonant mode, n=2, which would respond to pressure in a similar manner. For example, if we considered the bending terms and the longitudinal term to be negligible we would find from equation 26 that for n=2, $\frac{h}{a} = 0.1$ and P in mmHg then $f_2 \approx 9.5 \frac{P}{a}^{\frac{1}{2}}$. Thus the resonant frequency would be dependent on the square root of pressure as well as the radius, which will also vary throughout the cardiac cycle. If we assumed that the radius was constant at 0.25cm then we can obtain an estimate of the pressures from the peak systolic frequency of 600 Hz and the diastolic level of 360Hz. This would correspond to a blood pressure of 250/95 whose absolute values appear too high. However when the assumptions made are considered, this result may not be too bad. The possibility of both a smaller radius and

a thicker wall are likely due to the arteriosclerosis present. The smaller radius and the need for including the bending terms would both lower these values to a range that may be more acceptable. It is interesting to note the increased intensity of the murmur as it falls to a lower frequency, similar to that discussed in a previous section.

Plate 2B shows another musical murmur that was due to a calcific aortic valve. The same pressure sensitivity is noted here, although the intensity drops off during the diastolic phase, presumably as the turbulent jet decreases. Note the lower systolic frequency of 280Hz for the dominant peak with a higher order one at 560Hz, which may correspond to n=3. The lower frequency of the dominant peak, in comparison with the previous murmur, would be expected from the larger radius of the aorta, if it corresponds to n=2.

Using a similar approach to that above, and noting the different inertial response of the aorta (externally), we find a systolic pressure related to the radius by $P \simeq 470\ a^2$ mmHg. To obtain a reasonable estimate of pressure, therefore, we would have to assume a radius of 5 to 7 mm which appears too low. It seems clear, that without a specific knowledge of the wall stress and geometry further comparison is useless.

There are other hypotheses for musical murmurs, notably the 'flittering' phenomenon of Rodbard (1957) and

the periodic vortex shedding of Bruns (1959b). As discussed earlier, the instability known as 'flitter' occurs at low pressures which do not seem characteristic of the two musical murmurs discussed. The vortex shedding due to stiffened aortic cusps, on the other hand, can lead to a periodic fluctuation in the flow. However, in the presence of a transverse resonating mode the vortex shedding periodicity would be expected to occur at that of the resonance. This resulting feedback can lead to large scale motion of the fluid and the wall.

If the aortic resonance around 280Hz in plate 2B is correct then the second contour plot of the sound from an aortic stenosis (Plate 1B) may reveal a resonance around 270Hz. Note that this type of murmur was considered noisy. The decreasing frequency of this peak contour with decreasing pressure, that gives a 'christmas tree' effect, common to aortic stenosis, appears similar to that of the musical murmur just discussed and that expected of a circumferential resonance.

One of the general characteristics of musical murmurs is that they are intense. The dominance of their frequency content over that of the noisy murmurs may be related to the nature of the stimulating pressure field. The increased high frequency energy content due to severe obstruction or higher Reynolds numbers, for example, may accentuate the response in the resonant modes. Recall

that the pressure field was proportional to $f^2 \frac{Wo}{a}$ so that the high frequency accentuates the resulting pressure field. The correlation properties of the turbulent field also play a role in the modal response, so that the localized response of an obstruction may produce a different result than that from increased Reynolds number, for example.

In summary, the range of frequencies that are characterized by murmurs or bruits appear to contain those of several resonant modes of the arterial wall. It seems clear, therefore, that the wall is being stimulated to vibrate at several resonances which are probably an important factor in their detection, particularly with musical murmurs.

VI Summary

It is well known that vibration of a structure can lead to damage, possibly failure and biological tissue appears to be no exception. The vibratory stress that is induced in arteries as a result of turbulent flow can lead to a structural alteration of the wall properties. When these stresses are localized as with a partial occlusion or stenosis a dilatation of the arterial wall occurs (Roach, 1972).

An observation of discrete amplitude peaks in the wall vibration spectra distal to an occlusion, (Foreman and Hutchison, 1970), in vitro, led to the conclusion that the artery was being stimulated at its resonant frequencies. Such a result offers significant implications with respect to fatigue and the generation of sound. The relatively large vibratory strain possible at resonance offers a plausible explanation for the structural degeneration that is observed. Furthermore, these relatively large vibrations of the vessel wall can act as a sound source, such that they may become the dominant factor in the production of murmurs or bruits.

It seems clear that the question of arterial resonance is critical to a further understanding of structural fatigue and the associated cardiovascular sound. The scope of this thesis, therefore, has been to examine this question of resonance and to determine what factors are involved in determining the resonant frequencies.

What were the resonant modes that have been observed or are possible?

A solution was achieved by first examining the problem analytically. This was done by considering a membrane analysis of the radial equation of motion for a cylindrical elastic vessel that was under constant tension. This assumption removed most of the complexity associated with the vibration of continuous systems. Thus, an approach analogous to that of a simple string was followed which revealed that (as in the string) the wall stress (or tension) and geometry were the dominating factors determining the resonant frequencies. The tension governs the speed of propagation while the geometry determines the distance that the perturbation must travel. At the lower values of prestress or when considering the higher frequency modal patterns, however, the bending energy becomes important. Bending terms reflecting this contribution were therefore included in the final description.

A perturbation of the vessel wall also reflects a similar motion of the surrounding tissue or the enclosing fluid. The significance of this loading of the wall was considered in the theoretical development (Chapter III) where the resulting inertial terms demonstrated the importance of the internal and external acoustic media on the resonant frequencies. In the case of a fluid media the inertial term prediced a different response, dependent on the circumferential mode shape, n.

An experimental evaluation of this model, therefore, had to consider the effect of wall stress, geometry and the acoustical environment, as the three dominant factors describing the resonant frequencies.

As discussed in chapter IV this problem was first evaluated, experimentally, by considering the radial vibrations (measured with an optical sensor) of cylindrical segments of penrose tubing exposed to either acoustical stimulation (by a loudspeaker) or the random pressure fluctuations of turbulent flow (created by a stenosis). The use of the synthetic material provided a continuity for study under the three acoustic environments considered (air-air, air-fluid, and fluid-fluid), since its properties remained constant. The predicted changes in frequency for the various resonant modes due to wall stress was simply determined by varying the longitudinal tension (changing the length) or the circumferential tension (changing the pressure) under the three acoustic environments. The effect of geometry was similarly evaluated by using samples of different resting lengths and diameters. While these variations were sufficient to determine the resonant modes analytically, it was the spatial determination of amplitude and phase that confirmed them.

Having established that the model (see equation 26) adequately described the resonant modes of the synthetic tubing under the three acoustic environments, a series of disturbed flow studies were then performed on isolated arteries. The results were similarly successful and the

analysis was extended to the data from Foreman and Hutchisons study, where the predictions were also seem to be accurate.

The objective of this thesis was therefore met. An accurate analytical expression for the resonant modes of vibration was developed and the experimental analysis confirmed it. Those resonant modes can be determined from a knowledge of the wall stress, geometry and acoustic environment. Although only arterial segments were examined a similar extension to other tissues seems possible.

The response of the vessel to disturbed flow was that of an elastic system exposed to a random force that has a frequency content containing several resonant modes of the system. The radial vibrations of both the synthetic and biological material had an energy content of vibration that was confined to relatively narrow regions around the resonant frequencies.

The evidence for the wall vibrations being stimulated at several resonant modes under turbulent flow suggested that this may be the dominant factor involved in 'fatigue' of the vessel wall. From the discussion it seemed possible that the type of resonant mode excited may result in different structural alterations and that the occurrence of poststenotic dilatation may require stimulation of the circumferential resonant mode, $n \neq 2$.

Finally, the frequency range that is characteristic of murmurs and bruits is one which contains several resonant modes of vibration. It seems likely, therefore, that stimulation of those modes and the resulting vibrations may be a dominant factor in the sounds that are heard.

VII Suggestions for Future Research

The logical extension of these results, in vitro, would be to consider the response, in vivo. With two photonic sensors these studies would also provide information on the viscous attenuation of the disturbances.

An evaluation of the sound produced from wall vibration should be examined, correlating the external sound field (measured with a high quality pressure tranducer) with the wall vibration spectra.

Knowing the parameters of wall stress, geometry and the acoustical environment the specific murmurs or bruits could be evaluated in view of the present model. In this respect the use of better filtering techniques would be necessary to improve the quality of the frequency information.

The question of fatigue in biological tissue has been poorly examined. An approach similar to the fatigue tests done on synthetic materials would seem necessary. That is, both the effect of amplitude of the dynamic stress and the number of cyclic deformations should be considered. Another important factor to consider, in the regard, is the anisotropic effect of the dynamic stresses.

APPENDIX I

A list of the equipment used and their specifications.

Bruel and Kjaer (B&K) 2107 Frequency Analyzer

- continuously variable constant percentage band pass filter.
- maximum selectivity used was 6% (at 3dB bandwidth).
- ± 0.5 dB from 2-40,000 Hz (±0.3dB from 5-20,000 Hz).
- mechanically linked with Level Recorder to obtain an automatic precalibrated frequency sprectra of input signal.

Hewlett Packard 3580A Spectrum Analyzer

- low frequency constant bandwidth signal analyzer.
- six constant bandwidth from 300Hz to 1Hz (3dB) selectivity.
- ± 0.5 dB from 5-50,000 Hz.
- output stored on display or an XY recorder.

B&K 1022 Beat Frequency Oscillator

- precision signal generator with output from 125 uv to 125V.
- ± 0.2 dB from 20 to 20,000 Hz.

- the output voltage can be controlled from an external source by means of a regulating amplifier. The external voltage can be maintained to within 2dB over a 45dB change in output voltage.
- mechanically linked with Level Recorder to sweep over the range 20 - 20,000 Hz.

B&K 2305 Level Recorder

- full wave true RMS, average and peak detection of input voltage to within 1dB over the range 2-200,000Hz.
- variable writing and paper speeds of 4-2000mm/sec and 0.003-100mm/sec. respectively.
- six interchangeable logarithmic and linear potetiometers of which the 25dB and 50dB ranges were used.
- mechanically linked to drive either the 2107 Frequency Analyzer or the 1022 Beat Frequency Oscillator.

Physical Data Model 820A Random Signal Analyzer

- this unit performs auto and cross correlation (as well as amplitude probability distribution and amplitude probability density distribution) of input signals over the frequency range 10 to 250,000Hz.

- scanning rate of 10 seconds to 160 minutes permissible with a maximum delay of 1 second possible in the correlation mode.

Uher 4000 Report L Tape Recorder

- dynamic range 52dB
- ± 3dB from 60 to 13000 Hz at 7½ ips (± 5dB from 40 to 20,000Hz)
- Wow and flutter 0.2% maximum at 7½ips

Kudelski S.A. Nagra IVL Tape Recorder

- dynamic range 69dB
- ± .2dB from 30 to 15,000 Hz at 7½ips
- wow and flutter 0.05% maximum at 7½ips.

Mechanical Technology Model KD-45A 'Fotonic Sensor'

- electronic circuitry with planer photo diode has a flat frequency response from DC to 50 kHz and 3dB down at 100 kHz.
- KD-P109R fibre optic probe with active head of 2.18 mm diameter
- linear sensing range of 126 or 840 microns for a flat surface.

Fisher Scientific Flowmeter Kit - #11-164-5

- variable area Pyrex tube code 2L-150 with glass float used.

- flow rates from 0 to 3800 cc/min in air and 0 to 1130 cc/min in fluid.
- the extremes of the manufacturers calibration graph at 130, 600 and 1040 cc/min were checked with a one litre flask and stopwatch.

The results agreed within 5% so that the manufacturers calibration graph was used.

REFERENCES

Anliker, M. and J.A. Maxwell (1966). Dispersion of waves in blood vessels, pp. 46-67. In Y.C. Fung (ed.). Biomechanics symposium. ASME, New York.

Anliker, M. (1972). Toward a nontraumatic study of the circulatory system, pp. 337-380. In Y.C. Fung (ed.). Biomechanics. Prentice-Hall Inc., New Jersey.

Anne, A., Attinger, E.O., Sugawara, H., and A. Navarro. (1964). Frequency spectra of arterial flow parameters. 17th. Annual Conference of Engineering in Medicine and Biology.

Bergel, D.H. (1972). The properties of blood vessels, pp. 105-140. In Y.C. Fung (ed.). Biomechanics. Prentice-Hall Inc., New Jersey.

Botwin, M.R. (1973). Determination of viscoelastic moduli of arteries. J. Biomechanics 6 : 711-718.

Boughner, D.R. (1971). Vibration as a cause of arterial dilatation. Ph.D. thesis, University of Western Ontario, London, Canada.

Bruns, D.L., Connolly, J.E., Holman, E., and R.C. Stofer. (1959). Experimental observations on poststenotic dilatation. J. Thoracic Surgery. 38 : 662-669.

Bull, M.K. (1968). Boundary layer pressure fluctuations, pp. 169-180. In E.J. Richard (ed.). Noise and Acoustic Fatigue in Aeronautics. John Wiley & Sons, New York.

Clark, C. and D.L. Schultz (1973). Velocity distribution in aortic flow. Cardiovascular Rec. 7 : 601-613.

Clinch, J.M. (1969). Measurements of the wall pressure field at the surface of a smooth-walled pipe containing turbulent water flow. J. Sound vib. 9 : 398-419.

Clinch, J.M. (1970). Prediction and measurement of the vibrations induced in thin-walled pipes by the passage of internal turbulent flow. J. Sound vib. 12 : 429-451.

Dawes, G.S., Mott, J.C., and J.C. Widdicombe (1955). Cardiac murmur from the patent ductus arteriosus in newborn lambs. J. Physiol. (London) 128 : 344-360.

Dym, C.L. (1974). Introduction to the theory of shells. Pergamon Press, New York.

Ferguson, G.G. (1970). Turbulence in Human intracranial saccular aneurysms. J. Neurosurgery 33 : 485-497.

Ferguson, G.G. (1972). Physical factors in the initiation, growth, and rupture of human intracranial saccular aneurysms. J. Neurosurgery. 37 : 666-677.

Foreman, J.E.K., and K.J. Hutchison (1970a). Fluid Pressure Spectra in Turbulent Flow and Arterial Wall Vibration Distal to a Stenosis. Research Report, Engineering Science, University of Western Ontario.

Foreman, J.E.K., and K.J. Hutchison (1970b). Arterial wall vibration distal to stenosis in isolated arteries of dog and man. Circulation Res. 26 : 583-590.

Giddens, D.P., Mabon, R.F., Cassanova, R.A., Menon, R.K., and J. Chandler (1973). Experimental observations of the velocity field distal to partial occlusions in arteries. 10th. Anniversary Meeting, Society of Engineering Science, Raleigh, North Carolina.

Gutstein, W.H., Schneck, D.J., and J.O. Marks (1968). In vitro studies of local blood flow disturbance in a region of separation. J. Atherosclerosis Res. 8 : 381-388.

Hayden, H.W., Moffatt, W.G., and J. Wulff. (1965). The Structure and Properties of Materials III. Mechanical Behavior. John Wiley and Sons Inc., New York.

Holman, E. (1954a). The obscure physiology of poststenotic dilatation:its relation to the development of aneurysms. J. Thoracic Surgery. 28 : 109-133.

Holman, E. (1954b). "On circumscribed dilatations of an artery immediately distal to a partially occluding band." Poststenotic dilatation. Surgery. 36 : 3-24.

Kim, B.M., and W.H. Corcoran. (1973). Spectral analysis of turbulence and sound distal to a stenosis. 26th. Annual Conference of Engineering in Medicine and Biology. Minneapolis, Minnesota, p. 415..

Lees, R.S., and C.F. Dewey Jr. (1970). Phonoangiography. A new noninvasive diagnostic method for studying arterial disease. Proc. National Acad. Science 67 : 935-942.

Lepeschkin, E. (1957). Symposium on cardio-vascular sound. Circulation 16 : 428-431.

Maxwell, J.A. and M. Anliker. (1968). Dissipation and dispersion of small waves in arteries and veins with viscoelastic wall properties. Biophysical J. 8 : 920-950.

McKusick, V.A. (1958). Cardiovascular sound in health and disease. Williams and Wilkins, Baltimore.

Mead, D.J. (1968). Linear dynamical systems under random loading, p.p. 298-316. In E.J. Richards (ed.). Noise and Acoustic Fatigue in Aeronautics, John Wiley and Sons, New York.

Meisner, J.E., and R.F. Rushmer, (1963a). Eddy formation and turbulence in flowing liquids. Circulation Res. 12. 455-463.

Meisner, J.E., and R.F. Rushmer (1963b). Production of sounds in distensible tubes. Circulation Res. 12 : 651-658.

Moritz, W.E., and M. Anliker (1974). Wave transmission characteristics and anisotropy of canine carotid arteries. J. Biomechanics 7 : 151-154.

Nerem, R.M., Seed, W.A., and N.B. Wood (1972). An experimental study of the velocity distribution and transition to turbulence in the aorta. J. Fluid Mechanics 52 : 137-160.

Noordergraaf, A. (1969). Hemodynamics, pp. 391-545. In H.P. Schwan (ed.). Biological Engineering. McGraw-Hill, New York.

Prestigiacomo, A.J. (1962). Amplitude contour display of sound spectrograms. J.A.S.A. 34 : 1684-1688.

Patel, D.J., Janicki, J. and Carew, T. (1969). Static anisotropic elastic properties of the aorta in living dogs. Circ. Res. 25:765-779.

Roach, M.R., and A.C. Burton (1957). The reason for the shape of the distensibility curves of arteries. Canad. J. Biochem. Physiol. 35 : 681-690.

Roach, M.R. (1963a). Changes in arterial distensibility as a cause of poststenotic dilatation. Am. J. Cardiol. 12 : 802-815.

Roach, M.R. (1963b). An experimental study of the production and time course of poststenotic dilatation in the femoral and carotid arteries of adult dogs. Circulation Res. 13 : 537-551.

Roach, M.R. and K. Harvey (1964). Experimental investigation of poststenotic dilatation in isolated arteries. Canad. J. Physiol. Pharmacology 42 : 53-63.

Roach, M.R. and A.G. MacDonald (1970). Poststenotic dilatation in renal arteries. Preliminary report. Investigative Radiology 5 : 311-315.

Roach, M.R. and E. Melech (1971). The effect of sonic vibration on isolated human iliac arteries. Canad. J. Physiol. Pharmacology, 49: 288-291.

Roach, M.R. (1972). Poststenotic dilatation in arteries, p.p. 111-140. In D.H. Bergel (ed.). Cardiovascular Fluid Dynamics II. Academic Press, New York.

Rodbard, S., and H. Saiki (1953). Flow through collapsible tubes. Am. Heart J. 715-725.

Rodbard, S., (1957). Symposium on cardiovascular sound. Circulation 16 : 282.

Rushmer, R.G., and C. Morgan. (1968). Meaning of murmurs. Am. J. Cardiol. 21 : 722-730.

Sacks, A.H., Tickner, E.G. and I.B. MacDonald (1971). Criteria for the onset of vascular murmurs. Circulation Research 29 : 249-256.

Sinclair, A.S. (1972). The elastic properties of, and the effect of vibratory stress on dog bronchi. M. Sc. thesis, University of Western Ontario, London, Canada.

Skalak, R. (1966). Wave propagation in blood flow, pp. 20-46. In Y.C. Fung (ed.). Biomechanics Symposium. ASME, New York.

Wallace, J.D., Brown, J.R., Lewis, D.H., Deitz, G.W., and A. Ertugrul. (1959). Intra cardiac acoustics. J. Acoust. Soc. Am. 31: 712-723.

Warburton, G.B. (1961). Vibration of a cylindrical shell in an acoustic medium. J. of Mechanical Engineering Science. 3 : 69-79.

Willmarth, W.W. (1959). Space-time correlation and spectra of wall pressure in a turbulent boundary layer. N.A.S.A. T.M. 3-17-59W.

Winer, D.E., Perry, L.W., and G.A. Caceres. (1965). Heart sound analysis: a three dimensional approach. Contour plotting of sound for study of cardiovascular acoustics. Am. J. Cardiol. 16 : 547-551.

Yellin, E.L. (1966). Hydraulic noise in submerged and bounded liquid jets. In Biomedical fluid mechanics symposium, Fluid Mechanics Committee. A.S.M.E. Fluids Engineering Division, New York. pp. 209-221.

Young, D.F. and F.Y. Tsai (1973a). Flow characteristics in models of arterial stenosis. I. Steady flow.

Young, D.F. and F.Y. Tsai (1973b). Flow characteristics in models of arterial stenosis II. Unsteady flow. J. Biomechanics 6 : 547-559.